NASA Technical Paper 1056

F100 Multivariable Control Synthesis Program - Evaluation of a Multivariable Control Using a Real-Time Engine Simulation

John R. Szuch, James F. Soeder,
Kurt Seldner, and David S. Cwynar

OCTOBER 1977

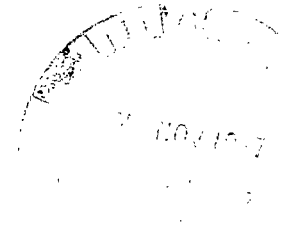

NASA

NASA Technical Paper 1056

F100 Multivariable Control Synthesis Program - Evaluation of a Multivariable Control Using a Real-Time Engine Simulation

John R. Szuch, James F. Soeder,
Kurt Seldner, and David S. Cwynar
Lewis Research Center
Cleveland, Ohio

National Aeronautics
and Space Administration

**Scientific and Technical
Information Office**

1977

CONTENTS

F100 MULTIVARIABLE CONTROL SYNTHESIS PROGRAM - EVALUATION OF A MULTIVARIABLE CONTROL USING A REAL-TIME ENGINE SIMULATION

by John R. Szuch, James F. Soeder, Kurt Seldner, and David S. Cwynar

Lewis Research Center

SUMMARY

Over the past several years, aircraft operational requirements have dictated the development of today's sophisticated turbofan engines. Classical control synthesis techniques have worked for the older, simpler engines. However, a need exists for a control synthesis procedure that can account for multiple loop interactions and can make use of them to optimize engine performance. One approach to solving the multivariable control problem is to apply the optimal control theory. The linear quadratic regulator is one specific area of optimal control theory that has been applied to the engine control problem. The F100 Multivariable Control Synthesis program is a cooperative effort by the Air Force Aero-Propulsion Laboratory and the NASA Lewis Research Center aimed at extending earlier linear quadratic regulator work to accomplish the design, evaluation, and testing of a practical multivariable control for the F100 turbofan engine. This report covers the NASA evaluation of the multivariable control logic and implementation. The evaluation utilized a real-time, hybrid computer simulation of the engine. Results of the evaluation are presented, and recommendations concerning future engine testing of the control are made. The results of the evaluation indicated that the engine testing of the control should be conducted as planned. With minor modifications, the multivariable control logic and its implementation on the NASA digital computer/controller should provide acceptable steady-state and transient performance at all flight conditions and power settings. It was concluded that the computer-aided, optimal control approach to designing multivariable controls does result in a practical solution to the engine control problem.

INTRODUCTION

Over the past several years, aircraft operational requirements have dictated the de-

velopment of gas turbine engines having increased performance capabilities over a wider operating envelope. These development efforts have resulted in today's sophisticated turbofan engines and will, undoubtedly, lead to increasingly complex engines in the future. For example, future variable-cycle engines may incorporate variable fan, compressor, turbine, and exhaust nozzle geometry to optimize overall engine performance (ref. 1). The trend toward more complex engines has resulted in additional requirements for the control system. Controls for future engines will require measuring more engine variables (perhaps 10 to 20) to control engine fuel flows, and the variable geometry. The use of a closed-loop control to achieve increased control accuracy and response is replacing the scheduling type (open-loop) controls used on older engines.

Classical control design (synthesis) techniques, which involve the design and evaluation of single-input, single-output control loops, have worked for the older, simpler engines. However, such techniques are cumbersome and time consuming when applied to the multivariable control problem. This is due to the inherent loop interactions that exist but are not considered in the classical design process. A need exists for a more suitable control synthesis procedure - that is, one that can account for these loop interactions and, possibly, make use of them to optimize engine performance.

One approach to solving the multivariable control problem is to apply the modern (optimal) control theory. This approach appears to be suited to the engine control problem due to the emphasis on maintaining optimum engine performance in the presence of a wide variety of external disturbances (i. e., aircraft maneuvers, horsepower extraction, etc.). The linear quadratic regulator (LQR) is one specific area of modern control theory that has been successfully developed and applied to a wide variety of linear, multivariable control problems (ref. 2). There have also been some initial research and development efforts aimed at applying the LQR theory to the design of controls for the nonlinear engine process (refs. 3 to 7). These efforts, however, have been limited to engine control over a narrow operating range (usually sea-level, static, standard-day conditions).

The F100 Multivariable Control Synthesis (MVCS) program, which is a cooperative effort by the Air Force Aero-Propulsion Laboratory (AFAPL) and the NASA Lewis Research Center, is aimed at extending the earlier LQR work to accomplish the design and testing of a "practical" multivariable control for a state-of-the-art turbofan engine - that is, one capable of operating the engine over its entire operating envelope. The engine selected for the MVCS program is the Pratt & Whitney F-100-PW-100(3) afterburning turbofan. In addition to the design of a control for the F100 engine, the MVCS program goals include the identification of advantages and disadvantages of the LQR method of designing engine controls, the evaluation of the control design using a real-time, hybrid computer simulation of the engine (ref. 8), and, finally, the demonstration of multivariable control of the F100 engine in a NASA altitude test facility.

Figure 1 illustrates the design and evaluation process used in the MVCS program. The program is highly dependent on cooperation and coordination between the various participants. The Air Force has provided the contract vehicle for the two contractors (i. e., the engine manufacturer and the controls research organization) and is therefore responsible for monitoring the activities of the two contractors. Pratt & Whitney has been contracted (F33615-75-C-2048) to provide the necessary engine support, while Systems Control Inc. has been contracted (F33615-75-C-2053) to design the control.

Pratt & Whitney has the prime responsibility of defining the F100 engine performance (both steady-state and transient) by means of a nonlinear, digital computer simulation (CCD 1103-1. 0) of the engine (ref. 9). This simulation has been supplied to both Systems Control Inc. and NASA for use in their preliminary evaluations of the control design. The digital engine simulation also forms the basis for the set of linear engine models that Pratt & Whitney has supplied to Systems Control Inc. for use in the LQR design procedure (ref. 9). The real-time, hybrid computer simulation of the engine (ref. 8) was developed by NASA to match steady-state and transient data obtained from the Pratt & Whitney digital simulation.

Pratt & Whitney has also defined the basic requirements of an F100 control system. These requirements (described in CONTROL REQUIREMENTS section) form the basis for the control evaluation criteria used by NASA in the hybrid evaluation. By participating in both the hybrid evaluation and subsequent engine tests, Pratt & Whitney has an opportunity to evaluate this new control concept using their intimate knowledge of the design problems associated with controlling gas turbine engines.

Systems Control Inc. has the prime responsibility for developing the multivariable control logic (refs. 10 to 11). They must demonstrate that this logic can successfully control the Pratt & Whitney digital simulation of the engine, be adequately programmed on the NASA digital computer/controller (ref. 12), successfully control the hybrid computer simulation of the engine, and, ultimately, control the F100 engine in a NASA altitude test facility. The controls contractor participates in both the hybrid computer evaluation and the engine tests to ensure that the control implementation reflects the design intent and that the design is well understood by the other participants.

NASA is responsible for providing the digital computer/controller and the manpower required to (1) program the multivariable control logic on that computer, (2) develop the real-time, hybrid computer simulation of the F100 engine, (3) carry out the hybrid evaluation, and (4) plan and conduct the engine tests. NASA is also responsible for providing the necessary engine-computer interface hardware. The total MVCS program involves a 19-month phase I effort culminating in the hybrid evaluation and a 6-month phase II effort concluding with the F100 engine tests.

This report covers the hybrid evaluation phase of the MVCS program. Results of the evaluation are presented and recommendations concerning future engine testing of the control are made. Separate NASA reports will cover the implementation of the mul-

tivariable control logic on the NASA digital computer/controller and the results of the engine tests.

Detailed discussions of the work performed by Pratt & Whitney and Systems Control Inc., as part of the MVCS program, are found in references 9 to 11.

SYMBOLS

A	cross-sectional area, m^2
ALT	altitude, km
BLC	fraction of compressor inlet airflow used for bleed
C_d	discharge coefficient
CHIGH	high power gain matrix, 5×15, appropriate units
C_I	integral gain matrix, 5×8, appropriate units
CIVV	fan inlet guide vane angle, deg
CLOW	low power gain matrix, 5×15, appropriate units
C_p	LQR gain matrix, 5×5, appropriate units
DPE	fan discharge $\Delta P/P$ parameter
FTIT	low-pressure (fan) turbine inlet temperature, K
F	thrust, N
GPARM	gain interpolation parameter
MN	aircraft Mach number
N_1	fan speed, rpm
N_2	compressor speed, rpm
P	total pressure, N/cm^2
PLA	power lever angle, deg
PLAM	effective power lever angle, deg
ΔP	total minus static pressure difference, N/cm^2
$\Delta P/P$	(total minus static)/total pressure parameter
Q_C	compressor torque, N-cm
Q_{FAN}	fan torque, N-cm
Q_{HT}	high-pressure turbine torque, N-cm

Q_{LT} low-pressure turbine torque, N-cm

RCVV compressor stator vane angle, deg

S Laplace operator, sec^{-1}

T total temperature, K

$\vec{U}$ control vector, 5-dimensional, appropriate units

$\dot{w}$ mass flow rate, kg/sec

$\dot{w}_F$ fuel flow rate, kg/hr

$\vec{X}$ state vector, 5-dimensional appropriate units

$\vec{Y}$ output vector, 5-dimensional, appropriate units

δ_2 fan inlet total pressure, divided by sea level atmospheric pressure

θ_2 fan inlet total temperature divided by standard day temperature

τ time constant, sec

Subscripts:

ADJ adjusted

BLC compressor discharge bleed

BLLT bleed for low-pressure turbine cooling

BLHT bleed for high-pressure turbine cooling

BOM hybrid with bill of material control

com command

DIG CCD1103-1.0 with bill of material control

ID fan hub

i station number (i = 0, 2, 2.1, 2.2, 3, 4, 4.1, 5, 6, 7, 8, 13, 16)

m measured

max maximum

min minimum

MVC hybrid with multivariable control

N net

nom nominal, rate-limited reference-point trajectory

OD fan tip

RAM ram drag

ss reference-point schedule

Superscript:

(i)' entrance to mixing volume at station i

ENGINE DESCRIPTION

The engine selected for the MVCS program is the Pratt & Whitney F100-PW-100(3) afterburning turbofan (ref. 9). This engine is representative of current high-technology engines and is illustrated in figure 2. The F100 engine is a low-bypass-ratio, twin-spool, axial-flow turbofan. A single inlet is used for both the fan airflow and the engine core airflow. Airflow leaving the fan is separated into two flow streams: one stream passing through the engine core and the other stream passing through the annular fan duct. A three-stage fan is connected by a through-shaft to the two-stage, low-pressure turbine. A ten-stage compressor is connected by a hollow shaft to the air-cooled, two-stage, high-pressure turbine. The fan has variable, trailing edge, inlet guide vanes (CIVV's). The inlet guide vanes are positioned to improve inlet distortion tolerance and fan efficiency. The compressor has a variable inlet guide vane and two variable stator vanes (RCVV's). These vanes are positioned to improve starting and to provide good high Mach number characteristics. Airflow bleed is extracted at the compressor exit and is discharged through the fan duct for starting. Bleed is also extracted to satisfy installation requirements and to provide turbine cooling. The main burner consists of an annular diffuser and a chamber with 16 fuel nozzles. The engine core and fan duct streams combine in an afterburner which consists of a diffuser and five concentric fuel manifolds. The afterburner discharges through a variable convergent-divergent nozzle. The exhaust nozzle is a balanced-beam design with an actuated divergent flap. The variable nozzle geometry provides near-optimum nozzle area, expansion ratio, and boat-tail drag throughout the operating range.

The current, bill of material (BOM) control system is basically hydromechanical with an engine-mounted, digital, electronic supervisory control. The BOM control logic sets the main burner fuel flow, fan inlet guide vanes, compressor stator vanes, afterburner fuel flow, and exhaust nozzle area to satisfy the pilot's throttle command (PLA) and flight condition (i. e., altitude and Mach number). In the MVCS program and its associated control design, the afterburner fuel flow is not being considered as a control variable due to the cost associated with providing the necessary interface hardware. The compressor discharge bleed is being utilized in the multivariable control, however.

The F100-PW-100(3) engine is being made available for testing of the multivariable control as part of the NASA-AFAPL Full-Scale Engine Research (FSER) program.

Among the FSER program objectives is the engine testing of advanced control concepts such as the multivariable control.

CONTROL REQUIREMENTS

One of the responsibilities of the engine manufacturer in the MVCS program is the definition of the control system requirements. These requirements serve as a guide for the control designer and are the driving force for making the control practical. These requirements also serve as the basis for the evaluation of the control design. Pratt & Whitney has provided a set of requirements for the F100 engine control (ref. 9). These requirements are intended to ensure that (1) engine limits are not exceeded, (2) steady-state and transient specifications are met, (3) the engine performance is compatible with aircraft requirements, and (4) the control can maintain satisfactory performance in the presence of component deterioration, horsepower and bleed extractions, inlet distortion, and afterburner ignition pulses. The following sections provide more detailed information on these requirements and are included as an aid in interpreting the results of the hybrid evaluation.

Engine Protection

In the current BOM control, the fan speed is limited as a function of the fan inlet total temperature as shown in figure 3. Normally, the fan speed would be scheduled below the limit because of performance and stability considerations. The compressor speed is limited to a fixed maximum value. Normally the control would maintain the compressor speed safely below this value since any overspeed requires at least a visual inspection of the high speed rotor.

The temperatures that must be maintained within limits to protect the engine are the compressor discharge temperature T_3 and the high-pressure-turbine-inlet temperature T_4. The compressor discharge temperature limit is based on maximum allowable metal temperature and the fact that turbine cooling effectiveness decreases rapidly above the limiting value of the temperature. The high-pressure-turbine-inlet temperature limit is based on maximum allowable metal temperature and turbine life considerations. The current control limits the low-pressure (fan) turbine inlet temperature FTIT to maintain the previously described temperatures within their limits. The FTIT limit is a function of the fan inlet temperature as shown in figure 4. In order to help meet transient response requirements, it is allowable to exceed the FTIT limit by up to 27 kelvins for a period of not more than 0.5 second.

To ensure structural integrity, the burner pressure P_4 is also limited. The limit

is normally encountered only at low altitude, high Mach number conditions.

To ensure structural stability, the fan and compressor variable geometry must be scheduled in accordance with the predicted blade flutter boundaries. These boundaries are shown in figures 5 and 6 for the fan and compressor, respectively. Also shown are the current BOM van schedules. The ground rule for fan and compressor stability is to maintain the fan surge margin above 0.15 and the compressor surge margin above 0.05. Since at some conditions this is not possible, the minimum allowable value is that predicted by the CCD1103-1.0 simulation.

Engine Performance

Engine thrust and fuel consumption requirements are contained in the F100 specification document CP2903B. These specifications are classified. For the purpose of the multivariable control design and evaluation, the thrust and fuel consumption goals were considered to be equal to the performance predicted by the CCD1103-1.0 simulation. The relation between thrust and PLA must be essentially linear and free of abrupt changes.

The required performance must be maintained by the control regardless of engine deterioration, except where the level of deterioration is such that engine limits would be exceeded. Fan and compressor efficiency decrements of 1.0 and 2.0 percent, respectively, are typical. High-pressure turbine efficiency losses of 2.5 percent have also been experienced.

Transient thrust requirements are specified for sea-level/static, standard-day, uninstalled conditions. These requirements are listed in table I. With maximum horsepower and bleed extractions, the response times cannot exceed 125 percent of the tabulated values. Idle thrust is defined as the lowest attainable thrust at the particular flight condition. Intermediate thrust is the highest nonaugmented thrust, and maximum thrust is the highest augmented engine thrust. For thrust increments of ±13.34 kilonewtons, if you start from a stabilized thrust between 25 and 45 percent of the available intermediate thrust, the time to achieve 90 percent of the thrust change should not exceed 1.2 seconds. For smaller thrust increments, this response criterion may be used as a measure of goodness.

Aircraft Compatibility

Engine airflow limits are set by inlet constraints. Airflow variations are restricted for supersonic operation to help maintain the inlet shock at a desired location. The current airflow limits are shown in figure 7.

In order to provide accessory airflow to various aircraft subsystems, the engine burner pressure P_4 should be maintained at a minimum level of 33.09 newtons per square centimeter. At very high altitudes, the value of P_4 at intermediate thrust will be lower than this value. Under these conditions, no reduction in the power setting below intermediate is allowed.

The engine should be controlled so that thrust is insensitive to variations in horsepower and bleed extractions up to the point where engine limits would be exceeded. For evaluation purposes, typical aircraft power extraction and bleed requirements are shown in figures 8 and 9, respectively.

Control Sensitivity

The engine must operate satisfactorily in the face of inlet pressure and temperature variations and rates of change of inlet conditions common to the operation of a highly maneuverable aircraft. Steady-state inlet variations of less than 1.0 percent are typical. For aircraft accelerations, rates of change of 0.103 newton per square centimeter per second and 1.111 kelvins per second are representative. For aircraft decelerations, the rates of change may be as much as -0.345 newton per square centimeter per second and -3.89 kelvins per second.

The control must be able to tolerate certain levels of afterburner ignition pulses. Figure 10 defines the maximum allowable level of afterburner ignition pressure pulses as a function of the fan discharge pressure P_{13}.

MULTIVARIABLE CONTROL

A simplified block diagram of the F100 multivariable control system is shown in figure 11. The control mode is basically proportional plus integral with a feed-forward path to provide rapid response. The proportional control action is provided by the LQR with the regulator gains C_p able to affect changes in all of the available control variables $\vec{U}$ to reduce deviations in all of the state variables $\vec{X}$ relative to the specified reference point $\vec{X}_{nom}$. The state, control, and output variables used in the multivariable control are as follows:

State variables	Control variables	Output variables
Fan speed	Fuel flow	Thrust
Compressor speed	Nozzle area	Fan airflow
Afterburner pressure	CIVV	Burner temperature
Fuel flow	RCVV	Fan surge margin
Burner pressure	Bleed flow	Compressor surge margin

The integral control provides steady-state trimming of the engine operating point to satisfy performance requirements and engine limits. The integrators are controlled by the engine protection logic through the limit flags. The integrators limit fuel flow and geometry excursions to provide safe stable engine operation.

The steady-state reference values of the state and control variables (i.e., $\vec{X}_{SS}$ and $\vec{U}_{SS}$) are scheduled as functions of the pilot command (PLA) and the flight condition. The outputs of the reference point schedules are rate limited in the transition control to prevent excessive deviations which could saturate the controller. The transition control provides a transient "model" for the regulator to follow.

Because of the nonlinear nature of the engine process, a single set of LQR and integrator gains will not result in satisfactory closed-loop responses at all operating conditions. To provide wide-range operation, the gains are scheduled as functions of the fan inlet conditions and the transition value of the compressor speed as shown in figure 11. It should be noted that the reference point and gain scheduling problems were not addressed in references 3 to 7.

The current F100 control system uses lead compensation to correct for a slow fan turbine inlet temperature sensor. The Systems Control Inc. design utilizes an FTIT "estimator" during transient operation to predict whether an overtemperature will occur. The estimated value of FTIT is compared with the limiting value (see fig. 3) and, if required, will cause the integral control to downtrim the engine before the overtemperature can actually occur.

The following sections provide a more detailed description of the various elements that make up the F100 multivariable control. An understanding of the control structure will serve as an aid in interpreting the results of the hybrid evaluation.

Reference Point Schedules

One of the tasks that must be accomplished in the multivariable control design is the calculation of steady-state, reference values for the five state variables, five control variables, fan turbine inlet temperature, and fan discharge $\Delta P/P$. These steady-state values are required for biasing the LQR inputs, unbiasing the LQR outputs, and

providing references for the trim integrators. The reference point schedules represent a steady-state model of the engine. Where schedule outputs feed trim integrators, the control will force the engine to match the schedules. For this reason, the fan discharge $\Delta P/P$, fan speed, fan inlet guide vane, compressor stator vane, and compressor bleed flow schedules must be sufficiently accurate to satisfy the performance requirements. Figure 12 illustrates the Systems Control Inc. approach to the reference point scheduling. The airflow schedule is basic to the fan match point. The scheduled values for fan speed N_1, fan discharge $\Delta P/P$, afterburner pressure P_6, and fuel flow $\dot{W}_{F4}$ are all functions of the scheduled airflow. The scheduled airflow is a function of the "effective" power lever angle PLAM, the fan inlet total temperature T_2, and the flight Mach number MN. The required inlet compatibility is provided by limiting the scheduled airflow to the allowable inlet corridor (see fig. 7). Compressor speed is also scheduled as a function of PLAM and T_2. The scheduled compressor speed (corrected to station 2) is used to schedule both the burner pressure and the fan turbine inlet temperature. If the pilot-set PLA will result in a scheduled burner pressure below 33.09 newtons per square centimeter, PLAM is uptrimmed to match the minimum allowable burner pressure. The scheduling of the fan and compressor variable vanes is accomplished in the integral trim logic, which is discussed in a following section (p. 13). The bleed is scheduled closed.

The reference point schedules have been simplified to reduce computer requirements. This has been accomplished by using corrected parameters. To ensure that the control requirements are still satisfied, absolute limits are provided in the reference point schedules. In addition to the inlet corridor, these include maximum fan speed (fig. 3), maximum and minimum burner pressure, maximum compressor speed, maximum FTIT (fig. 4), combustor blowout limits, and maximum and minimum fuel flows.

Transition Control

The transition control logic operates on the reference point schedule outputs to provide a transient model for the controller to follow during changes in either the flight condition or the pilot command. Figure 13 illustrates the concept used to accomplish this. Scheduled values of rate limits are applied to rate limited, first-order lags driven by the outputs of the reference point schedules $\vec{X}_{SS}$ and $\vec{U}_{SS}$. The rate limits are scheduled as functions of the fan inlet conditions P_2 and T_2 and the transition value of the compressor speed. The first-order lag time constants are set for each variable to give a smooth transition from the rate limited portion of the transient to the steady-state condition and to provide rapid movement of the reference point for small perturbation transients. The rate limits were determined from an analysis of linear engine models. The rates were established to provide the desired rates of change of

thrust, high-pressure turbine inlet temperature T_4, and compressor surge margin. The rates were determined at flight conditions (altitude/Mach number) of sea-level/static, 9.144 kilometers (km)/0.9, 13.72 km/0.9, and sea-level/1.2 for low, middle, and high power settings. The interpolation of control gains and rates as functions of the instantaneous flight condition and power setting is discussed in a later section (p. 14).

This rate limiting approach does not provide "hard" protection for temperature and surge margins due to the dependence on linear analysis. This hard protection is accomplished by the engine protection logic and the trim integrators to be described later (p. 14).

The transition logic also provides for an initial fuel flow and nozzle area rate "kick" for gross decelerations. The magnitude of the rate kick is a function of the scheduled and rate-limited compressor speed reference values, the fan inlet conditions, and PLAM. This kick logic is also used to signal the occurrence of gross transients to the integrator mode control.

The hybrid evaluation of the multivariable control covered both small perturbations and gross transients. The transition control logic was fully tested to determine the adequacy of the rates and switching logic. In addition, transition rates, designed for fast engine response, were also evaluated.

LQR Control (Proportional)

The LQR consists of a set of proportional gains which act through all of the control variables to reduce deviations in all of the state variables (relative to a specified reference). The basic regulator is described by

$$\vec{U} = \vec{U}_{nom} + C_p(\vec{X} - \vec{X}_{nom}) \tag{1}$$

where

$\vec{U}$ 5-dimensional control vector

$\vec{U}_{nom}$ 5-dimensional control vector (nominal trajectory)

$\vec{X}$ 5-dimensional state vector

$\vec{X}_{nom}$ 5-dimensional state vector (nominal trajectory)

C_p 5×5 LQR gain matrix

The LQR proportional gains were calculated by solving the matrix Ricatti equation at an operating point defined by a linear, state-variable model of the engine. A per-

formance index (measure of goodness), which contains weightings on all state deviations and all control deviations, was specified. The LQR design is intended to minimize this index.

An analysis by Systems Control Inc. of the approximately 30 linear engine models provided by Pratt & Whitney indicated that the full range of flight conditions and power settings could be covered by six LQR designs. Gain matrices were obtained at intermediate power (PLA = 83^{o}) for flight conditions of sea-level/static, 9.144 km/0.9, 13.72 km/0.9 and sea level/1.2. Idle power (PLA = 20^{o}) gains were calculated for the sea-level/static and 9.144 km/0.9 conditions. Analyses indicated that designs at mid-power conditions were not required since the engine dynamics appeared to change distinctly depending on exhaust nozzle and low-pressure turbine choking/unchoking.

Figure 14 shows the form of the resulting gain matrices. Of the 25 proportional gain terms, Systems Control Inc. found that 9 could be eliminated (zeroed) without significantly affecting the closed-loop response characteristics. A later section (p. 14) will describe the scheduling or interpolation of the 6 gain matrices based on the flight condition and power setting.

The ability of the LQR to regulate the steady-state and transient performance of the hybrid simulation of the engine was thoroughly tested in the evaluation. Gross transients were run to test the gain scheduling concept while small perturbations were run to test specific LQR designs. Afterburner ignitions and aircraft accelerations and decelerations were simulated to test the regulation in the face of external disturbances.

Trim Control (Integral)

Integral control action is used in the multivariable control to either control the fan operating point or to track an engine limit. Systems Control Inc. determined that integral control was necessary to satisfy the F100 control requirements in the face of engine-to-engine variations, component deterioration, installation requirements, and associated reference-point scheduling errors. Integral gains C_I were calculated to provide trim action with a time constant of approximately 1.0 second without affecting the LQR closed-loop response. The integral gains were determined at the same six operating points used in the LQR design. This allowed the integral gains to be included in the LQR matrix structure with its interpolation mechanism. Figure 15 shows the form of the overall gain matrix. The integral control consists of five integrators (one for each control variable) with each integrator driven by a combination of eight error terms. The basic integral control mode uses fuel flow and nozzle area to eliminate the fan speed deviation and the fan discharge $\Delta P/P$ deviation. In this mode, the engine limits are inactive. The CIVV, RCVV, and compressor bleed integrators are single-input integrators designed to maintain the vanes on their nominal schedules and the

bleed closed in steady state. Engine limits such as maximum allowable FTIT or minimum burner pressure will cause the appropriate limit error to be substituted for the fan speed error in both the fuel flow and nozzle area integrators.

Integration is normally allowed only near steady-state conditions. The fuel flow integrator, however, is allowed to trace engine limits whenever they are reached. Control saturation will cause the appropriate integrator to be clamped. Integrators are allowed to wind down during transients if the sign of the error term is such to reduce the absolute value of the integrator output. Dead-bands are applied to all integrator inputs to avoid limit cycling which might be caused by actuator hysteresis.

The hybrid evaluation was intended to fully test the operation of the integral control under both steady-state and transient conditions. The ability of the integral control modes to satisfy the steady-state performance requirements was determined. Particular attention was directed toward the integral tracking of engine limits.

Gain Scheduling

The LQR and integral control gains are scheduled in the multivariable control to reflect shifts in the engine dynamics as changes occur in the flight condition or engine power. The gain scheduling algorithm is shown in figure 16. It interpolates between gains that were determined at the four high-power conditions and the two low-power conditions. For a particular flight condition, a set of low- and high-power gains is computed by the gain scheduling algorithm based on fan inlet air density. The transition value of the scheduled compressor speed SNCTR is then used to interpolate the low- and high-power gains. The break between the low- and variable-power gains occurs at compressor speeds which correspond to a PLA of approximately 36°. The break between variable-power gains and the high-power gains occurs at a PLA of approximately 70°. The 36° setting corresponds to the point where the low-pressure turbine unchokes. This unchoking causes a significant change in the engine's dynamic behavior.

Engine Protection

The engine protection logic in the multivariable control provides hard limits on the commands to the control actuators. The engine protection algorithm is shown in figure 17. The engine protection logic includes fuel flow limits, variable vane limits (figs. 5 and 6), bleed limits (0.0 to 6.0 percent of the compressor inlet airflow), and exhaust nozzle area A_7 limits. The fuel flow limits include the maximum and minimum flows and an acceleration schedule which is a function of the measured compressor speed. The exhaust nozzle area limits are functions of the PLAM. The maximum and minimum

allowable area commands converge at idle power so as to prevent limit cycling in this sensitive operating regime. This feature was included as a result of early results from the hybrid evaluation. Flags are set when any unlimited commands exceed the specified limits or when control saturation is detected. The flags are used to clamp the appropriate trim integrators.

FTIT Estimator

The current F100 BOM control system uses lead compensation to predict an impending FTIT overshoot. This is necessary because of slow FTIT sensor dynamics. High downtrim gains are used to avoid excessive temperature overshoots. In the multivariable control, however, another method of estimating FTIT is used. As shown in figure 18, the FTIT "estimator" uses a combination of the sensed FTIT ($FTIT_m$), the steady-state reference value of FTIT ($FTIT_{ss}$), the transition value of fuel flow ($\dot{W}_{F,4,nom}$), and the commanded fuel flow ($\dot{W}_{F,4,com}$) to predict the final value of FTIT during a transient. The predicted value is compared with the maximum allowable FTIT (fig. 4). If an overtemperature is predicted, the fuel flow integrator downtrims the fuel flow before an overtemperature can occur.

A detailed description of the F100 multivariable control logic can be found in reference 11.

CONTROL IMPLEMENTATION

The F100 multivariable control logic was implemented on the SEL810B digital computer (ref. 12) shown in figures 19 and 20. The salient features of that computer are listed in table II. Although this computer is not flight-qualified hardware, its memory, speed, and word size are believed to be representative of the computers that will be used to control engines in the 1980's. All of the SEL810B programming was performed in assembly language in order to reduce the core requirements and computation time. The total software package, including the control algorithms, matrix data, reference point schedule data, and general-purpose input/output subroutines consumed approximately 12 000 words of core storage. The multivariable control algorithm consumed approximately 7000 words of core storage. A complete breakdown of the memory allocation is given in table III. The core requirements listed in table III are not a direct measure of the control complexity, however. While the schedules and matrix data would consume the same amount of core on any 16-bit computer, the control algorithm requirements are highly dependent on the computer architecture, instruction set, and objectives of the programmer. In the MVCS program, a determining factor was the

stated goal of achieving a 10-millisecond control update time, as compared with the 14-millisecond update time for the F100 electronic supervisory control and the 20-millisecond update time for the IPCS (ref. 13) implementation of the TF30 BOM control logic. To achieve the desired 10-millisecond update time, it was necessary to write the entire program using inline code. This had the effect of eliminating the overhead associated with multilevel subroutine calls and indexing. While speeding up the computations, this required additional core storage.

In addition to performing the multivariable control calculations, the SEL810B was used to simulate the control actuators and for collecting transient data. All of these tasks were performed in the 10-millisecond update interval.

EVALUATION OF MULTIVARIABLE CONTROL

The principle objective of the MVCS program is to demonstrate the multivariable control of the F100 engine in a NASA altitude test chamber. To that end, the multivariable control logic was developed by Systems Control Inc. and implemented on the NASA digital computer/controller. The implementation was described in the preceding section. Prior to the altitude tests, however, it is necessary to evaluate the control logic and its implementation to ensure safe, stable engine operation throughout the F100 flight envelope.

This evaluation was accomplished using a real-time, hybrid computer simulation of the F100 engine (ref. 8). The hybrid computer simulation provided a convenient and economical means of evaluating both the steady-state and transient performance of the multivariable control and its implementation. The simulation did not, however, provide sufficient precision and repeatability for determining the control's sensitivity to installation and engine component deterioration. For those evaluation items, the CCD1103-1.0 simulation was run by Systems Control Inc. using compatible FORTRAN coding of the multivariable control logic. The results of that study will be presented in their final report.

Figure 21 illustrates, schematically, how the various computers were configured for the hybrid evaluation. An Electronic Associates Inc. model 690 hybrid computer provided the real-time engine simulation. The analog signals, representing the engine variables to be sensed, were trunked to a TR48 analog computer which provided real-time sensor simulations. The simulated sensor outputs were digitized and processed in the SEL810B digital computer. The SEL810B computer was used to compute the commands to the control actuators and to simulate, digitally, the actuator dynamics. The digital actuator outputs were converted to analog signals for input to the engine simulation. The following sections provide a more detailed description of the engine, sensor, and actuator simulations.

Real-Time Engine Simulation

A real-time, hybrid computer simulation of the F100-PW-100(3) turbofan engine (ref. 8) was developed by NASA to support controls research programs involving that engine. The simulation has both wide-range steady-state and transient computing capabilities. The mathematical model describing the performance of the F100 engine was patterned after the CCD1103-1.0 digital simulation (ref. 9). Wide-range, overall performance maps for the engine's rotating components (i.e., fan, compressor, turbines) were utilized so as to provide the wide-range steady-state accuracy. Factors such as fluid momentum, mass and energy storage, and rotor inertias were included to provide transient capability.

Figure 22 contains a computational flow diagram of the real-time simulation. It can be seen that the mathematical model consists of a number of individual elements and their related volumes, each of which requires a number of input variables and generates one or more output variables. However, unlike a digital simulation, all calculations are considered to be performed in parallel.

The equations describing the F100 mathematical model were implemented on the Lewis Research Center's hybrid computing system. The Electronic Associates Inc. model 690 hybrid computer consists of a model 640 digital computer, model 680 analog computer, model 681 analog computer, and an interface unit which allows communication between the individual computers. A photograph of the hybrid computer system is shown in figure 23. The digital portion of the hybrid computer was used primarily to perform the bivariate function generation associated with modeling the performance of the engine components. In addition to this function generation, the digital computer was also used for computing the fan and compressor surge margins and the engine net thrust. The digital portion of the simulation consumed 12 440 words of core storage and had an update time of approximately 7.5 milliseconds. The digital portion of the simulation was structured to provide accurate, real-time dynamics with this update time (ref. 8). The remaining calculations were performed on the analog computers. The analog computers provided continuous integration with respect to time, multiplication, division, univariate function generation, etc. The two analog computers were fully utilized. For example, the full complement of 54 multipliers and a total of 189 potentiometers were required. The use of peripheral equipment such as X-Y plotters and strip-chart recorders allowed continuous monitoring of computed variables. Setup and checkout of the analog portion of the simulation was accomplished using the digital computer and general-purpose software.

Sensor and Actuator Simulations

To demonstrate multivariable control of the real-time engine simulation, it was

necessary to simulate, in real time, the dynamic characteristics of the engine-control interfaces. This included the sensors and the control actuators. Since the hybrid evaluation was aimed at verifying the multivariable logic and its implementation prior to engine testing of the control, it was concluded that the interface simulations should reflect the hardware to be used in the altitude tests. In most cases, the dynamic characteristics of the research actuators and sensors differ from those of the BOM control interface hardware.

Table IV lists the simulated sensors and their dynamic characteristics. With the exception of the FTIT and the fan discharge temperature T_{13} sensors, the sensors were represented by first-order lags. The time constants for the rotor speed sensors were based on the CCD1103-1.0 simulation values. The time constants for the P_2, P_4, and P_6 sensors were based on the use of strain-gage-type transducers with fairly short sensing line lengths. Because of the uncertainty in estimating the dynamic characteristics of the research temperature instrumentation, the BOM sensor models were used in the hybrid evaluation.

In the altitude tests of the control, measurements of the fan discharge total pressures and total-minus-static pressure differences (ΔP) will be used to compute the Systems Control Inc. fan discharge $\Delta P/P$ parameter DPE. The following equation is to be used:

$$\mathrm{DPE} = \frac{(\Delta P)_{13} + (\Delta P)_{2.2}}{P_{13} + P_{2.2}} \tag{2}$$

Since similar transducers are to be used for the four separate measurements, it was assumed that they would have similar dynamic characteristics. Since the ratio would effectively cancel their dynamic effects, no sensor dynamics were considered in the computation of DPE. In the hybrid computer simulation of the engine, static pressures are not calculated. However, the individual $\Delta P/P$ parameters are computed as functions of the corresponding corrected airflows. In the hybrid evaluation, the following method of computing DPE was used:

$$\mathrm{DPE} = \frac{(\Delta P/P)_{13}P_{13} + (\Delta P/P)_{2.2}P_{2.2}}{P_{13} + P_{2.2}} \tag{3}$$

The sensor dynamics were simulated in real time using an Electronic Associates model TR48 desk-top analog computer which is shown in figure 24.

The actuators associated with the five control variables had to be simulated in real time also. Because of equipment limitations, the SEL810B was used for the actuator

simulations.

The exhaust nozzle and CIVV actuators were designed by NASA to support fan flutter studies that were conducted as part of the FSER program. The exhaust nozzle interface consists of an electrohydraulic servo which positions, by means of a cable linkage, an air motor control valve on the engine-mounted actuation system. This is shown schematically in figure 25. Experimental data indicated that the response of the electrohydraulic servo was fast compared with the actuation system slew rate. Therefore, the dynamics of the servo were neglected. The remainder of the actuation system was simulated in the SEL810B computer.

The CIVV actuator consists of an electrohydraulic servo which drives dual engine-mounted piston-in-cylinder actuators. The CIVV system is shown schematically in figure 26. For the multivariable control tests, the servovalve has been sized to provide the desired CIVV slew rate. Prior to the hybrid evaluation, the servoamplifier gain was adjusted to provide satisfactory simulation response characteristics.

NASA must also provide the fuel flow, RCVV, and bleed flow interface hardware for the multivariable control tests. The Bendix Energy Controls Division was contracted (NAS3-20245) to provide the fuel flow and RCVV interface hardware. The fuel flow actuator is shown schematically in figure 27. This system consists of a basic F100 metering valve positioned by a fuel-actuated power piston. This piston is driven by an electrically controlled servovalve. A resolver is attached to the metering valve shaft to provide metering valve position feedback to the servoamplifier. The pressure drop across the metering valve is sensed by the F100 fuel pump controller and is maintained at 41.37 newtons per square centimeter. The pump controller dynamics are represented by a first-order lag with a time constant of 0.1 second. This lag was simulated on the analog computer while the remainder of the fuel actuation system was simulated in the SEL810B computer. The nonlinear resolver characteristic was included in the simulation.

The RCVV actuator is shown schematically in figure 28. This system consists of dual, fuel-powered pistons driven by an electrically controlled servovalve. The servovalve is designed to drive both the tandem cylinder and the RCVV slave cylinder. A resolver is attached to the tandem cylinder to provide position feedback to the servoamplifier. The RCVV resolver characteristic is essentially linear and was assumed to be linear in the actuator simulation. Based on the CCD1103-1.0 simulation, RCVV hysteresis of $\pm 1.0^{o}$ was included in the SEL810B simulation.

Prior to the hybrid evaluation no information was available on the bleed flow valve characteristics. For the evaluation the bleed system was assumed to be fast acting with the bleed flow computed from

$$\dot{w}_{BLC} = BLC\dot{w}_{2.2} \tag{4}$$

where BLC is the fraction of the compressor inlet airflow used for bleed in the multivariable control. In the altitude tests a dynamic measurement of the compressor inlet airflow will not be available. An analysis of CCD1103-1.0 data has shown that the required bleed valve opening can be related to the BLC command by

$$A_{BLC} = \frac{0.01774\ BLC}{C_{d,\,BLC}}\ m^2 \tag{5}$$

Procedure

Table V lists the flight conditions and types of tests covered in the evaluation. The flight conditions were selected to cover the full range of F100 operation. They included conditions to be run in the altitude facility and, additionally, low altitude and high inlet temperature conditions that cannot be run in the facility. The range of power settings at each flight condition was limited so as to satisfy the inlet airflow requirements (fig. 7).

The EAI640 and SEL810B digital computers provided digital listings of steady-state engine and control data, respectively. A total of 192 engine and control variables were listed at each of the 56 evaluated operating points.

The usual peripheral analog equipment was used to monitor transient data during the evaluation. Because of the vast amount of available data, however, a more convenient means of recording and processing transient data was desired. Therefore, the SEL810B digital computer was also utilized as a transient data sampler and storage device as shown in figure 21. A total of 72 variables were sampled and stored for each of the 77 transient runs. These variables included engine variables, sensed engine variables, internal control variables, actuator commands, and actuator outputs. Two hundred samples per variable per run were stored with the sampling rate adjusted to match the duration of the transient. For example, each of the 72 variables was sampled every 100 milliseconds during a 20-second run. After the completion of a particular transient run, the stored data were transferred to a disk storage device for later processing.

Prior to taking data at a particular flight condition, it was necessary to "trim" the engine simulation to match CCD1103-1.0 data (ref. 8). The fan and compressor discharge specific heats and the main combustor efficiency were adjusted (if necessary) to match the baseline values of fan speed, compressor speed, and FTIT. During this trimming process, the control inputs to the hybrid simulation were fixed at their CCD1103-1.0 intermediate thrust values. No trimming of the simulation was done at part-power conditions.

In order to avoid transients when switching to the multivariable control, the following procedure was used. After the trimming of the engine simulation, the multivariable

control was put in a "TRACK" mode whereby the control's trim integrators were continuously updated to match the open-loop control inputs to the engine. The integrators were then clamped and the loops between the control implementation and the engine simulation were closed. The trim integrators were then released without an accompanying transient. This procedure proved successful and will be used in the altitude tests when switching from the BOM mechanical controls to the multivariable control.

During the initial phase of the evaluation, a number of anomalies were discovered which required modifications to the control logic and its implementation. With the assistance of the control designer, causes were identified and corrective action was taken. Table VI lists the symptoms, causes, and required control modifications. In general, the observed behavior was associated with the nonideal hybrid simulation environment. The control logic and implementation were changed to accommodate noisy signals and observed differences between the hybrid and CCD1103-1.0 simulations.

RESULTS AND DISCUSSION

Steady-State, Uninstalled Performance

The steady-state, uninstalled performance of the F100 engine simulation under multivariable control was evaluated at those flight conditions listed in table V. Figures 29 to 35 show the results of that evaluation.

For each flight condition, the observed values of fan speed, compressor speed, burner pressure, afterburner pressure, fan turbine inlet temperature, and fan discharge $\Delta P/P$ are plotted against the corresponding scheduled values over the allowable range of power settings. Depending on the integral trim mode, a matching of the reference point schedules may be forced by the trim integrators. A match of the reference point schedules for uncontrolled variables, however, indicates that the schedules represent an accurate, steady-state model of the simulated engine. On the other hand, large deviations from the reference point schedules can result in the saturation of the regulator and/or the integral controller and produce degraded steady-state performance.

For each flight condition, the observed values of net thrust, fan surge margin and compressor surge margin are plotted against PLA. However, because of possible hybrid simulation errors caused by simplified thrust and surge margin calculations, a direct evaluation of those aspects of the control performance was not possible. An attempt was made to estimate those errors at each operating point and to adjust the simulation data accordingly. Hybrid simulation values of fan surge margin, compressor surge margin, and net thrust, obtained with an SEL810B implementation of the BOM control logic, were compared with the corresponding CCD1103-1.0 data. Any observed differences were attributed to the hybrid simulation and were applied to the multivariable

control results. The "adjusted" values of the surge margins and net thrust were thus computed from

$$\vec{Y}_{ADJ} = (\vec{Y}_{DIG} - \vec{Y}_{BOM}) + \vec{Y}_{MVC} \tag{6}$$

The resultant data were then judged relative to the previously described control requirements. It should be remembered, however, that the primary objective of the evaluation was to verify the control implementation and to identify control problems prior to the engine tests. A quantitative evaluation of the steady-state, closed-loop performance was a secondary objective that could be accomplished using the CCD1103-1.0 simulation. The hybrid simulation is sufficiently accurate, nonetheless, so as to provide a realistic test of the multivariable control logic as well as the implementation.

Figures 29 and 30 show the steady-state results for the sea-level/static and 3.048 km/0.6 flight conditions, respectively. The 3.048 km/0.6 condition will serve as a substitute for the sea-level/static condition in future engine tests since simulating altitudes lower than about 3 kilometers in the NASA altitude test facility is not possible. At these two flight conditions the control action was quite similar. At intermediate power (PLA = 83^{o}), the trim integrators for fuel flow and nozzle area maintained FTIT at its limit and the fan discharge $\Delta P/P$ parameter at its scheduled value. This is shown in figures 29(e) and (f) for the sea-level/static condition. The observed agreement between the other engine variables and their schedules indicated that the reference point schedules did match the engine simulation quite well at these conditions. At part-power settings, the trim integrators maintained the fan speed and the fan discharge $\Delta P/P$ parameter at their schedules values. This is shown in figures 29(a) and (f) for the sea-level/static condition. However, at PLA settings of 30^{o} and below, the nozzle area was constrained by the multivariable control to be 0.274 square meter to satisfy the idle thrust requirement and to prevent limit cycling in the low power portion of the operating line. Therefore, only integral control of the fuel flow was available to maintain the fan speed at its scheduled value. The area constraint was active at each of the evaluated subsonic conditions below the 13.72-kilometer altitude. Figures 29 and 30(g) show that the multivariable control did satisfy the intermediate thrust requirement at the three flight conditions. The idle thrust results varied, however, with a match of the CCD1103-1.0 idle thrust at the sea-level/static condition, but a higher thrust was observed at the 3.048 km/0.6 condition.

The control requirements specified minimum allowable fan and compressor surge margins of 0.15 and 0.05, respectively. These requirements are relaxed at those operating points where the CCD1103-1.0 simulation predicts lower values. In these two cases, however, the multivariable control produced slightly lower surge margins than the CCD1103-1.0 simulation. At the sea-level/static condition, a minimum fan surge margin of 0.074 was observed as shown in figure 29(h). This was slightly lower

than the CCD1103-1.0 value of 0.079. Also, at the 3.048 km/0.6 condition, the multivariable control resulted in a minimum fan surge margin of 0.134 as compared with the baseline value of 0.144. This is shown in figure 30(h).

Two different aspects of the multivariable control were introduced and verified at the 9.144 km/0.9 and 13.72 km/0.9 conditions. Those results are shown in figures 31 and 32, respectively. For these conditions, the trim integrators for fuel flow and nozzle area maintained both the fan speed and fan discharge $\Delta P/P$ parameter at their scheduled values at the intermediate thrust setting. At this setting, the FTIT was lower than the limit. This is shown in figures 31(a), (e), and (f) for the 9.144 km/0.9 condition. At idle power the trim integrators switched from fan speed control to burner pressure control so as to maintain a minimum burner pressure of 33.09 newtons per square centimeter. This is shown in figures 31(a) and (c) for the 9.144 km/0.9 condition. Figures 32(a) and (c) show that the minimum burner pressure limit was active at a higher power setting due to the higher altitude. PLAM was uptrimmed to 22.7° at the 9.144 km/0.9 condition and to 38.1° at the 13.72 km/0.9 condition. Figure 31(f) shows that the nozzle area constraint was also active at low power settings at the 9.144 km/0.9 condition.

Figures 31 and 32(g) show that the multivariable control again satisfied the intermediate thrust requirement. In both cases, however, the idle thrust was lower than that predicted by the CCD1103-1.0 simulation. This was caused by the BOM control limiting the burner pressure to a higher value than 33.09 newtons per square centimeter. The surge margin requirements were satisfied at both flight conditions as shown in figures 31(h) and (i) and 32(h) and (i). At the 13.72 km/0.9 condition, the multivariable control matched the CCD1103-1.0 minimum fan surge margin of 0.142.

Figures 33 and 34 show the results from the evaluation of the multivariable control at two low altitude, high Mach number conditions. The sea-level/1.2 condition produced the highest engine pressures and flows. The 3.048 km/1.2 condition will be a substitute for the sea-level/1.2 condition in the altitude tests with the engine. Figures 33(a) and (f) and 34(a) and (f) show that the integral trims for fuel flow and nozzle area maintained the fan speed and fan discharge $\Delta P/P$ at their scheduled values over the entire operating line. PLA settings below 50° were not run since the control criteria do not permit lower settings due to inlet airflow requirements at these supersonic flight conditions. The results of the evaluation showed that the multivariable control did maintain the intermediate operating point below the maximum burner pressure and maximum FTIT at at the sea-level/1.2 condition. The resultant thrust exceeded the CCD1103-1.0 value at intermediate power but was considerably lower at part-power settings as shown in figure 33(g). Figure 34(g) shows that the intermediate thrust at the 3.048 km/1.2 condition was also low. The surge margin requirements were satisfied at both flight conditions.

At the sea-level/1.2 condition, the intermediate value of the compressor speed, shown in figure 33(b), exceeded the maximum allowable value. While this was attributed

to a simulation anomaly at this operating condition, it does point up the need for some form of hard limit on compressor speed in addition to the limit provided in the reference point schedule. The steady-state portion of the evaluation was performed with the acceleration schedule of fuel flow removed from the engine protection logic. Since this schedule has a high and low compressor speed cutback feature, it is felt that this schedule will provide sufficient protection against a compressor overspeed during engine testing.

Figure 35 shows the steady-state results for the evaluation points where part-power operation was not permitted. At these conditions, only intermediate power settings were run. For all but the 12.19 km/2.2 condition, the integral trims maintained FTIT at its limit. At the 12.18 km/2.2 condition, the fan speed was maintained at its scheduled value. The fan discharge $\Delta P/P$ parameter was maintained at its scheduled value at all of the flight conditions.

At three of the flight conditions, however, the authority limits on the fuel flow and nozzle area trim integrators had to be relaxed to match the schedules. At the 6.096 km/1.8 condition, the fuel flow uptrim limit was increased to permit 878.6 kilograms per hour of uptrim to match the FTIT limit at that condition. At the 12.19 km/2.2 condition, the fuel flow uptrim limit was increased to permit 838.2 kilograms per hour of uptrim to match the fan speed schedule. Finally, at the 19.81 km/2.5 condition, the nozzle area downtrim limit was increased to 0.073 square meter to match the fan discharge $\Delta P/P$ schedule.

At the 19.81 km/0.9 and 22.86 km/1.8 conditions, conflicting control requirements existed. That is, the burner pressure was lower than the minimum allowable value while the FTIT was at its limit. The integral control logic places FTIT control on a higher priority. Therefore, the burner pressure was lower than 33.09 newtons per square centimeter at these conditions as shown in figure 35(c).

A problem with the FTIT estimator logic was discovered at the 19.81 km/0.9 condition. Figure 35(e) shows a large discrepancy (140°) between the maximum and scheduled values of FTIT at that condition. It was observed that changes in the fan inlet conditions due to changes in the flight condition or noise could produce sufficient changes in the scheduled value of FTIT so as to reinitialize the estimator. The estimator was designed to reset to the scheduled value when a transient was indicated by a sudden change in the schedule output. At the 19.81 km/0.9 condition, the resetting of the estimator to the low value and the low burner pressure resulted in a fuel flow uptrim and a corresponding increase in the FTIT. An overtemperature could not be prevented by the existing estimator logic. Modifications to the FTIT reference point schedule to better match the engine at this flight condition could not conveniently be made. However, the estimator logic was modified to prevent the reset action when low burner pressure conditions existed.

Figure 35(g) compares the actual net thrust obtained with the multivariable control

and the adjusted net thrust. While all of the flight conditions resulted in thrust in excess of the CCD1103-1.0 values, only the 19.81 km/0.9 condition resulted in adjusted thrust meeting the thrust requirement. This could be attributed to the fact that no supersonic conditions were considered in the establishment of the reference point schedules. Figure 35(h) shows that the surge margin requirements were satisfied at all of the flight conditions. The 19.81 km/0.9 condition produced a minimum fan surge margin of 0.137 which exceeded the CCD1103-1.0 value of 0.126.

In general, the results of the steady-state evaluation of the multivariable control indicated that the control logic and its implementation did satisfy most of the control requirements. Engine limits were maintained throughout the flight envelope. The uncertainties associated with the simulation calculation of net thrust and surge margins made it difficult to make a quantitative assessment of those aspects of the control performance. It appears that those instances where thrust and surge margin requirements were not satisfied do not warrant changes to the control design.

The reference point schedules appeared to accurately represent the engine simulation at subsonic flight conditions. In spite of differences between the hybrid and CCD1103-1.0 simulations, the control provided good steady-state regulation of the operating point; thus, the control should be able to accommodate expected engine-to-engine variations.

Although thrust requirements were specified only at low altitude, low Mach number conditions, it appears that some modifications to the reference point scheduled might be required to match CCD1103-1.0 values of thrust at supersonic flight conditions. Those modifications would probably eliminate the trim saturations observed at three of the supersonic flight conditions.

Power Lever Transients

The transient response characteristics of the F100 real-time simulation under multivariable control were investigated at those flight conditions where part-power settings were permitted. Those conditions are listed in table V. The transients included small and large amplitude PLA snaps and cyclic movements of the power lever. For all but the cyclic movements, the PLA was ramped at a constant rate of $\pm 126^{o}$ per second to match the altitude facility rate limit. As described in preceding sections, the engine and control variables were sampled by the SEL810B computer and the resulting data were stored on disks for later processing.

Figures 36 to 45 contain plots of selected transient data. Figures 36 and 37 show the responses of engine and internal control variables, respectively, to a power lever snap from 30 percent thrust (PLA = 35^{o}) to intermediate thrust (PLA = 83^{o}) at the 3.048 km/0.9 condition. The corresponding deceleration is also shown. Figures 36(b)

to (f) show the responses of the five control variables. As shown in figure 36(b), the fuel flow was not constrained by the acceleration schedule for this transient. As the intermediate thrust was approached, a dip in the fuel flow was observed. This was followed by a slow increase to its final value. This behavior was attributed to the switch from the untrimmed, regulator control mode to the integral trim mode as the steady-state condition was approached. Figure 36(f) indicates that the compressor discharge bleed was utilized during the deceleration. A peak outflow bleed of 1.09 kilograms per second was observed. This represented about 1.7 percent of the compressor inlet airflow. Figures 36(g) to (o) show the resultant responses of selected engine variables. As shown in figures 36(g) and (h), the fan and compressor rotor speed responses exhibited no overshoot during the acceleration and only a slight compressor overshoot during the deceleration. Figures 36(i) to (l) show that the burner pressure, FTIT, afterburner pressure, and net thrust exhibited the same characteristics as the fuel flow response. The responses of the FTIT sensor and estimator are also shown in figure 36(j). At the 30 percent thrust condition, the estimator matched the sensor output. During the acceleration, the estimator led the actual temperature response and exceeded the FTIT limit by 40 kelvins, 0.5 second after the initiation of the transient. This resulted in downtrimming the fuel flow and the subsequent limiting of the FTIT peak value. Figure 36(l) shows that no thrust overshoots were observed during the acceleration and deceleration. The response time (time to achieve 90 percent of the thrust increase) of 2.1 seconds was acceptable. Figures 36(m) and (n) show the responses of the fan and compressor surge margins, respectively. No loss of fan surge margin was observed during the acceleration. A minimum value of 0.15 was observed for the compressor surge margin during the deceleration. This did not violate the 0.05 minimum requirement. Figure 36(o) shows the response of the fan discharge $\Delta P/P$ parameter. In steady-state, this parameter was maintained at its scheduled value by the trim integrators. During the acceleration, a maximum deviation of 0.013 was observed while the trim integrators were clamped. A smaller deviation of 0.007 was observed during the deceleration.

While the data presented in figure 36 provide a measure of the multivariable control performance, it was desirable to monitor internal control variables to verify the control logic. Figure 37 shows plots of LQR outputs, integral trims, and state deviations for the same 3.048 km/0.9 transient shown in figure 36. Figures 37(b) and (c) show the responses of the LQR and integral control outputs of fuel flow, respectively. During the initial portion of the acceleration, the negative fan speed error (relative to the scheduled value) would have produced a fuel flow uptrim by means of the integrator. The multivariable control logic, however, clamped the integrator during this portion of the transient as shown in figure 37(c). The LQR did, however, uptrim the fuel flow to reduce the state deviations as shown in figure 37(b). About 0.5 second after the initiation of the transient, the high FTIT estimator output caused the fuel flow integrator to be

released to produce a fuel flow downtrim. The decreasing state deviations and the integral downtrim of fuel flow resulted in a reduction in the LQR output. At about the 1.5-second mark, the falling FTIT estimator output caused the fuel flow integrator to switch to fan speed control. At the initiation of the deceleration, the estimator output had not risen to the point where control of FTIT would have been restored at the intermediate thrust condition. At the beginning of the deceleration, the fuel flow integrator was again clamped since the positive fan speed error would have increased the amount of downtrim. At the 11.4-second mark, integral control of fan speed was restored. Figures 37(d) and (e) show the responses of the LQR and integral control outputs of nozzle area, respectively. During the initial portion of the acceleration, the trim integrator was allowed to uptrim to match the scheduled value of the $\Delta P/P$ parameter. Once the $\Delta P/P$ parameter exceeded the scheduled value, however, the integrator was clamped. The integrator was again released at the 1.4-second mark to provide steady-state trimming of the nozzle area. The LQR output of the nozzle area acted to reduce the state deviations of the fan speed, compressor speed, and afterburner pressure.

Figures 37(f) to (i) show the LQR and integral control outputs for the fan inlet guide vanes and compressor stator vanes. For both sets of vanes, the integrators were used to maintain the steady-state vane positions on their nominal schedules. In both cases, less than 1.0° of trim was required. The CIVV integrator was clamped at the 30 percent thrust condition due to the vanes being fully cambered. Similarly, the RCVV integrator was clamped at the intermediate thrust condition due to the vanes being fully axial. The LQR output of CIVV was used to reduce the state deviations of fan speed and afterburner pressure. Nearly 6.0° of downtrim (toward cambered) was used during the acceleration and 4.0° of uptrim (toward axial) during the deceleration. The LQR output of RCVV was used to reduce the state deviations of fan speed, compressor speed, and afterburner pressure. In this case, nearly 3.0° of downtrim were required during both the acceleration and deceleration.

Figures 37(j) and (k) show the LQR and integral control outputs of the bleed flow. The bleed flow integrator was used to close the bleed valve in steady state. For the entire acceleration and steady-state running at intermediate thrust, the negative LQR output (positive corresponds to outflow) caused the bleed flow integrator to be clamped. Only after the deceleration had reached steady state at the 11.4-second mark was the integrator released to balance the LQR output. The LQR output was used to reduce the state deviations of burner pressure, fan speed, and compressor speed. Figures 37(l) to (p) show the resulting state deviations. The fuel flow deviation shown in figure 37(p) is indicative of the slow increase to the final thrust that was shown in figure 36(l).

The preceding transient test demonstrated the ability of the multivariable to accelerate the F100 engine simulation to intermediate thrust while preventing a turbine overtemperature. The results shown in figures 36 and 37 indicated that the associated control logic performed as intended. However, another limit which must not be violated is

the minimum burner pressure limit. This limit is a factor at high altitude, low Mach number conditions. To demonstrate the multivariable control's ability to maintain suitable levels of burner pressure, the simulation was run at the 13.72 km/0.9 condition. The PLA was ramped from 30° to 83° and back to 30° after 10 seconds. At the 30° setting, it had been demonstrated that the control uptrimmed the PLAM to 38.1° to maintain the burner pressure at 33.09 newtons per square centimeter (see fig. 32(c)). The transient test was intended to show that the limit would not be violated during the rapid deceleration to idle power. Figure 38 shows the results of that test. Figure 38(b) shows that the acceleration schedule of fuel flow was, again, not a factor. Also, a slight dip in the fuel flow response was again observed. The nozzle area opened up to about 0.32 square meter during the acceleration as shown in figure 38(c). At this flight condition, both the CIVV and RCVV went fully axial at the intermediate thrust condition as shown in figures 38(d) and (e), respectively. It should be noted that the RCVV schedule was extended to permit actuator commands of 6.0° to overcome vane linkage hysteresis as indicated in table VI. Figure 38(f) shows that about 0.5 kilogram per second of bleed flow was utilized during the deceleration. This represented about 3 percent of the compressor inlet airflow. Figures 38(g) and (h) show a slight fan speed overshoot during the acceleration and a slight compressor speed overshoot during the deceleration, respectively. The burner pressure limit was maintained during the deceleration as shown in figure 38(i). A minimum burner pressure of 32.4 newtons per square centimeter was observed. The dead-band on the burner pressure error driving the fuel flow integrator was ± 0.69 newton per square centimeter. Figures 38(b) and (i) show that the fuel flow was rapidly uptrimmed once the minimum burner pressure limit was reached. Figure 38(j) shows that the FTIT limit was not reached during this test. The estimator output matched the actual temperature quite well at the idle condition and during the acceleration. However, the estimator output was observed to differ from the actual temperature after the deceleration. Similar behavior was observed for the 3.048 km/0.9 transient as shown in figure 36(j). This was not considered a serious problem, however, since the estimator did not perform a control function at the low power settings.

The corresponding thrust response is shown in figure 38(k). Ninety percent of the thrust increase was achieved in 2.0 seconds with a slow increase to the final thrust caused by the dip in fuel flow at the 3.0-second mark. A thrust overshoot was observed during the deceleration and was attributed to the fuel flow uptrim at the low burner pressure condition.

No loss of fan surge margin was observed during the acceleration as shown in figure 38(ℓ). An acceptable value of 0.155 was observed during the deceleration. During the acceleration, the compressor surge margin dropped to 0.055 as shown in figure 38(m). This was slightly lower than the 0.075 value observed during hybrid testing of the BOM logic but still larger than the 0.05 minimum requirement.

Transient tests were also run at sea-level/static, sea-level/1.2, and 3.048/1.2

flight conditions with commanded thrust changes larger than 60 percent. In general, the multivariable control produced transient behavior similar to that shown in figures 36 to 38. Table VII summarizes the results of the gross transient tests. The multivariable control satisfied the sea-level/static thrust response requirement and produced comparable response times at the other flight conditions.

In addition to the gross transients, a number of other power lever transients were run to ensure that the multivariable control logic and implementation worked properly. These tests included PLA "bodie" movements, medium and small amplitude perturbations of the PLA, and cyclic PLA movements designed to confuse the control logic.

Figure 39 shows the results of a power lever bodie between the intermediate and 40 percent thrust settings at the 13.72 km/0.9 condition. Figure 39 shows that the controlled engine response tracked the PLA movement quite well. No appreciable speed overshoots were observed as shown in figures 39(g) and (h). The FTIT estimator output, shown in figure 39(i), was observed to peak and remain below the actual temperature. This prevented downtrim of fuel flow during acceleration and resulted in the observed overshoot in FTIT. The FTIT limit was not reached, however, and the overshoot was not considered a serious problem. The thrust responded well to the PLA movement with no overshoots as shown in figure 39(j). There appeared to be about a 0.4-second lag in the response. Figures 39(k) and (*l*) show that the fan and compressor surge margins did not fall below the minimum requirements for this transient. PLA bodies were also run at other flight conditions as indicated in table V. The results of those tests were judged to be satisfactory. In general, the engine simulation responded well and tracked the PLA movement accurately with no overshoots in speeds, temperatures, thrust, etc., at those conditions.

Various medium amplitude movements of the PLA were run to test the LQR and integral control gain scheduling algorithm at selected flight conditions. In general, the gain switching was smooth and the resulting responses were judged satisfactory. However, an oscillatory response was observed for an acceleration from PLA = 50° to PLA = 70° at the 3.048 km/0.9 condition. Figure 40 shows the results from that transient. Figures 40(b) and (c) show the responses of fuel flow and compressor speed, respectively. It appeared that the LQR gains relating the compressor speed deviation to fuel flow may have been too high at this condition, which was not one of the LQR design points. This problem should be investigated and eliminated prior to engine testing of the multivariable control. Figure 40(d) shows the corresponding response of thrust. Ninety percent of the thrust change was achieved in 0.9 second. Both the fan and compressor surge margins were maintained at safe levels for this transient.

To test the small perturbation response characteristics of the multivariable control, $\pm 3^{\circ}$ PLA snaps were run at several flight conditions as indicated in table V. Prior to making the control modifications listed in table VI, data were obtained at sea-level/static, 3.048 km/0.6, and 9.144 km/0.9 flight conditions. Those results indicated that

the small perturbation response characteristics were, in general, satisfactory. Response times ranged from 0.5 second (at high altitude/high power conditions) to 2.0 seconds (at sea-level/static-idle power). However, an underdamped thrust response characteristic was observed in the 52° to 55° PLA range for all three flight conditions. The gain scheduling breakpoints were subsequently modified. Small perturbation tests were then conducted at the 3.048 km/0.9, 13.72 km/0.9, sea-level/1.2, and 3.048 km/1.2 conditions. Results from those tests indicated that the underdamped thrust response characteristics had been corrected. Response times ranged from 0.4 to 1.0 second for these conditions. These response times were judged acceptable relative to the small perturbation response requirement of 1.2 seconds. The small perturbation response times are summarized in table VII.

Figure 41 shows results from the 80° to 83° PLA snap at the 3.048 km/0.9 condition. A slight fan speed overshoot was observed as shown in figure 41(b). The FTIT estimator peak provided fuel flow downtrim and limited the FTIT as shown in figure 41(d). The 9° overtemperature was judged acceptable relative to the allowable 27.8° overtemperature for 0.5 second. The thrust response is shown in figure 41(e). Ninety percent of the thrust increase was achieved in 0.5 second.

Figure 42 shows similar results for the 3.048 km/1.2 condition. Figures 42(b) and (c) show about 30 rpm overshoots in both rotor speeds. The FTIT estimator peak exceeded the gas temperature by 27.8 kelvins and the limit by 16.7 kelvins as shown in figure 42(d). This caused a premature downtrim of fuel flow and a resulting dip in the thrust response as shown in figure 42(e). Ninety percent of the final thrust change was achieved in 0.6 second, prior to the dip in thrust.

Cyclic power lever movements were established by Pratt & Whitney (ref. 9) and used in their preliminary evaluation of the multivariable control logic. This type of test was run to ensure that the control logic could not be fooled by cyclic operation around a gain switching point. Three such maneuvers were selected for the hybrid evaluation and programmed on an analog function generators. The cyclic PLA tests were conducted at the flight conditions listed in table V. Figure 43 shows a typical result from that investigation. The PLA movement shown in figure 43(a) was run at the 13.72 km/0.9 condition. Figures 43(b) to (f) show the resulting engine responses. Figure 43(d) shows that the thrust tracked the PLA movement quite well with little phase lag. The fan and compressor surge margins were maintained at safe levels as shown in figures 43(e) and (f), respectively. Similar results were obtained at the other flight conditions.

Control Flexibility - Fast Acceleration Design

The results of Pratt & Whitney's preliminary evaluation of the multivariable control logic (ref. 9) indicated that the potential existed for achieving faster thrust response.

The previously discussed results from the hybrid evaluation also indicated this fact. While fast thrust response was not a specific objective of the MVCS program, it was felt that achieving faster response through a straightforward design iteration without changing the structure of the control would demonstrate the flexibility of the design approach and resulting implementation.

The Systems Control Inc. approach to achieving faster response with the multivariable control was to redesign the transition control rate limits. These rate limits define the transient model which the regulator attempts to follow. For the hybrid evaluation, the redesign was accomplished at sea-level/static conditions. The resulting rates were implemented in the SEL810B computer and were evaluated for PLA snaps from the idle to the intermediate thrust setting and from the 30 percent to the intermediate thrust setting. The resulting transient data were compared with the corresponding results obtained with the normal rate limits. Figure 44 shows the results of that comparison for the 30 percent to intermediate thrust transient. Figure 44(b) shows that the fast-acceleration rates resulted in the fuel flow approaching the acceleration limit (fig. 17) during the acceleration. The resulting responses of fan speed, compressor speed, FTIT, and thrust are shown in figures 44(c) to (f), respectively. No overshoots were observed during the acceleration and only slightly more overshoot was observed during the deceleration with the fast-acceleration rates. The FTIT estimator output caused fuel flow downtrim at the 0.6-second mark resulting in the dip in the FTIT response shown in figure 44(c). The faster thrust response, shown in figure 44(f), exhibited a 1.4-second response time as compared with the normal response time of 2.2 seconds. The faster thrust response was achieved with little or no loss in fan or compressor surge margin as shown in figures 44(g) and (h), respectively.

Similar results were obtained for the PLA snap from the idle to the intermediate thrust setting. A reduction in the response time from 3.2 to 2.2 seconds was achieved with a loss of 0.012 in fan surge margin and a loss of 0.07 in compressor surge margin.

Afterburner Ignition Tolerance

Although LQR control of afterburner fuel flow was not a part of the multivariable control task, the control requirements dictated that the control be tolerant of external disturbances such as afterburner ignition pulses. Figure 10 specified the maximum allowable amplitudes of afterburner pressure pulses. These values were based on BOM control results for which the exhaust nozzle is opened in anticipation of the afterburner ignition. It was hoped that the LQR would provide sufficient regulation based on the sensed afterburner pressure deviations.

Afterburner ignitions were simulated by a step-wise increase in the afterburner fuel flow. The amount of injected fuel was based on the current afterburner schedule and the

intermediate value of burner pressure for the flight condition being studied. Figure 45 shows the engine and control variable responses at the 13.72 km/0.9 condition. Figures 45(b) to (d) show the resultant deviations in fan speed, compressor speed, and afterburner pressure, respectively. The amplitude of the afterburner pressure spike was approximately 7.2 percent of the intermediate pressure. This was about 2 percent higher than the desired amplitude. Figures 45(e) and (f) show that losses of 0.065 in fan surge margin and 0.035 in compressor surge margin were observed. Figures 45(b) and (g) show the result of the integral control action which attempts to maintain the fan speed and the fan discharge $\Delta P/P$ parameter at their scheduled values. While one would expect the suppression of the pressure spikes to be accomplished by opening the nozzle area, the LQR, in fact, opened the nozzle only slightly (see fig. 45(h)) while moving the fan inlet guide vanes 2^{o} cambered. Figure 46 shows the results of the afterburner ignition tests at all of the evaluated flight conditions. These results indicated that the LQR design, without anticipatory nozzle opening, did provide pressure spike suppression. It appears that incorporating an extended nozzle area schedule and the necessary prefill logic for the afterburner fuel manifolds would be compatible with the multivariable control logic. The LQR action would, in that case, supplement the nozzle schedule in suppressing the pressure spikes.

Sensor Failure Accommodation

Although sensor failure accommodation was not a requirement for the multivariable control design, hybrid tests were conducted to identify critical sensors in order that appropriate software provisions could be made prior to full-scale engine tests. Various modes of sensor failure were studied at the 9.144 km/0.9 condition and an intermediate thrust setting. Both full-scale (saturation) and sensor loss tests were conducted. The results of the failure study are summarized in table VIII. The control structure with its engine protection logic proved adequate for most failures. Two critical failures were identified, however. They were saturation of the fan inlet total pressure (P_2) sensor and the loss of the fan speed sensor. Figure 47 shows the effects of the P_2 sensor saturation. The high P_2 signal resulted in a sudden increase in the scheduled values of fuel flow, burner pressure, and afterburner pressure. The feed-forward path for the scheduled control values drove the fuel flow command up as shown in figure 47(b). The 680 kilograms per hour downtrim limit on the fuel flow integrator prevented it from limiting the fan speed which exceeded its limit at about the 9.5-second mark as shown in figure 47(c). Similarly, the compressor speed exceeded its limit at about the 8.5-second mark as shown in figure 47(d). The FTIT estimator is dependent on having an accurate schedule of FTIT. The FTIT schedule is, however, a function of the sensed fan inlet air density. The high P_2 signal caused an erroneous estimator output as

shown in figure 47(e). In spite of the overtemperature at the 1.4-second mark, no downtrim of fuel flow was requested. Facility shutdown logic, based on the sensed FTIT, would not be active until 4.5 seconds after the sensor failure due to the slow sensor dynamics, thus pointing out the need for some form of P_2 sensor failure detection logic. Figures 47(f) through (h) show the corresponding thrust and surge margin responses. The loss of fan surge margin also indicates the necessity of some form on detection and accommodation logic for the P_2 sensor. The P_2 sensor saturation test was subsequently repeated with the downtrim limit removed from the fuel flow integrator. Nearly 2700 kilograms per hour of downtrim was requested but could not prevent the overtemperature and fan overspeed from occurring. The compressor speed was maintained within limits, however.

The loss of the fan speed sensor resulted in increased fuel flow and nozzle area trims from the regulator. The fuel flow integrator was also driven to its uptrim limit by the false fan speed deviation. This resulted in an overtemperature at the 0.2-second mark, a fan overspeed at the 0.28-second mark, and a compressor overspeed at the 0.57-second mark. Based on these results, it is clear that detection and accommodation logic are required for the fan speed sensor also.

Flight Condition Transition

The results from the previously described tests indicated that the multivariable control would provide satisfactory regulation at each of the evaluated flight conditions. However, it was noted that the FTIT estimator could be confused by sensor noise and/or changes in the flight condition. In changing flight conditions during the hybrid evaluation, no attempt was made to control the rates of change of the fan inlet conditions (P_2 and T_2). Therefore, a test was conducted which simulated representative aircraft accelerations and decelerations as defined in the CONTROL REQUIREMENTS section. At sea level, the flight Mach number was ramped from 0.0 to 0.6 in 32 seconds as shown in figure 48(a). This resulted in the fan inlet pressure and temperature responses shown in figures 48(b) and (c), respectively. The peak rates of change were 0.17 newton per square centimeter per second and 1.3 kelvins per second. Figures 48(d) to (f) show the resulting responses of fuel flow, FTIT, and thrust. Figure 48(d) shows that the fuel flow was not downtrimmed adequately until late in the acceleration. Although the fan and compressor speeds did not exceed their limits, the FTIT did exceed its limit by as much as 11.1 kelvins as shown in figure 48(e). The FTIT overtemperature indicated that the estimator output did not respond accurately to the FTIT sensor output and the commanded fuel flow. A slight thrust overshoot was also observed as shown in figure 48(f).

A corresponding sea-level deceleration was simulated with the Mach number ramped

from 0.6 to 0.0 in 11 seconds as shown in figure 49(a). This resulted in maximum rates of change of PT2 and TT2 of -0.59 newton per square centimeter per second and -2.8 kelvins per second as shown in figures 49(b) and (c). For this deceleration, the estimator provided adequate downtrimming of the fuel flow to maintain FTIT within limits as shown in figures 49(d) and (e). The results of the flight condition transition test point out the need to take a closer look at the estimator behavior prior to the engine tests.

SUMMARY OF RESULTS

The primary objective of the evaluation was to verify the multivariable control logic and its implementation so as to ensure safe and stable operation of the F100 engine during subsequent altitude tests. The results of the evaluation indicated that the control logic and its implementation on the SEL810B digital computer will be capable of controlling the engine throughout its operating range. The specified engine limits were not violated during normal steady-state and transient operation.

The results of the steady-state evaluation showed that the reference point schedules matched the simulation model of the engine at most operating conditions. Where discrepancies were noted, they did not affect the normal control action. An observed discrepancy in the FTIT schedule at the 19.81 km/0.9 condition, coupled with the low burner pressure at that condition, did result in an overtemperature whenever changes in the fan inlet conditions caused resetting of the FTIT estimator to the low scheduled value. A subsequent change in the FTIT estimator logic to prevent the reset action at the low burner pressure condition eliminated this problem.

The hybrid evaluation indicated that the multivariable control could accommodate the slight differences between the hybrid model and the CCD1103-1.0 simulation. While the control should be able to handle expected engine-to-engine differences, it is recommended that the reference point schedules be trimmed as soon as FSER engine data becomes available.

Simulation errors, caused by simplified thrust and surge margin calculations, did make it difficult to quantitatively evaluate the steady-state, closed-loop performance of the controls. However, previous studies involving a digital implementation of the BOM control logic and the hybrid simulation provided an opportunity to "adjust" the MVC data. The adjusted values of thrust indicated that the multivariable control matched the CCD1103-1.0 intermediate thrust values (within the specified 1 percent) at all but the supersonic flight conditions. This result is substantiated by data provided by SCI from their version of the CCD1103-1.0 simulation with FORTRAN coding of the multivariable control logic. Those data also showed low thrust values at the supersonic flight conditions. This is attributed to the fact that the supersonic flight points were not fac-

tored into the reference point schedules. It is recommended that adjustments (if possible) be made to the reference point schedules to improve the high Mach number performance.

Authority limits on the fuel flow and nozzle area trim integrators were implemented to provide protection in the event of sensor failures. It was determined, however, that the assumed limits of ±0.028 square meter and ±680.4 kilograms per hour did prevent the steady-state matching of the schedules at three supersonic flight conditions. This was caused by the aforementioned scheduling errors at the supersonic flight conditions. While no engine limits were violated due to the trim saturation, the schedules should be refined prior to the engine tests.

The proportional (LQR) plus integral control structure provided good fan operating point control over the range of engine operation. The integral control provided adequate limiting of fan speed, FTIT, and burner pressure at all flight conditions.

The LQR and transition control resulted in satisfactory transient responses at most operating conditions. The gain switching for gross transients was smooth. The break between low and high power gains was shifted to a higher power condition to eliminate underdamped behavior at low power settings. Unsatisfactory response characteristics were noted at only two conditions. Oscillatory behavior was observed during a 50^{o} to 70^{o} PLA snap at the 3.048 km/0.9 condition. This was attributed to a high regulator gain relating fuel flow to the compressor speed deviation at this condition. As described in the MULTIVARIABLE CONTROL section, the LQR gains at this condition are dependent on the gain scheduling algorithm since none of the stored LQR gain matrices were designed at this flight condition. It is recommended that this behavior be corrected prior to the engine tests. Also, an excessive FTIT estimator overshoot was observed during an 80^{o} to 83^{o} PLA snap at the 3.048 km/1.2 condition. This resulted in a premature downtrimming of fuel flow during the acceleration and a corresponding dip in the thrust response. FTIT anomalies were observed during various phases of the evaluation. In addition to the aforementioned overshoot, a slowly diminishing error between the estimator output and the actual gas temperature was observed at the conclusion of many of the transients. Although the estimator fulfilled its basic function of providing a form of anticipation of impending overtemperatures, it is recommended that the estimator design be refined prior to the engine tests so as to provide predictable behavior during transients and flight condition transitions.

The specified response requirements were satisfied for all small and large amplitude transients with the exception of the small (3^{o}) PLA snaps at the sea-level/static, idle condition. It should be noted that the 1.2-second response time requirement for small perturbations was adopted due to a lack of specificity in the requirements.

The flexibility of the control structure and the design methods was demonstrated by implementing a set of fast-acceleration rate limits in the transition control. The resulting sea-level/static acceleration from idle to intermediate thrust showed a reduction

in the response time from 3.2 to 2.2 seconds. This compared with the current BOM-controlled response time of 2.8 seconds.

Afterburner ignitions were simulated to test the multivariable control's tolerance to external disturbances. The results of those tests indicated that the LQR design did provide pressure spike suppression at all flight conditions. The LQR was observed to use both the exhaust nozzle area and the fan inlet guide vanes (CIVV) to suppress the pressure spikes.

The results of the sensor failure study of the 9.144 km/0.9 condition indicated that most sensor failures would result in a safe, downtrimming to a part-power condition. The saturation of the P_2 sensor or the loss of the fan speed sensor, however, resulted in a catastrophic overspeed and overtemperature condition. Therefore, it is recommended that some form of sensor failure detection and accommodation logic be implemented in the multivariable control if redundant sensors cannot be provided for the engine tests. It is further recommended that some form of the current acceleration schedule of $\left(\dot{W}_{F,4}/P_4\right)_{max}$ be implemented since it provides fuel flow cutback in the event of a loss of the compressor speed signal or a compressor overspeed. The results of the hybrid evaluation showed that the limiting of the reference point schedule of compressor speed is not sufficient to prevent overspeeds from occurring although normal engine operation would seem to preclude this from happening.

The results of the simulated aircraft accelerations and decelerations at sea level showed that the FTIT estimator logic could be confused by changing fan inlet conditions. This resulted in overtemperatures in some cases. Those results point out the need to take a closer look at the estimator design prior to the engine tests.

CONCLUDING REMARKS

The results of the evaluation indicate that the engine testing of the multivariable control should be conducted as planned. The multivariable control produced satisfactory performance for all but a few test conditions. With minor modifications, the control should provide acceptable steady-state and transient performance at all flight conditions and power settings.

Considering the fact that in approximately 10 months a control design for the F100 engine was accomplished, it must be concluded that the computer-aided approach to designing multivariable controls is a practical solution to the engine control problem. The results of the evaluation indicate that the Systems Control Inc. approach to solving the nonlinear control problem is also practical. The implementation of the control logic on the SEL810B digital computer has demonstrated that a practical LQR control can be implemented on a digital computer having many of the characteristics of flight-qualified computers. The core requirements (7.1 K) and update time (10 msec) are comparable

to the requirements of flight-qualified digital controls such as the IPCS control and the F100 electronic supervisory control.

Lewis Research Center,
National Aeronautics and Space Administration,
Cleveland, Ohio, June 22, 1977,
505-05.

REFERENCES

1. Beattie, Edward C.: Control Mode Studies for Advanced Variable-Geometry Turbine Engines. PWA-5161, Pratt & Whitney Aircraft. (AD-A009169), 1974.
2. Kwakernaak, Huibert; and Sivan, Raphael: Linear Optimal Control Systems, John Wiley and Sons, Inc., 1972.
3. Michael, Gerald J.; and Farrar, Florence A.: An Analytical Method for the Synthesis of Nonlinear Multivariable Feedback Control. UARL-M941338-2, United Aircraft Research Labs. (AD-762797), 1973.
4. Bowles, Robert John: Sub-Optimal Control of a Gas Turbine Engine. M.S. Thesis, Air Force Institute of Technology, Wright Patterson Air Force Base. (GE/EE/73A-1, AD-777852), 1973.
5. Michael, Gerald J.; and Farrar, Florence A.: Development of Optimal Control Modes for Advanced Technology Propulsion Systems. UARL-N911620-2, United Aircraft Research Labs. (AD-775337), 1974.
6. Stone, C. R.; et al.: Turbine Engine Control Synthesis, Vol. I. Honeywell F0164-FR-Vol-1, Systems and Research Division. (AFAPL-TR-75-14-Vol-1, AD-A014229), 1975.
7. Weinberg, Marc S.: A Multivariable Control for the F100 Engine Operating at Sea-Level Static, ASD-TR-75-28, Aeronautical Systems Division, Wright Patterson Air Force Base, 1975.
8. Szuch, John R.; and Seldner, Kurt: Real-Time Simulation of the F100-PW-100 Turbofan Engine Using the Hybrid Computer. NASA TM X-3261, 1975.
9. Miller, Ronald J.; and Hackney, Ronald D.: F100 Multivariable Control System Engine Models/Design Criteria. FR-7809, Pratt and Whitney Aircraft Group. (AFAPL-TR-76-74, AD-A033532), 1976.

10. DeHoff, Ronald L.; and Hall, W. Earl, Jr.: Multivariable Control Design Principles with Application to the F100 Turbofan Engine. Productivity; Proceedings of the 1976 Joint Automatic Control Conference, ASME, 1976, pp. 113-116.

11. DeHoff, Ronald L.; and Hall, W. Earl, Jr.: Design of a Multivariable Controller for an Advanced Turbofan Engine. Proceedings of the 1976 IEEE Conference on Decision and Control, IEEE, 1976, pp. 1002-1008.

12. Arpasi, Dale J.; Zeller, J. R.; and Batterton, Peter G.: A General Purpose Digital System for On-Line Control of Airbreathing Propulsion Systems. NASA TM X-2168, 1971.

13. Bentz, Charles E.; and Zeller, John R.: Integrated Propulsion Control System Program. SAE Paper 730359, April 1973.

TABLE I. - F100 TRANSIENT THRUST

RESPONSE TIME REQUIREMENTS

[All times for sea-level, static, standard day with no bleed flow or power extraction.]

Thrust change, percent	Power lever angle change			
	Idle to intermediate	30 Percent to intermediate	Intermediate to idle	Idle to maximum
	Time, sec			
90	4.0	3.5	3.0	8.0
98	15.0	15.0	20.0	15.0

TABLE II. - MULTIVARIABLE CONTROL COMPUTER SPECIFICATIONS

SEL810B digital computer
Two 16-bit accumulators Memory specifications: 24K magnetic core Cycle time, 0.75 μsec Expandable to 32K Two's-compliment, fixed-point multiply and divide: Add time, 1.5 μsec Multiply time, 4.5 μsec Divide time, 8.25 μsec Double precision arithmetic Infinite indirecting Infinite indexing Direct memory access 28 Levels of vectored priority interrupt 66 Total instructions
Analog acquisition unit[a]
Two multiplexors sample and hold circuits and analog to digital converters 64 Input channels for each multiplexor Input voltage range, ±10 V 12 Bit + sign data resolution (two's compliment) Digitizing rate, 50 μsec/sample Percent error with calibration, 0.073
Analog output unit[a]
26 Digital to analog conversion channels: 10 to 12 bit (plus sign) 16 to 11 bit (plus sign) Output voltage range, ±10 V Slew rate, 1 V/sec
Tektronix 4010A peripheral system[a]
Tektronix 4010 scope terminal: 1600 Baud capacity RS232 and teletype interface Paper tape reader punch Floppy disk: Store 262, 144 bytes/disk - ~660 meters of paper tape Write speed, 400 bytes/sec

[a]SEL810B peripherals.

TABLE III. - CORE REQUIREMENTS FOR

MULTIVARIABLE CONTROL

(MVC) PROGRAM

Software	Core storage, words
Block data:	
Schedules	1 226
Matrices	450
Total	1 676
MVC program:	
Main	1 305
FTIT estimator	315
Set point	547
Gain control	830
Transition control	634
Integral control	776
LQR control	332
Engine protection	202
Function generation	518
Total	5 459
General purpose input/output and debug routines:	
INFORM and DATAO and SAMPLE	3 613
Input/output drivers	674
Floating point software	519
Total	4 806
Grand total	11 941

TABLE IV. - F100 RESEARCH

SENSOR CHARACTERISTICS

Sensor	Characteristics
Fan speed	$\frac{1}{(0.03\,S + 1)}$
Compressor speed	$\frac{1}{(0.05\,S + 1)}$
Pressures	$\frac{1}{(0.05\,S + 1)}$
Fan inlet temperature	$\frac{1}{(1.5\,S + 1)}$
Fan turbine inlet temperature	$\frac{0.31}{(0.6\,S + 1)} + \frac{0.69}{(5.5\,S + 1)}$
Fan discharge temperature	$\frac{(3S + 1)(15.5\,S + 1)}{(\tau S + 1)(20S + 1)(0.6S + 1)}$ where $\tau = f(\dot{w}_{13})$

TABLE V. - F100 MULTIVARIABLE CONTROL SYNTHESIS PROGRAM-

HYBRID EVALUATION TESTS

Altitude (km) / Mach number	Steady state		Power lever angle (PLA) transients			Disturbances		Sensor failures
	PLA = 83°	PLA < 83°	Large	Small	Cyclic	After-burner	Maneuver	
0/0	•[a]	•	•	•	•	•	•[b]	
3.048/0.6	•	•	•	•	•	•	o	
3.048/0.9	•	•	•	•	•	•	o	
9.144/0.9	•	•	•	•	•	•	o	•
13.72/0.9	•	•	•	•	•	•	o	
19.81/0.9	•					•	o	
0/1.2	•	•	•	•		•	o	
3.048/1.2	•	•	•	•		•	o	
6.096/1.8	•					•	o	
22.86/1.8	•					•	o	
17.83/2.15	•					•	o	
12.19/2.2	•					•		
19.81/2.5	•					•	o	

[a]Specific test, •.

[b]Evaluated during flight condition transients between tests, o.

TABLE VI. - PREEVALUATION CONTROL MODIFICATIONS

Symptom	Remedy
Underdamped behavior at midpower for cyclic PLA inputs	Extension of gain transition region to lower gains in midpower range
Erratic FTIT estimator behavior	Dead-zone placed in estimator initialization logic
RCVV off-schedule at high-power due to actuator hysteresis	Extension of schedule at high compressor speeds
Bleed command noise	Negative bleed command bias with added downstream limits
Excessive nozzle area downtrims at 19.81 km/0.9 condition due to sensitivity to $\Delta P/P$ calculation accuracy	Authority limit placed on nozzle area trim
Anticipated problems caused by sensor failures or scheduling errors	Limits placed on fuel flow trim and trim rate

TABLE VII. - POWER LEVER ANGLE (PLA)

RESPONSE RESULTS

[Specified response time requirements in parentheses. A 1.2-sec response time requirement assumed for $\pm 3^{\circ}$ PLA changes.]

Altitude (km) / Mach number	PLA change, deg					
	20-23	30-33	52-55	80-83	Idle-83	35-83
	Thrust response times, sec					
0/0	2.0	1.4	0.8	0.7	3.2 (4.0)	2.2 (3.5)
3.048/0.6	1.2	1.0	.6	.6	---	---
3.048/0.9	1.0	1.0	.8	.5	3.0	2.1
9.144/0.9	---	.7	.5	.5	---	---
13.72/0.9	---	---	.4	.4	2.0	---
0/1.2	---	---	.6	.5	1.5	---
3.048/1.2	---	---	.75	.6	1.5	---

TABLE VIII. - RESULTS OF HARD SENSOR FAILURES ON MULTIVARIABLE CONTROL AT 9.144 km/0.9 AND PLA = 83°

Sensor	Mode	Result
MN	Loss	None
	Saturation	Slight downtrim
P_2	Loss	Downtrim to 38 percent thrust
	Saturation	Overtemperature, overspeed[a]
T_2	Loss	None
	Saturation	Downtrim to 63 percent thrust
N_1	Loss	Overtemperature, overspeed[a]
	Saturation	Downtrim to 60 percent thrust
N_2	Loss	Downtrim to 34 percent thrust
	Saturation	Downtrim to 58 percent thrust
P_4	Loss	Downtrim to idle
	Saturation	None
P_6	Loss	None
	Saturation	Downtrim to 74 percent thrust
$(\Delta P/P)_{13}$	Loss	Slight downtrim
	Saturation	None
$\dot{w}_{F,4}$	Loss	None
	Saturation	Downtrim to 68 percent thrust

[a]Catastrophic failure.

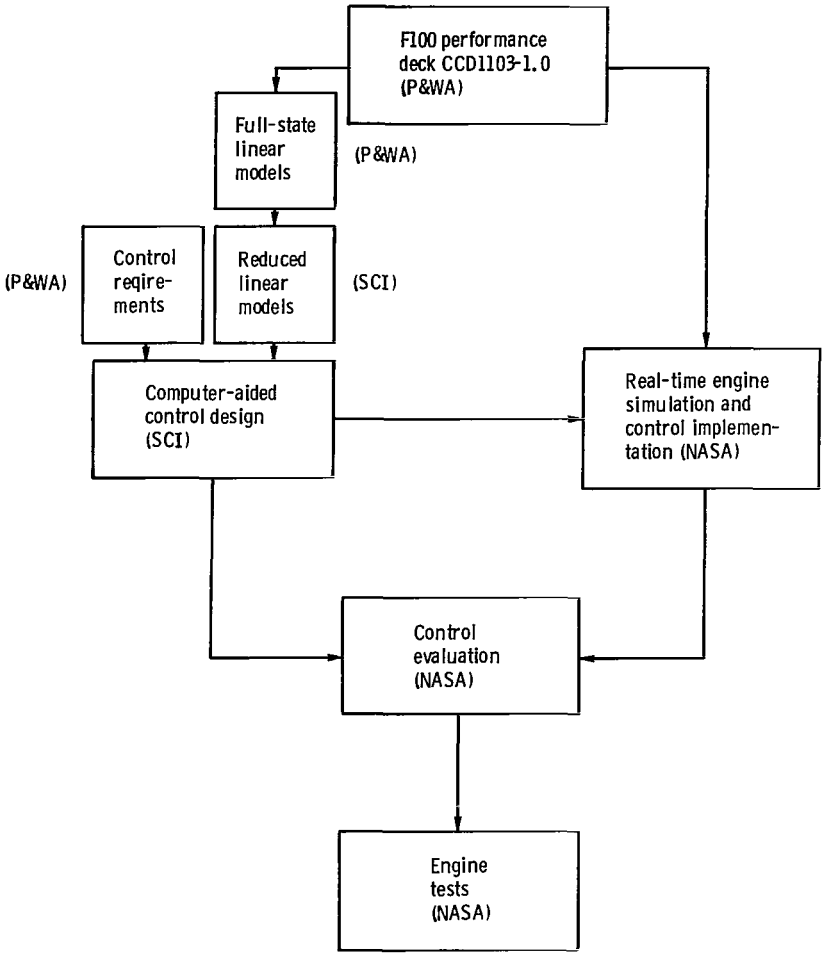

Figure 1. - Multivariable Control Synthesis program - design and evaluation process. Pratt & Whitney Aircraft, P&WA; Systems Control Inc., SCI.

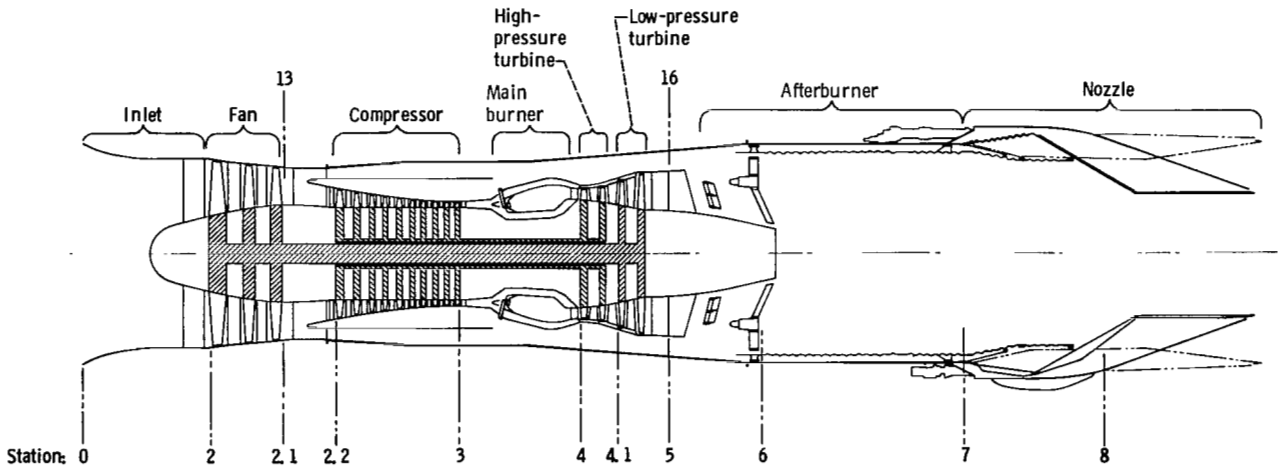

Figure 2. - Schematic representation of F100-PW-100 augmented turbofan engine.

CD-11819-07

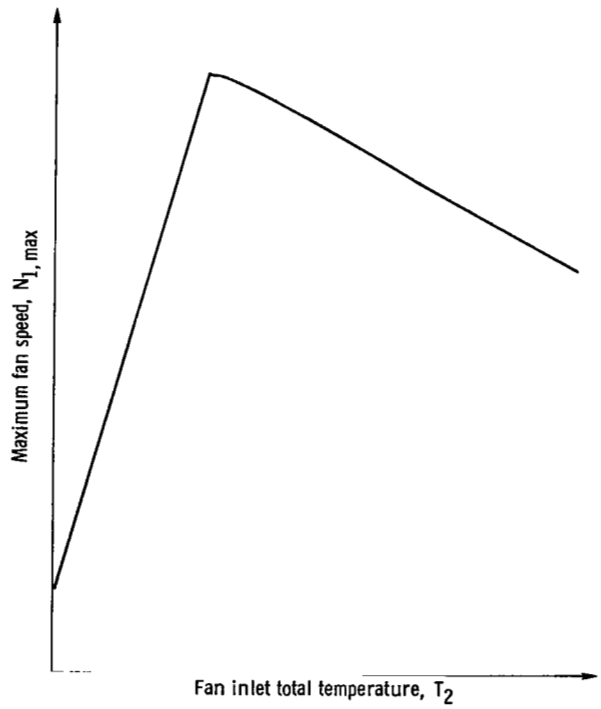

Figure 3. - Fan rotor speed limit.

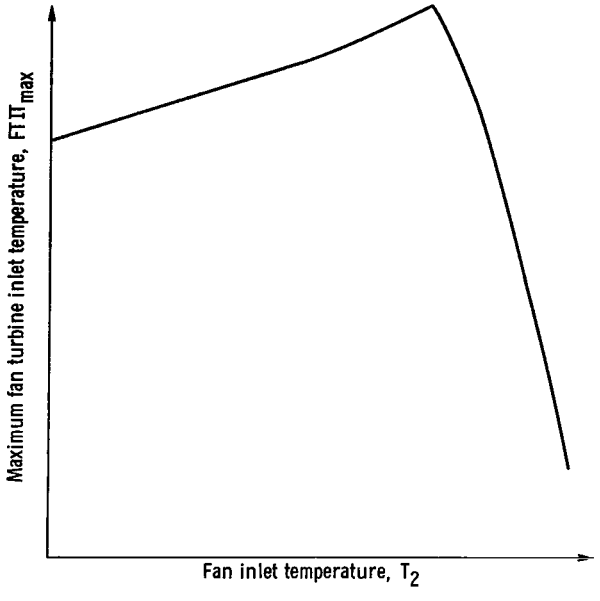

Figure 4. - Fan turbine inlet temperature limit.

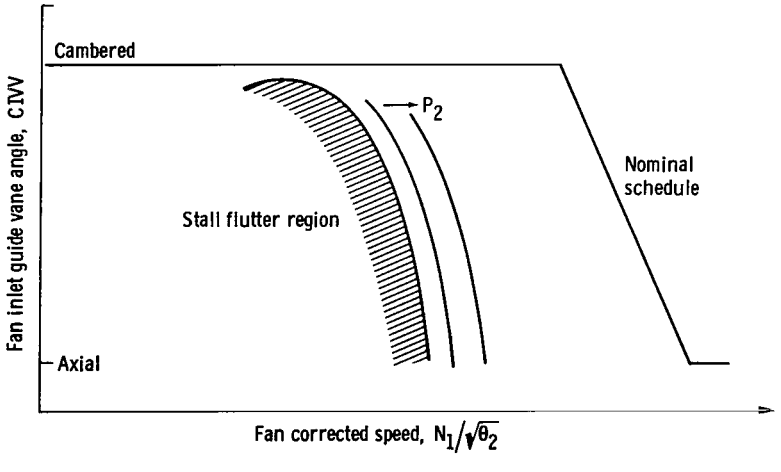

Figure 5. - Fan inlet guide vane schedule and limits.

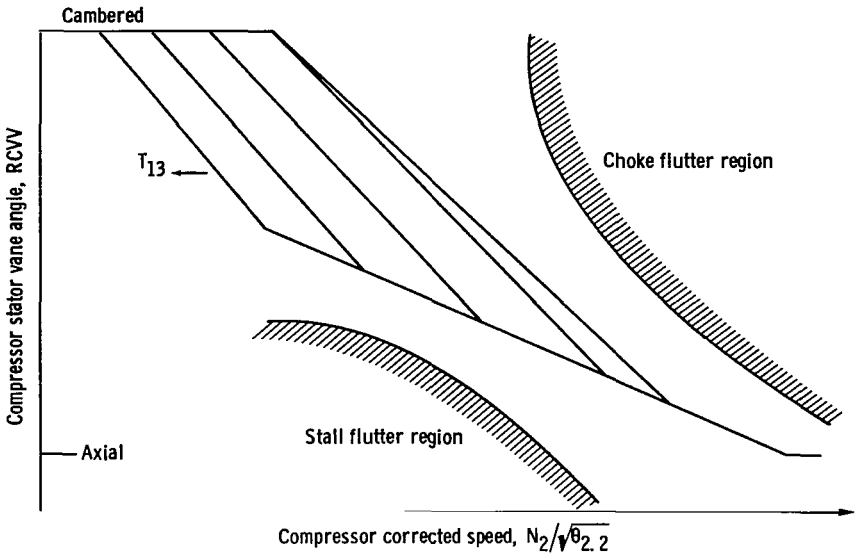

Figure 6. - Compressor stator vane schedule and limits.

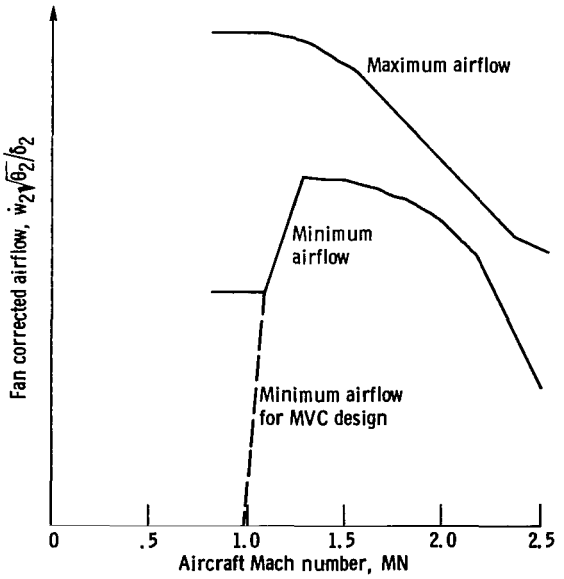

Figure 7. - Fan corrected airflow limits.

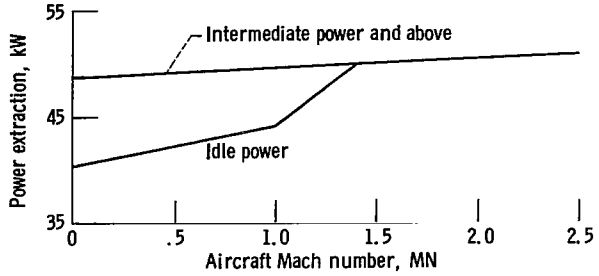

Figure 8. - Typical power extraction requirements: standard day.

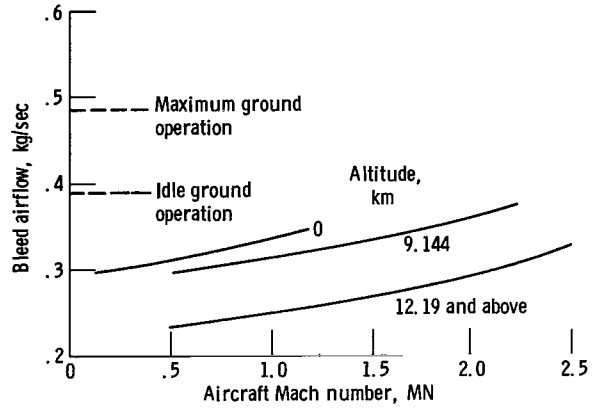

Figure 9. - Typical bleed requirements: standard day, all power settings.

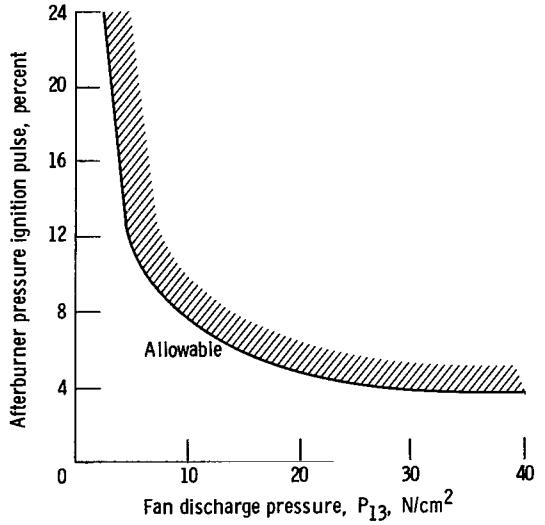

Figure 10. - Afterburner ignition pressure pulse requirements.

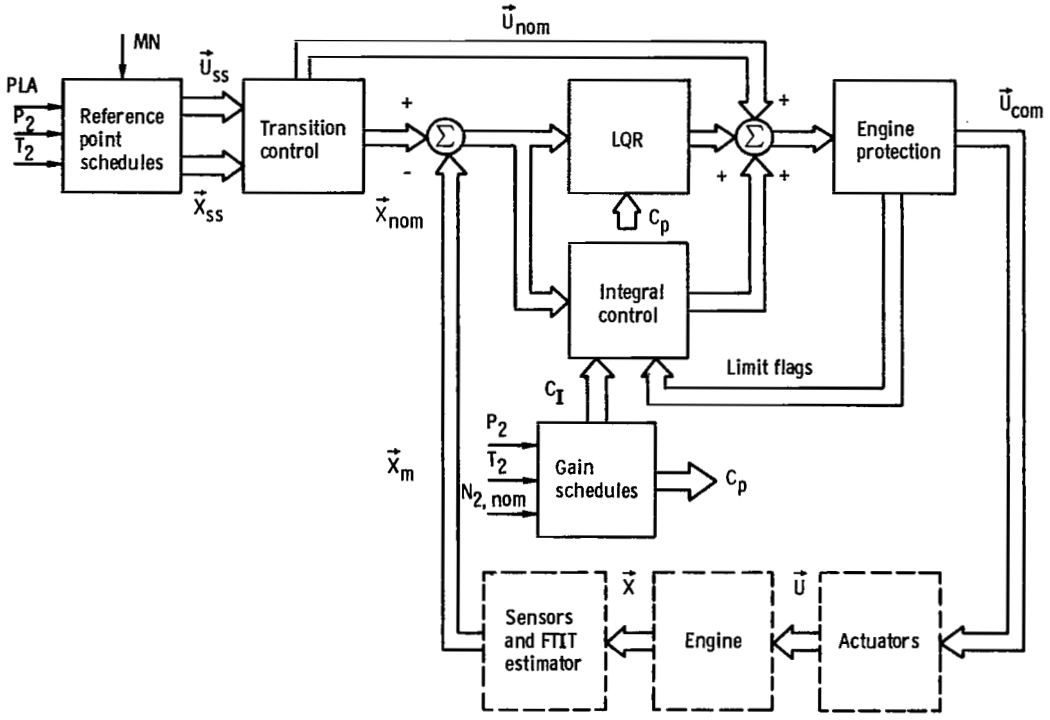

Figure 11. - F100 Multivariable Control System.

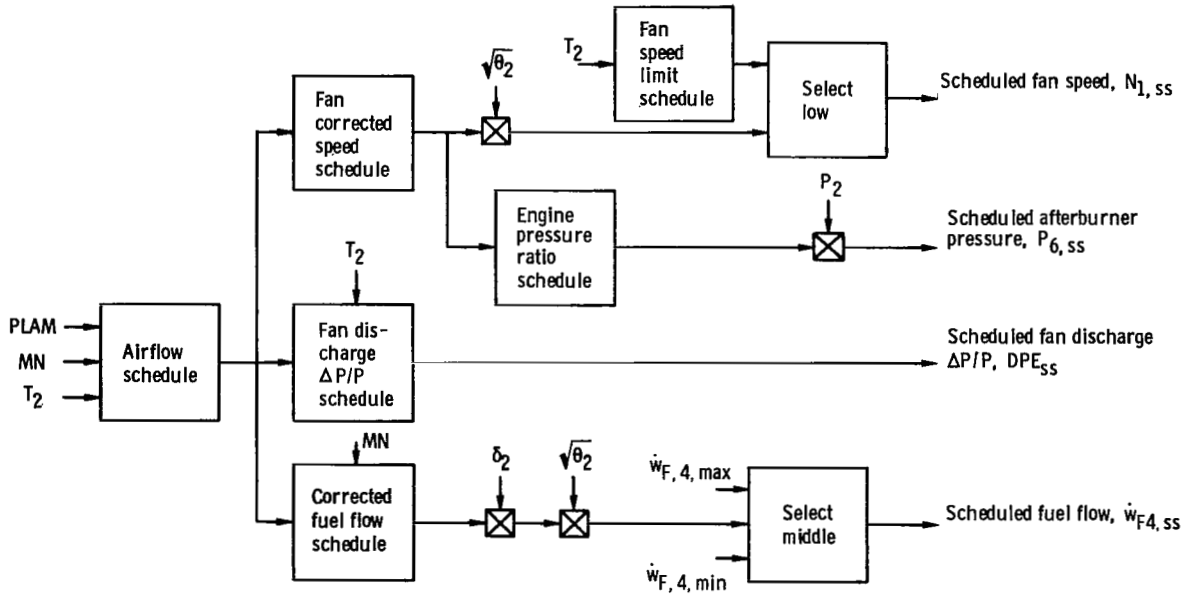

Figure 12. - Reference point scheduling algorithm.

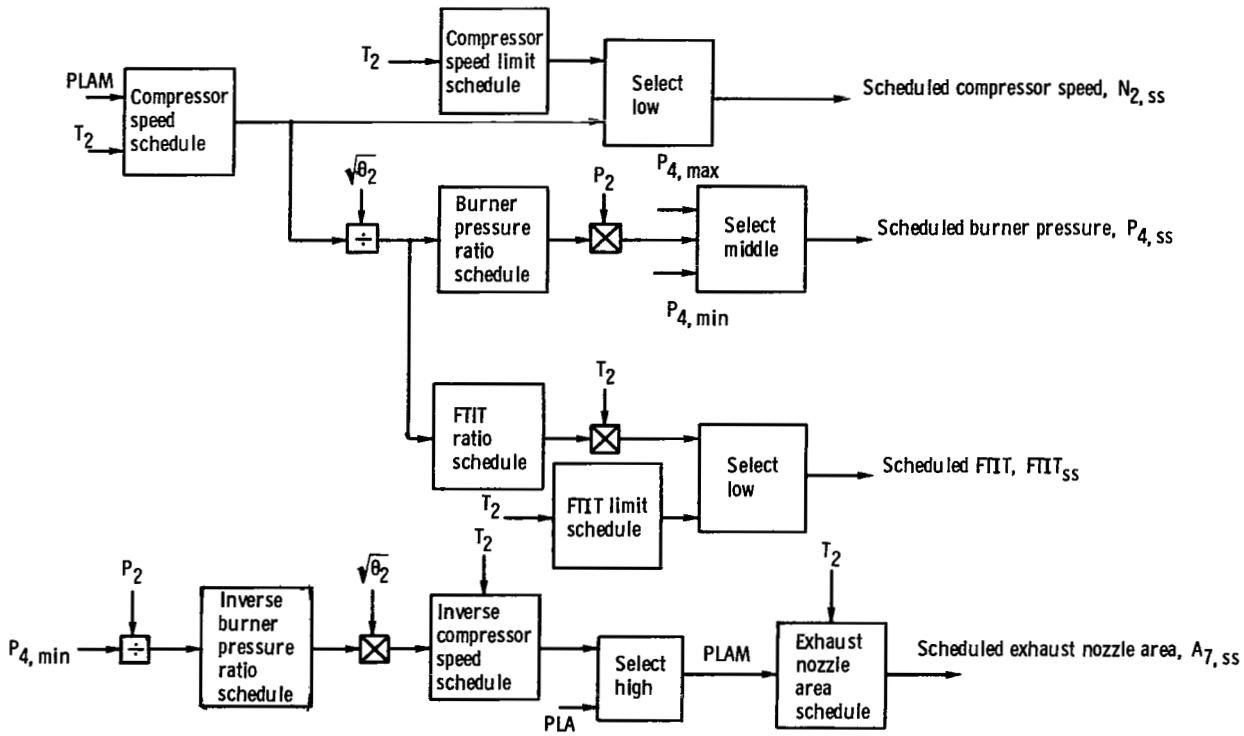

Figure 12. - Concluded.

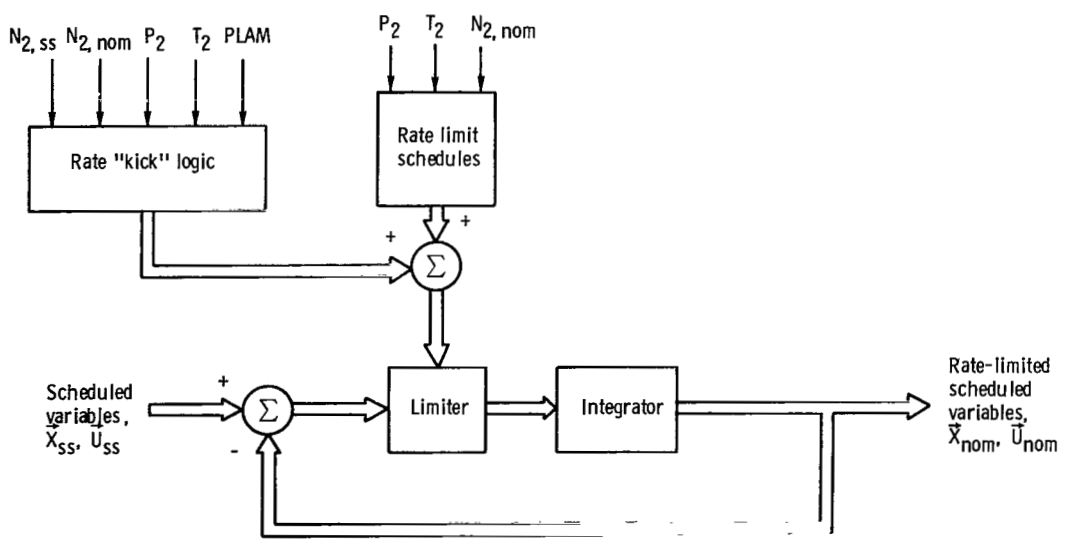

Figure 13. - Transition control algorithm.

		State deviations				
		Fan speed	Compressor speed	Afterburner pressure	Fuel flow	Burner pressure
Controls	Fuel flow	X	X	X	X	X
	Nozzle area	X	X	X	0	0
	CIVV	X	0	X	0	0
	RCVV	X	X	X	0	0
	Bleed flow	X	X	X	0	X

Figure 14. - LQR gain matrix structure.

		State deviations					Spares	Integral output deviations						
		Fan speed	Compressor speed	Afterburner pressure	Fuel flow	Burner pressure		ΔP/P parameter	CIVV	RCVV	Bleed flow	Fan speed	FTIT maximum limit	Burner pressure minimum limit	Burner pressure maximum limit
Controls	Fuel flow	X	X	X	X	X		X	0	0	0	X	X	X	X
	Nozzle area	X	X	X	0	0		X	0	0	0	X	X	X	X
	CIVV	X	0	X	0	0		X	X	0	0	X	0	0	0
	RCVV	X	X	X	0	0		0	0	X	0	0	0	0	0
	Bleed flow	X	X	0	0	X		0	0	0	X	0	0	0	0

Figure 15. - Gain matrix structure.

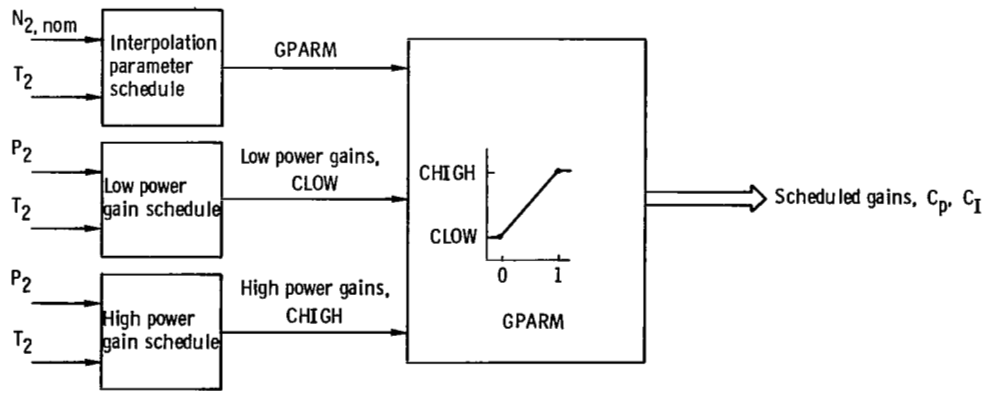

Figure 16. - Gain schedule algorithm.

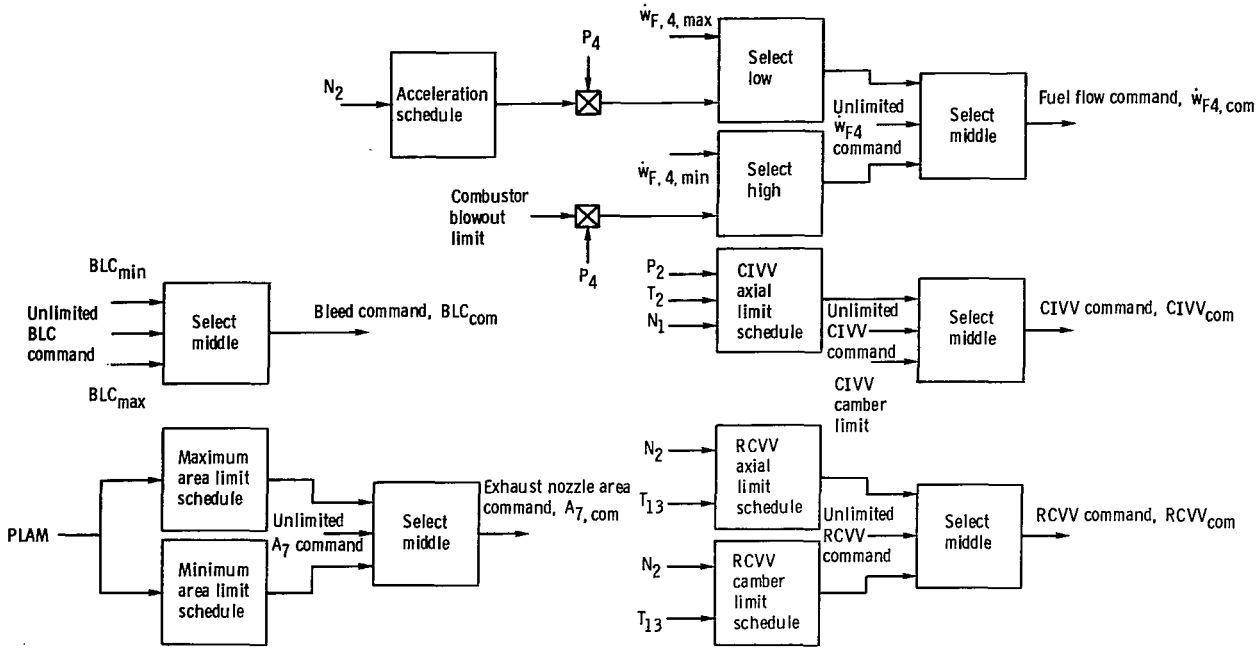

Figure 17. - Engine protection algorithm.

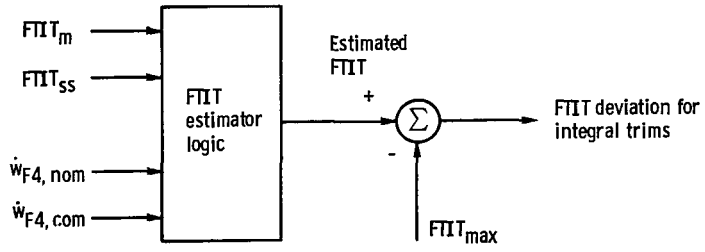

Figure 18. - Fan turbine inlet temperature estimator.

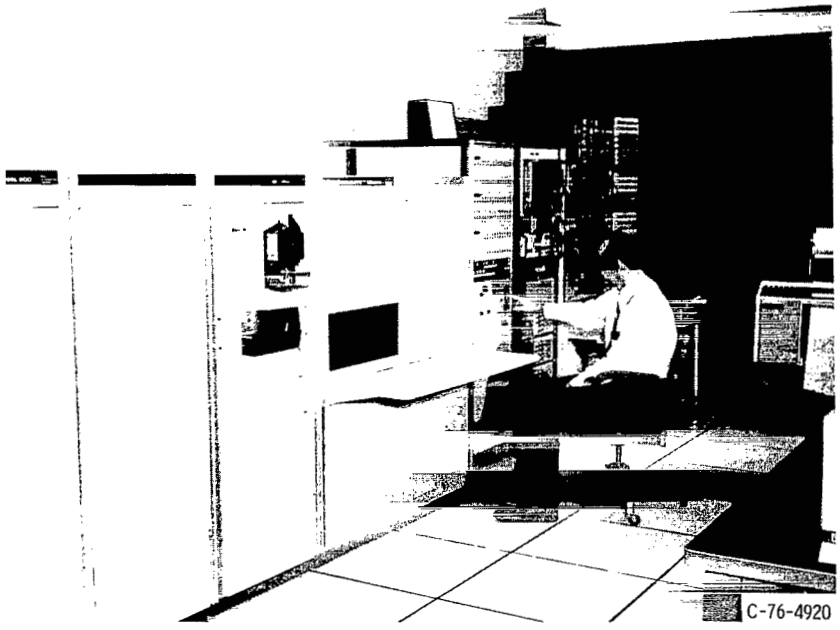

Figure 19. - NASA digital computer system used for on-line engine control.

Figure 20. - NASA digital computer system - input/output and peripheral subsystem.

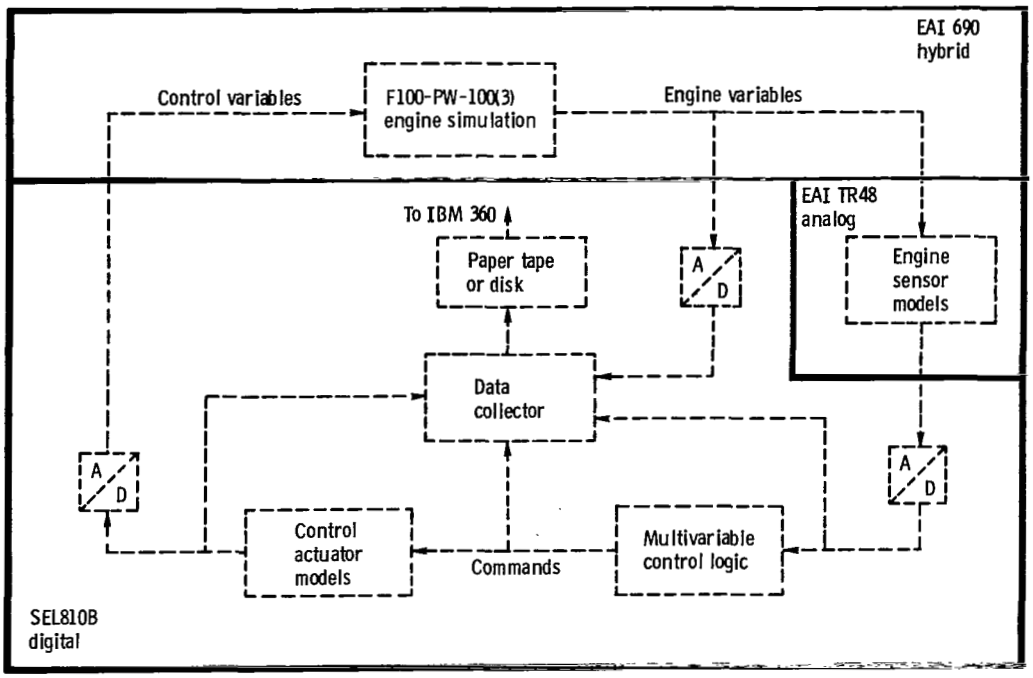

Figure 21. - Schematic representation of multivariable control evaluation.

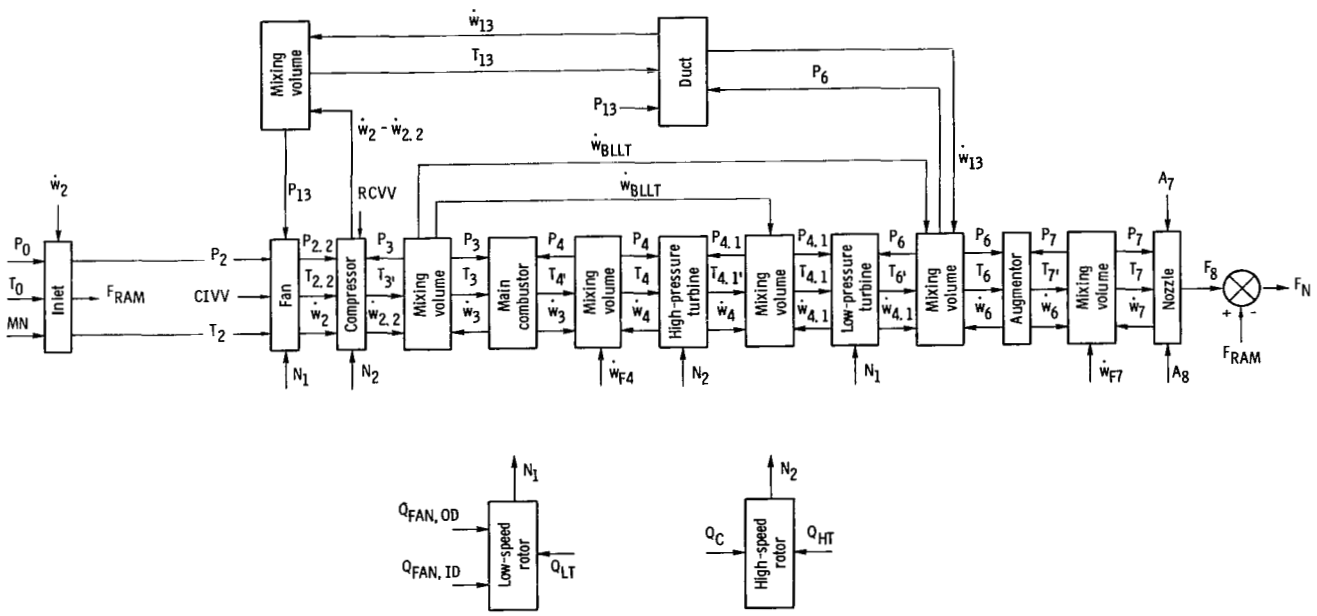

Figure 22. - Computational flow diagram of real-time turbofan engine simulation.

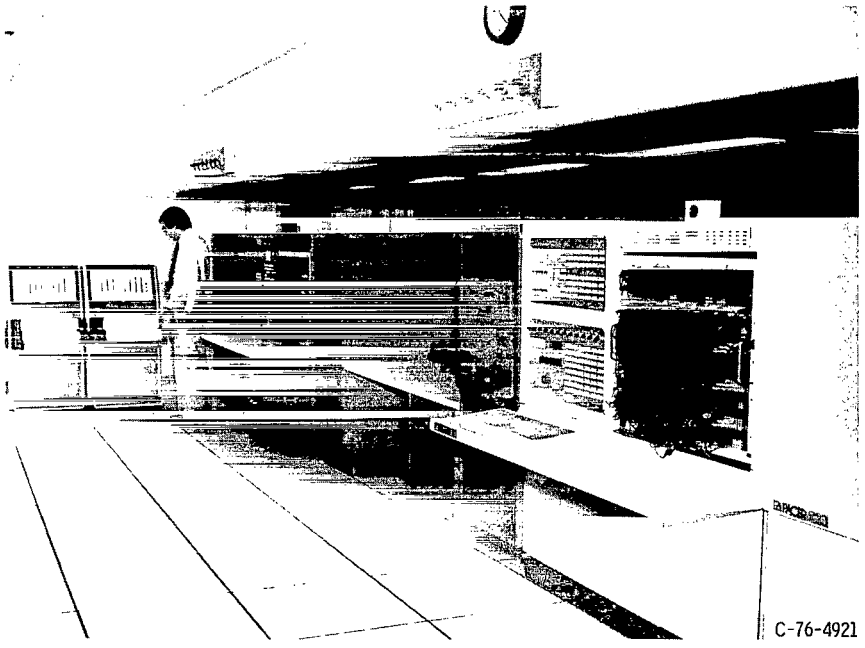

Figure 23. - NASA hybrid computing system used for real-time engine simulation.

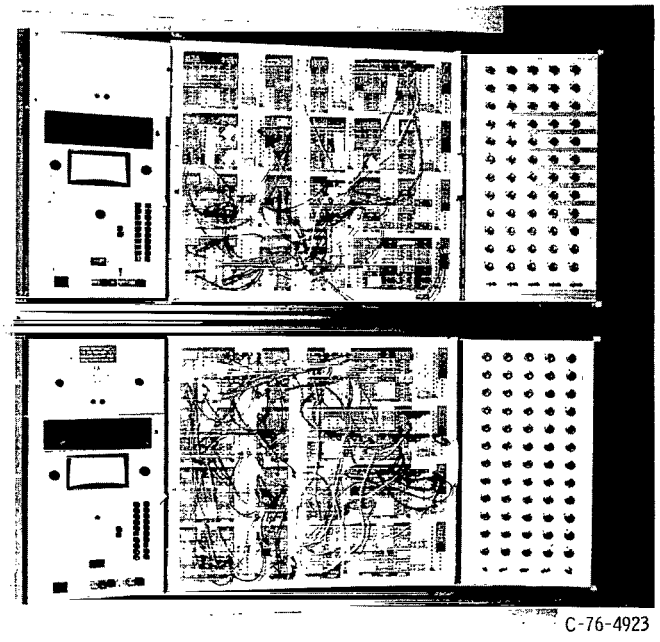

Figure 24. - NASA analog computers used for sensor simulations.

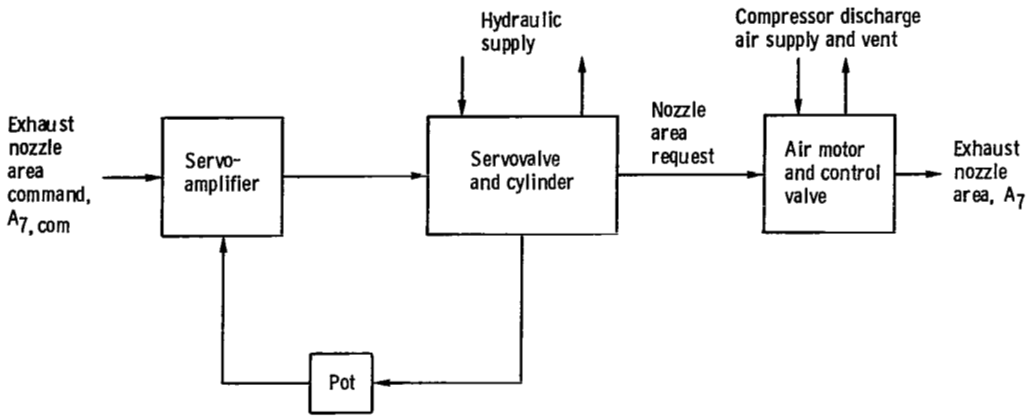

Figure 25. - Schematic representation of exhaust nozzle actuator system.

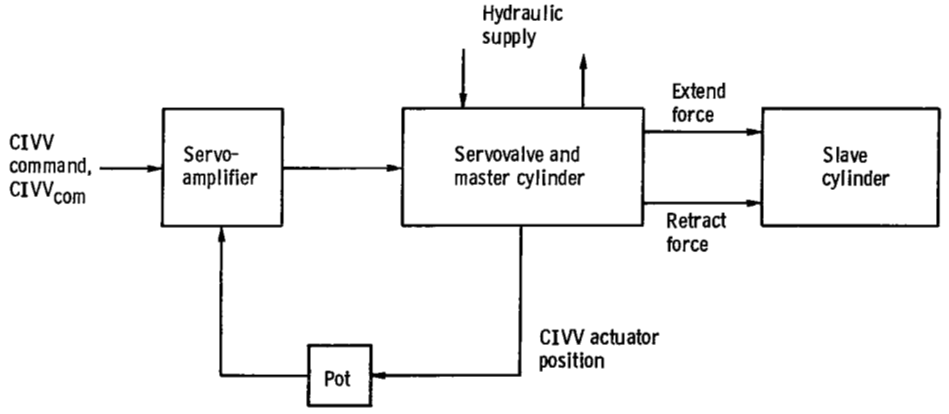

Figure 26. - Schematic representation of CIVV actuator system.

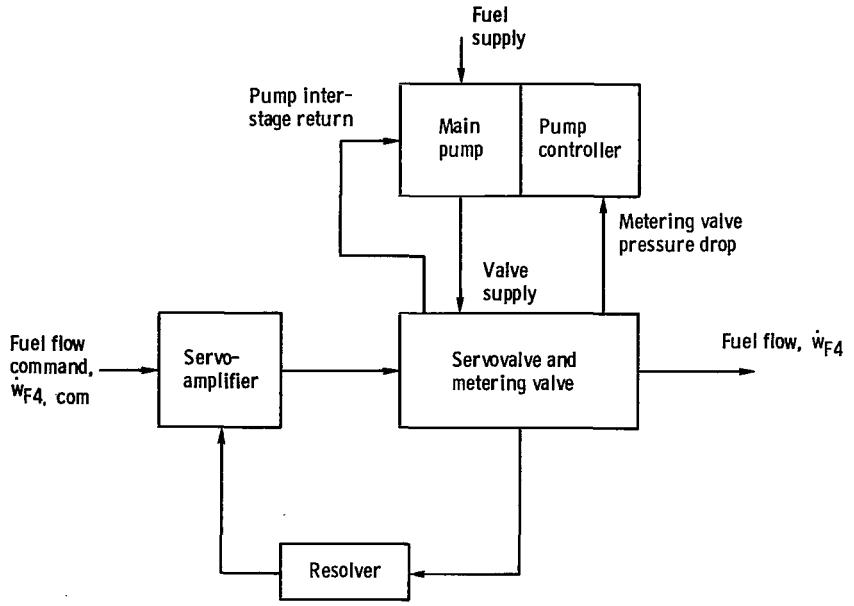

Figure 27. - Schematic representation of fuel valve actuator system.

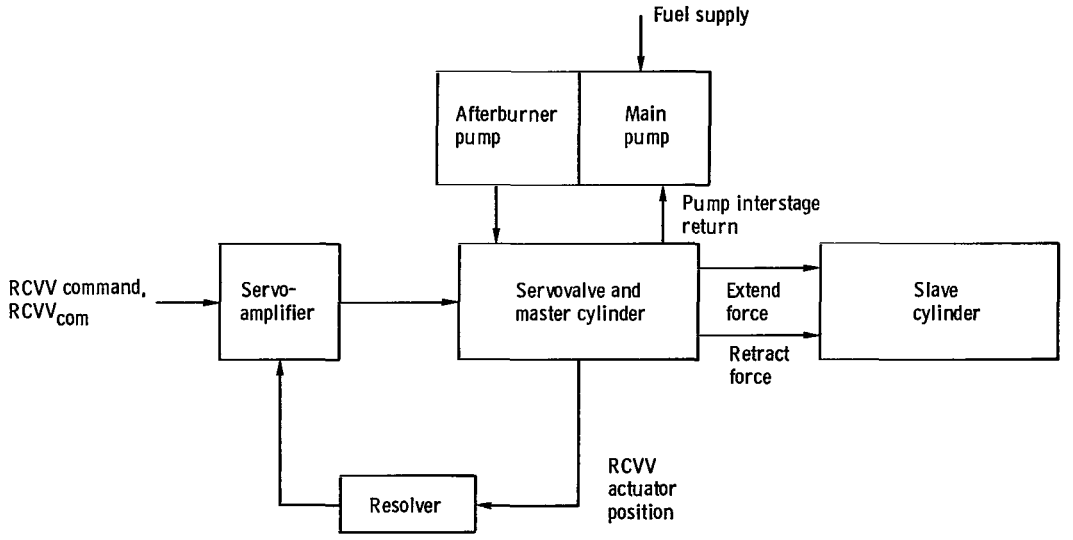

Figure 28. - Schematic representation of RCVV actuator system.

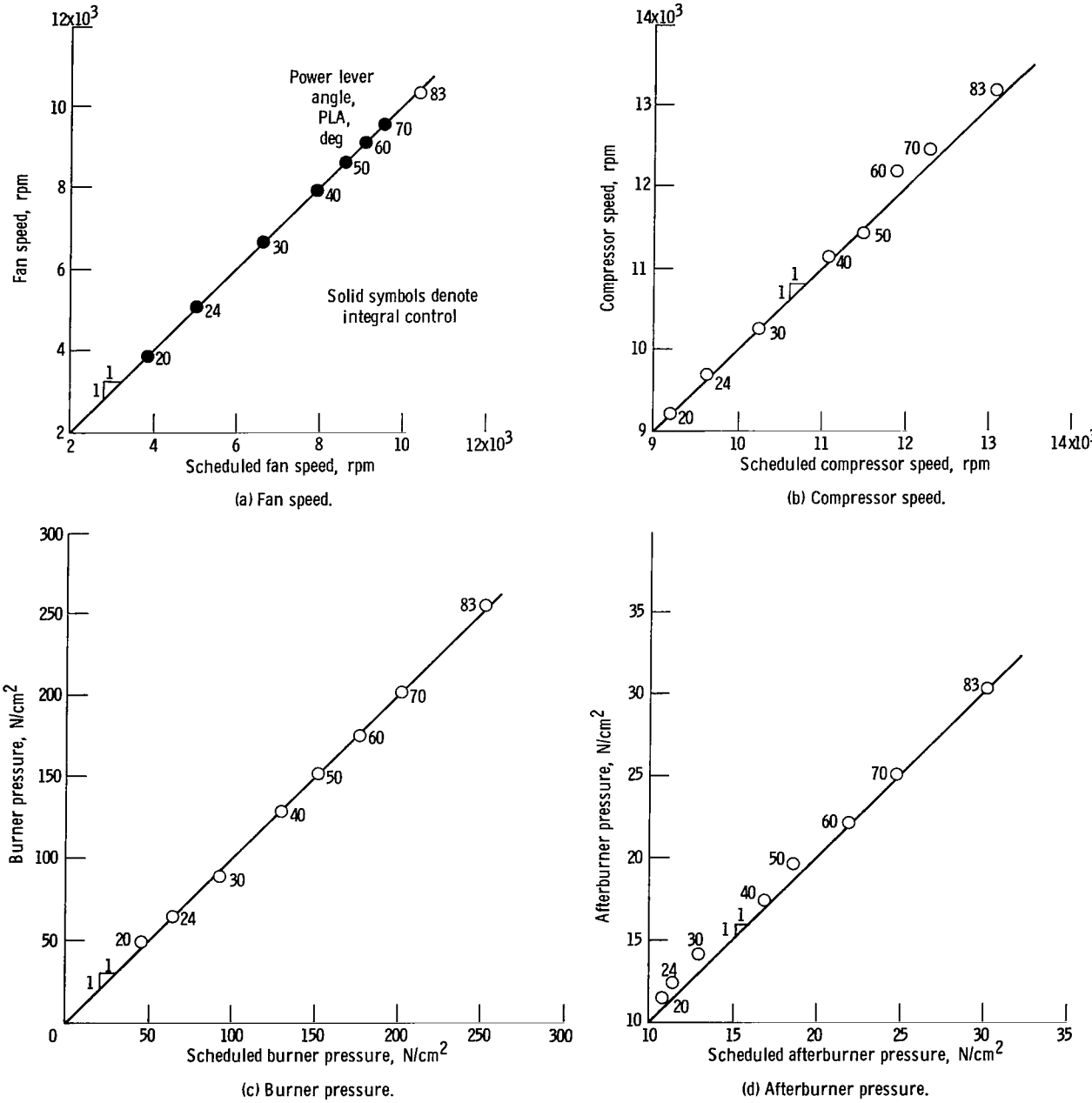

Figure 29. - Steady-state, uninstalled performance of F100 real-time simulation with multivariable control. Sea-level, static, standard-day conditions.

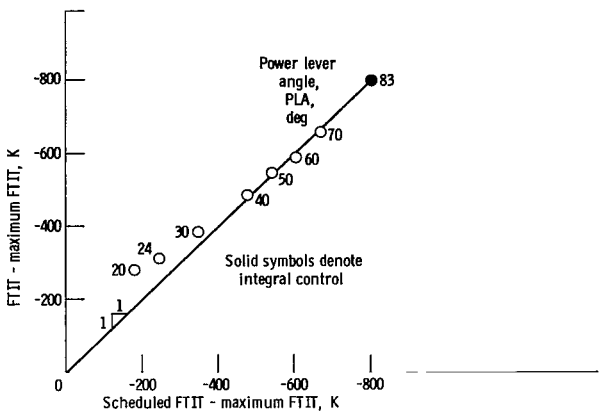

(e) Fan turbine inlet temperature.

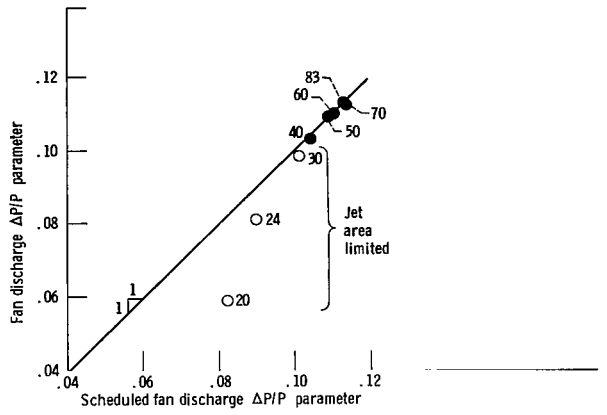

(f) Fan discharge ΔP/P parameter.

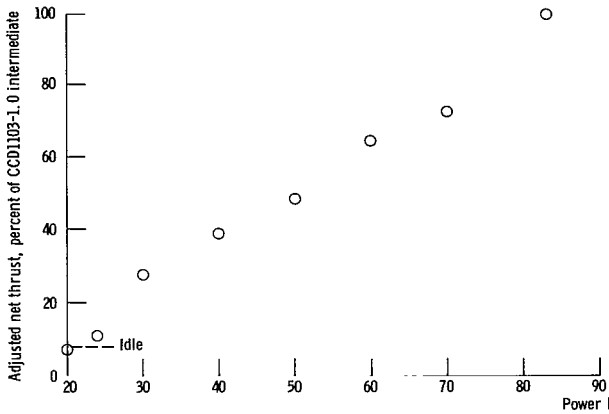

(g) Adjusted net thrust.

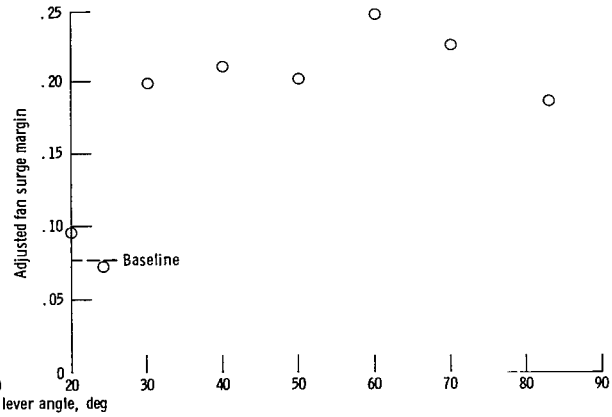

(h) Adjusted fan surge margin.

Figure 29. - Continued.

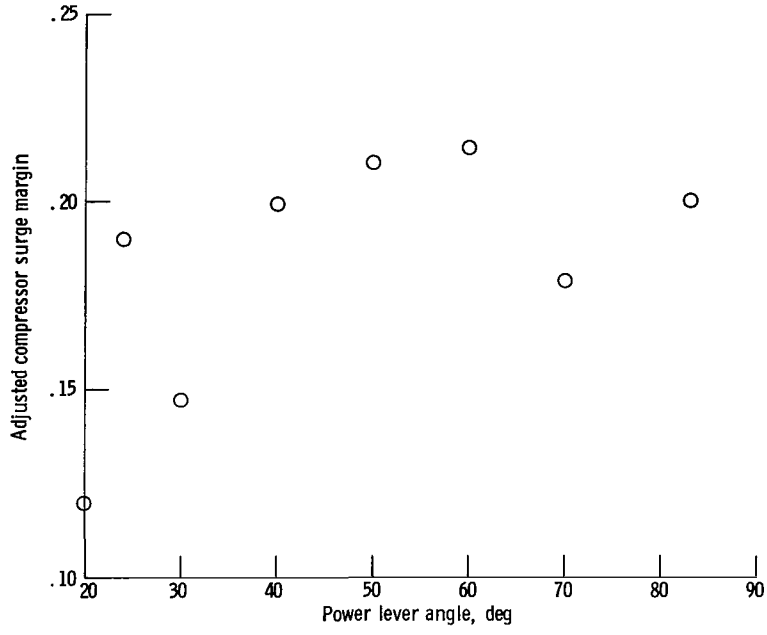

(i) Adjusted compressor surge margin.

Figure 29. - Concluded.

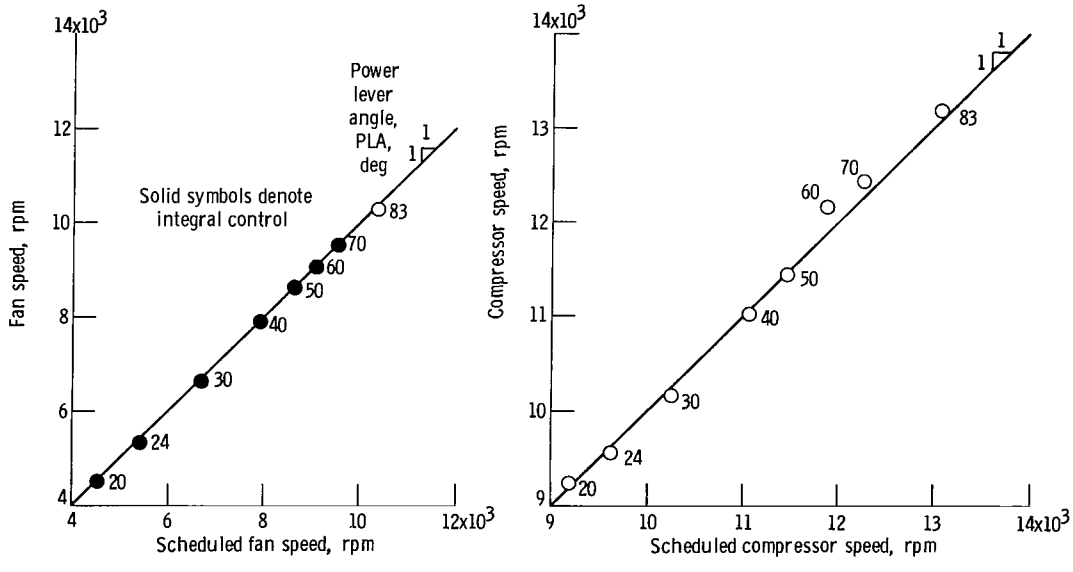

(a) Fan speed.

(b) Compressor speed.

Figure 30. - Steady-state, uninstalled performance of F100 real-time simulation with multivariable control. Altitude, 3.048 kilometers; Mach number, 0.6; standard-day conditions.

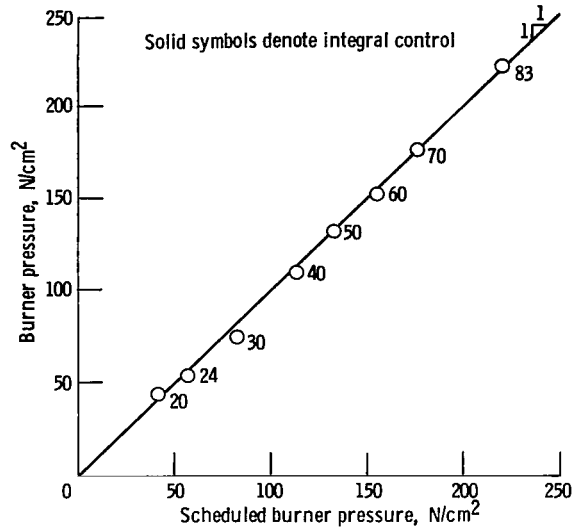

(c) Burner pressure.

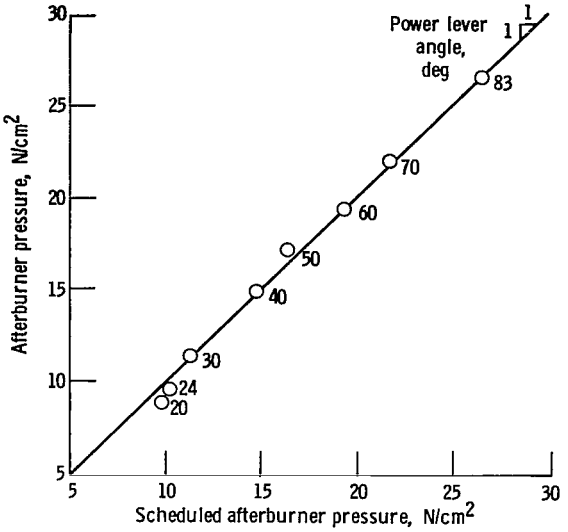

(d) Afterburner pressure.

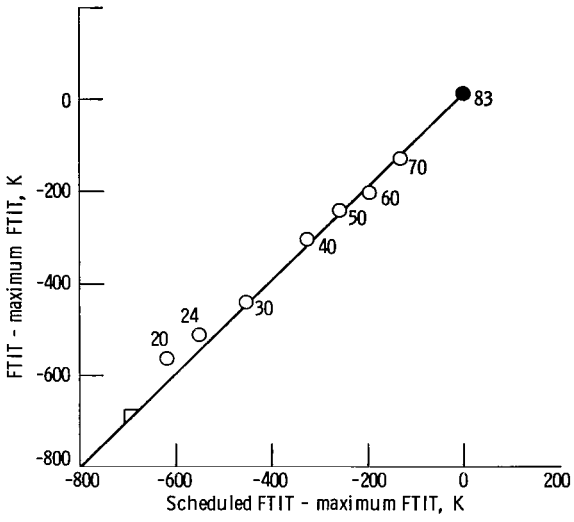

(e) Fan turbine inlet temperature.

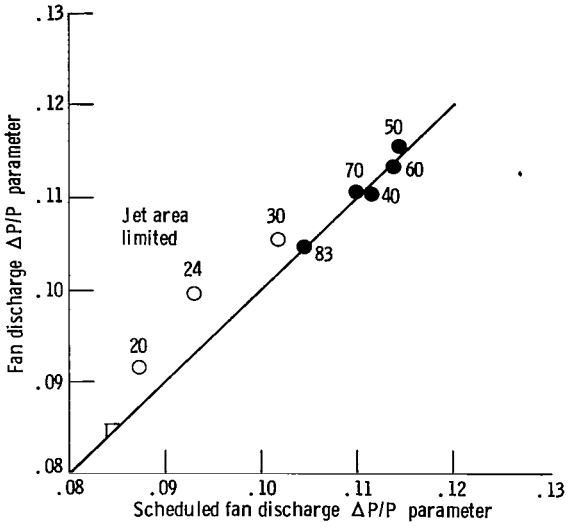

(f) Fan discharge ΔP/P parameter.

Figure 30. - Continued.

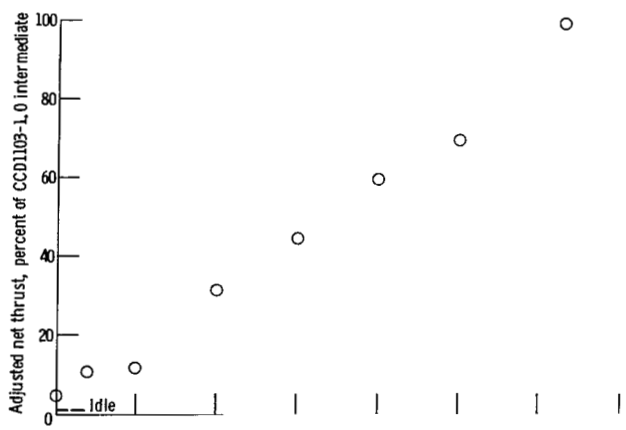

(g) Adjusted net thrust.

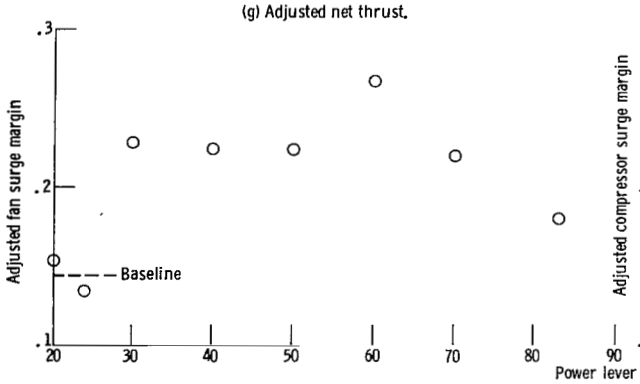

(h) Adjusted fan surge margin.

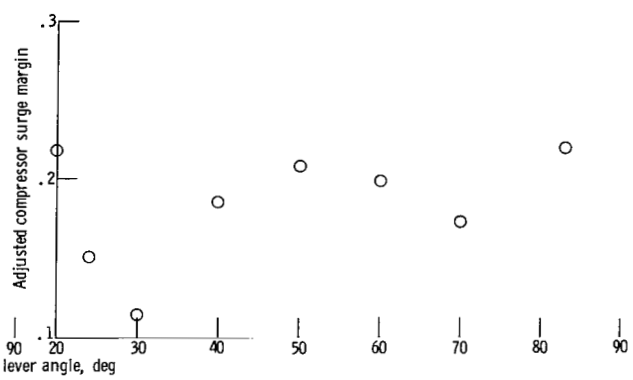

(i) Adjusted compressor surge margin.

Figure 30. - Concluded.

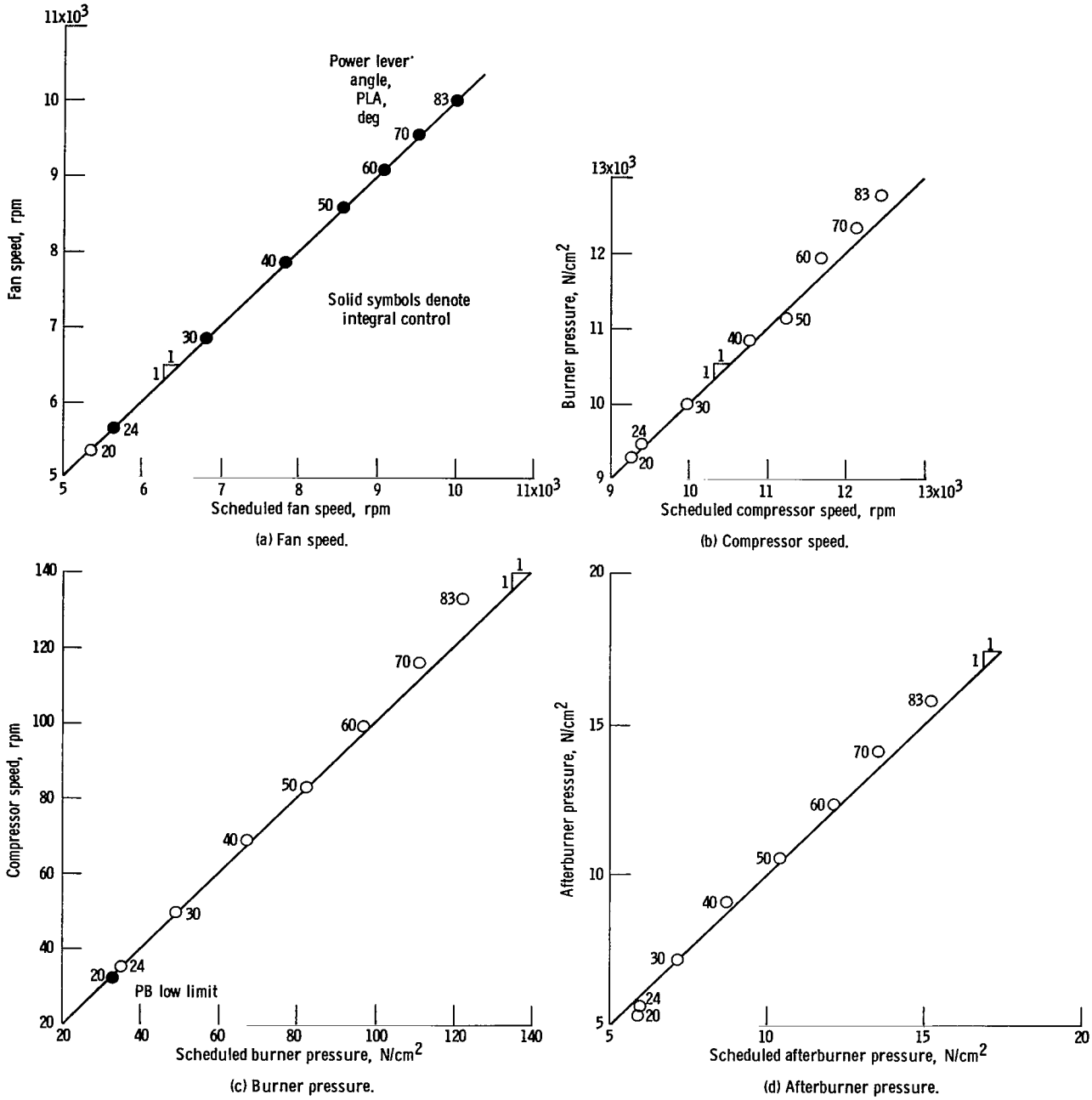

Figure 31. - Steady-state, uninstalled performance of F100 real-time simulation with multivariable control. Altitude, 9.144 kilometers; Mach number, 0.9; standard-day conditions.

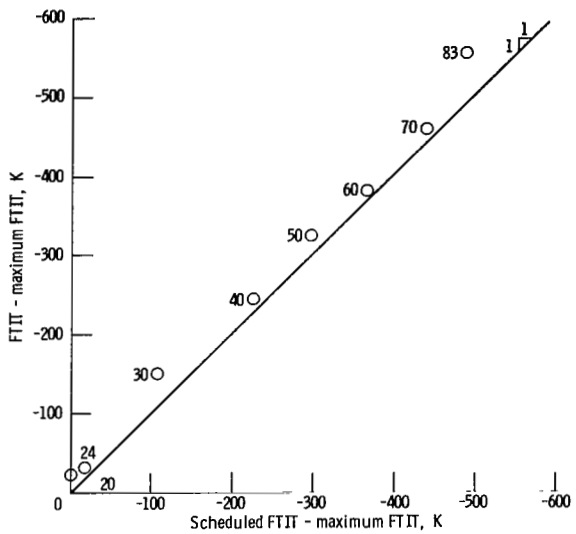

(e) Fan turbine inlet temperature.

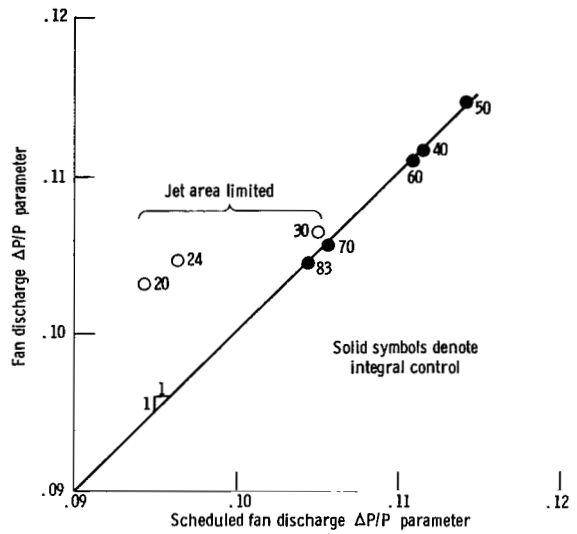

(f) Fan discharge ΔP/P parameter.

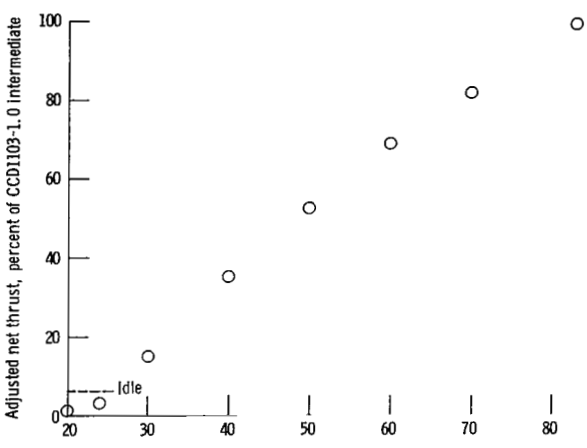

(g) Adjusted net thrust.

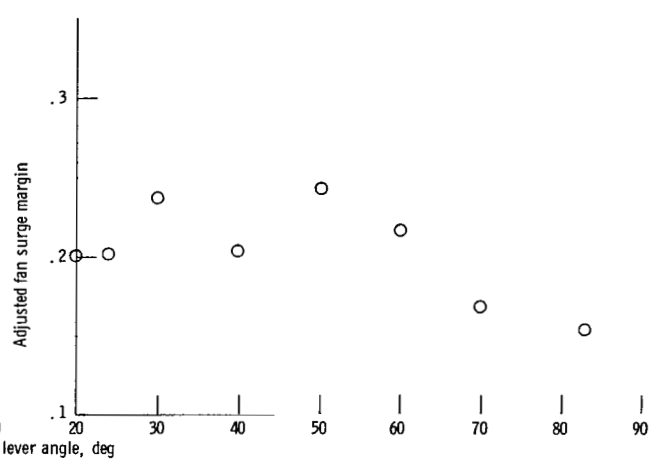

(h) Adjusted fan surge margin.

Figure 31. - Continued.

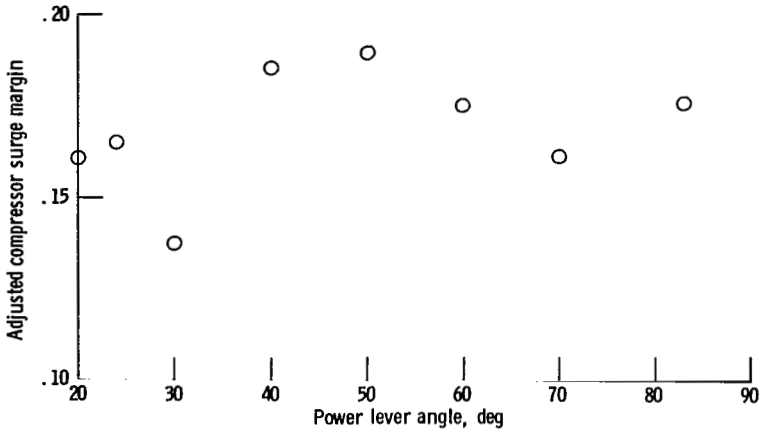

(i) Adjusted compressor surge margin.

Figure 31. - Concluded.

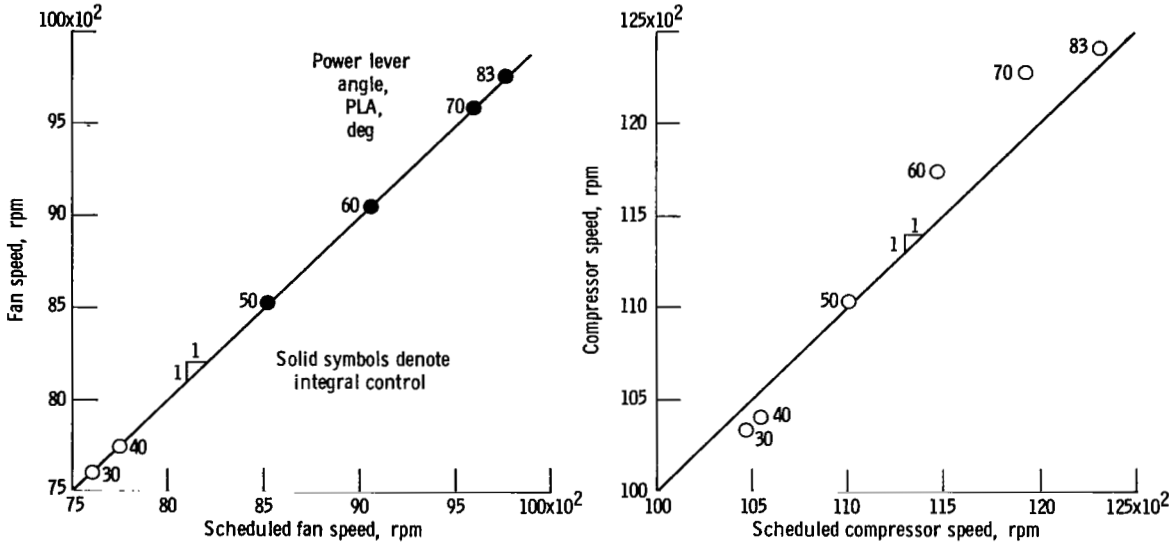

(a) Fan speed.

(b) Compressor speed.

Figure 32. - Steady-state, uninstalled performance of F100 real-time simulation with multivariable control. Altitude, 13.72 kilometers; Mach number, 0.9; standard-day conditions.

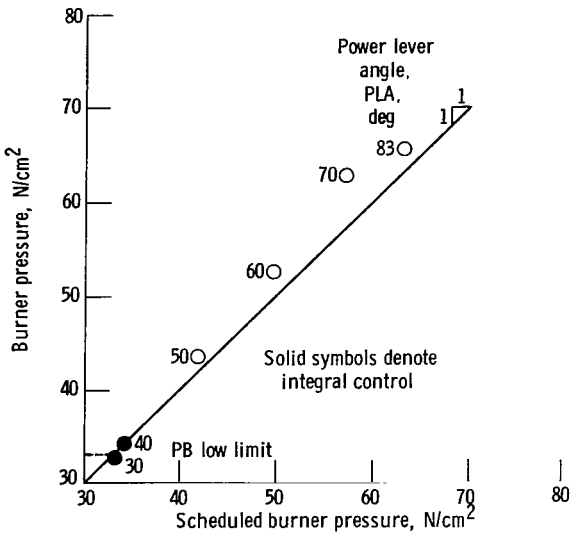

(c) Burner pressure.

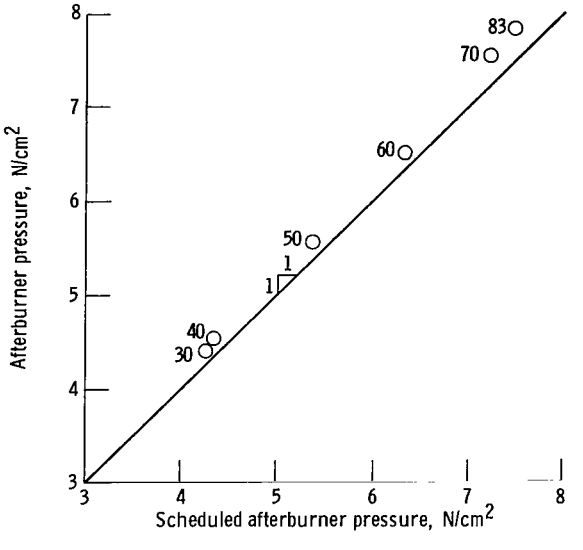

(d) Afterburner pressure.

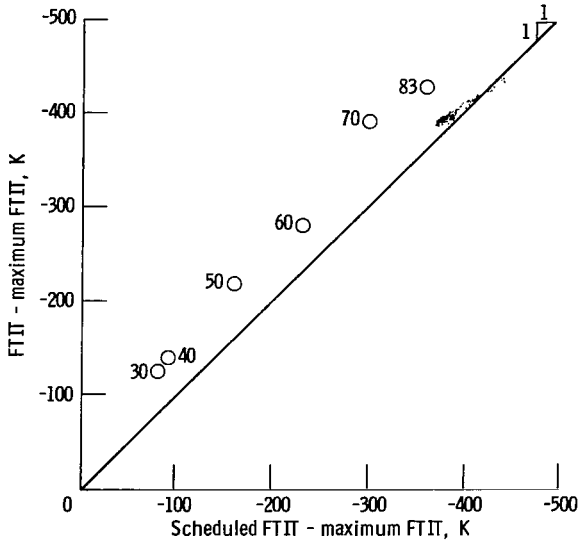

(e) Fan turbine inlet temperature.

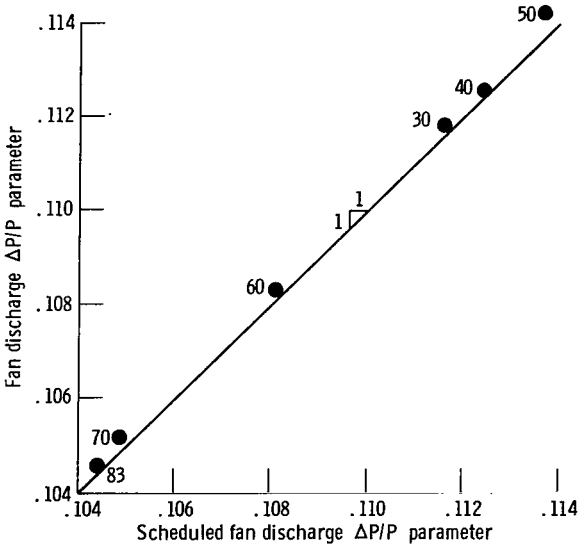

(f) Fan discharge ΔP/P parameter.

Figure 32. - Continued.

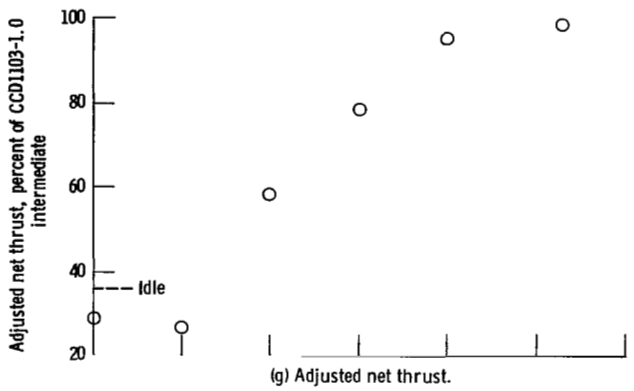

(g) Adjusted net thrust.

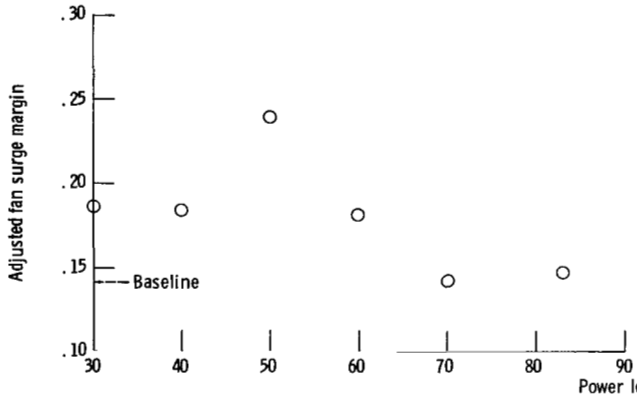

(h) Adjusted fan surge margin.

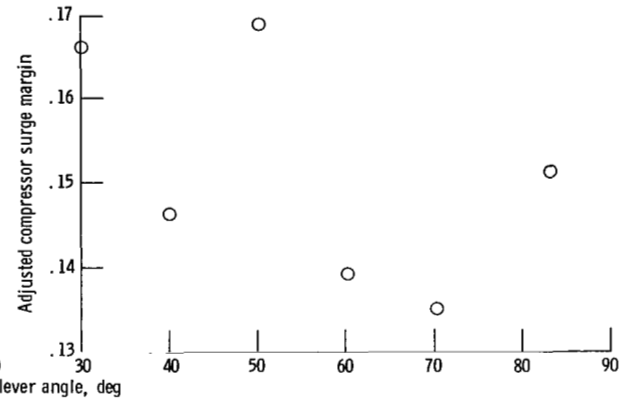

(i) Adjusted compressor surge margin.

Figure 32. - Concluded.

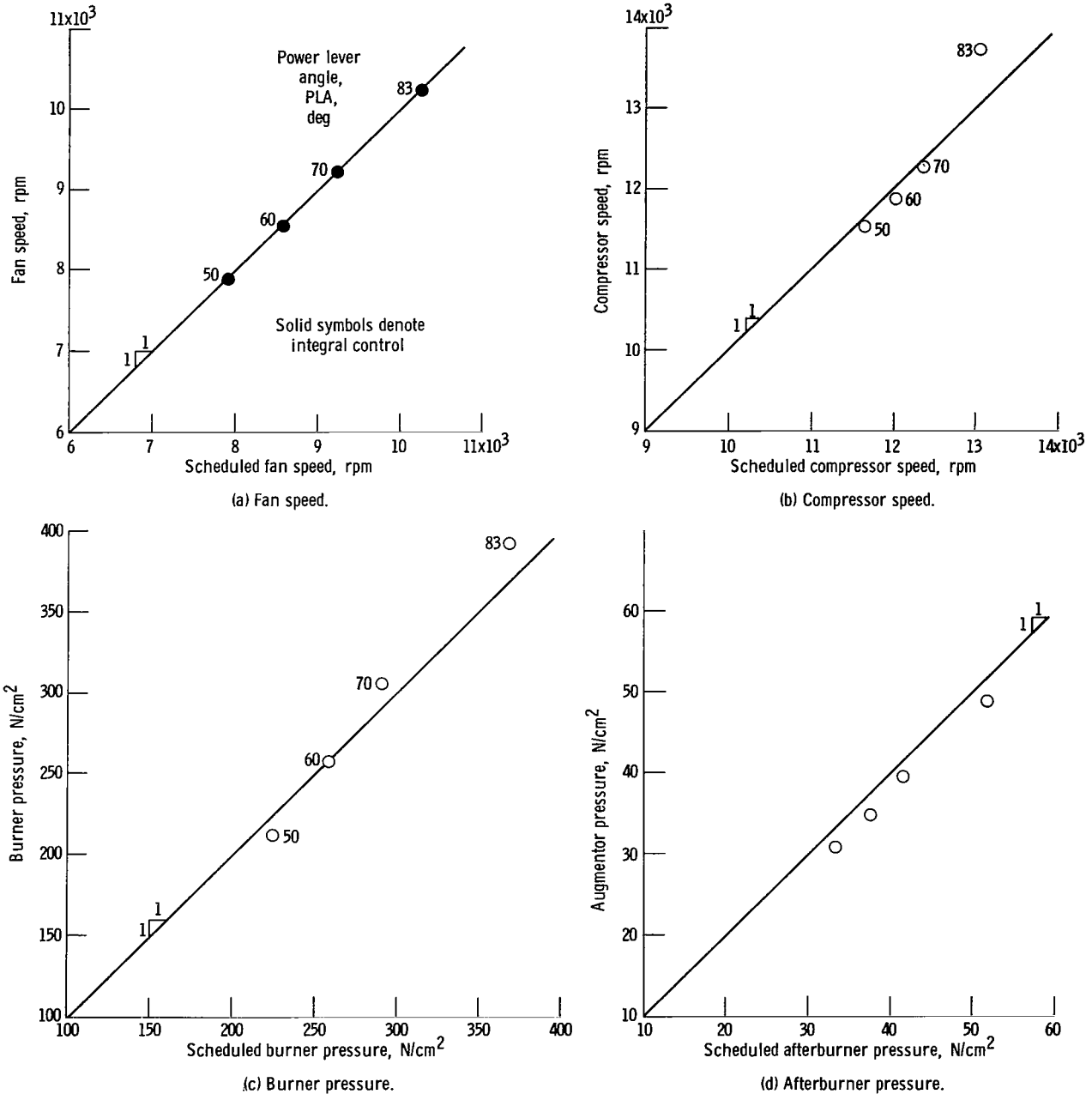

Figure 33. - Steady-state, uninstalled performance of F100 real-time simulation with multivariable control. Sea-level, Mach number 1.2, standard-day conditions.

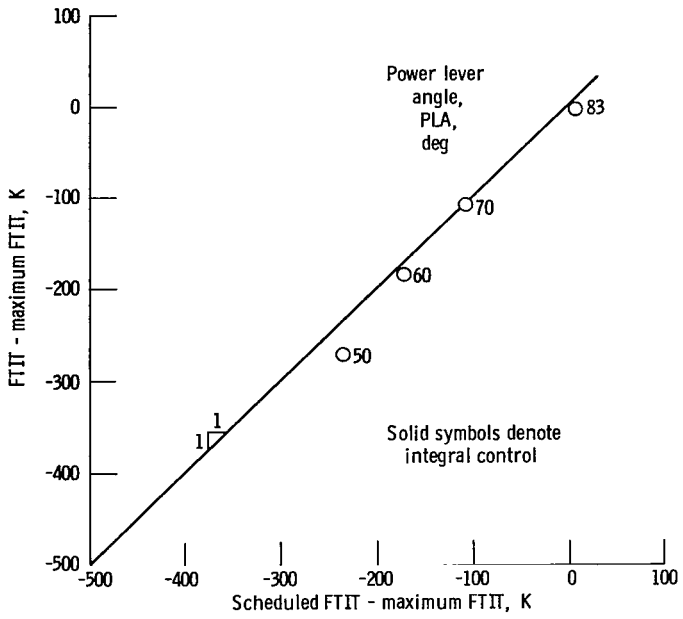

(e) Fan turbine inlet temperature.

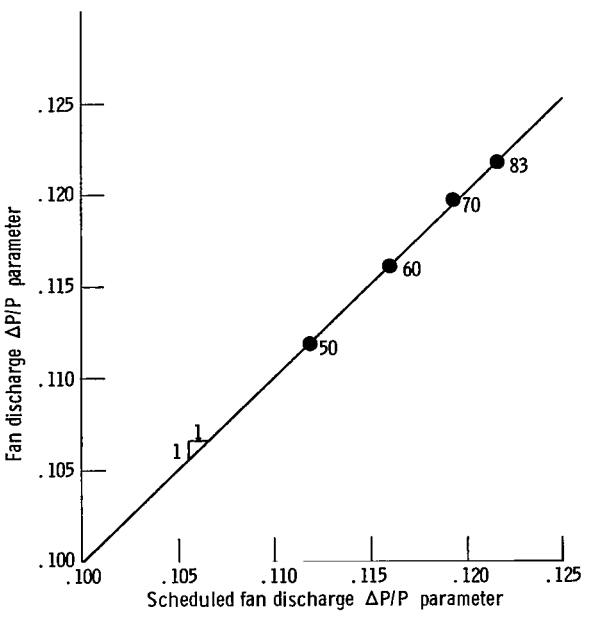

(f) Fan discharge ΔP/P parameter.

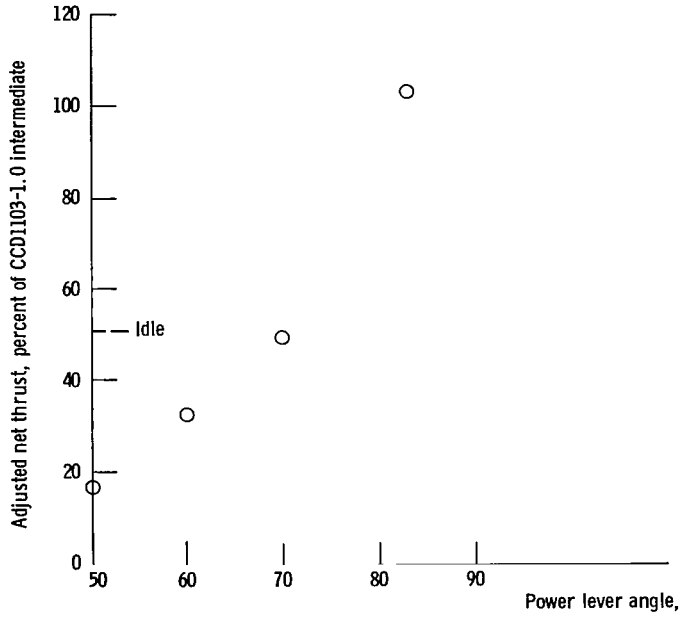

(g) Adjusted net thrust.

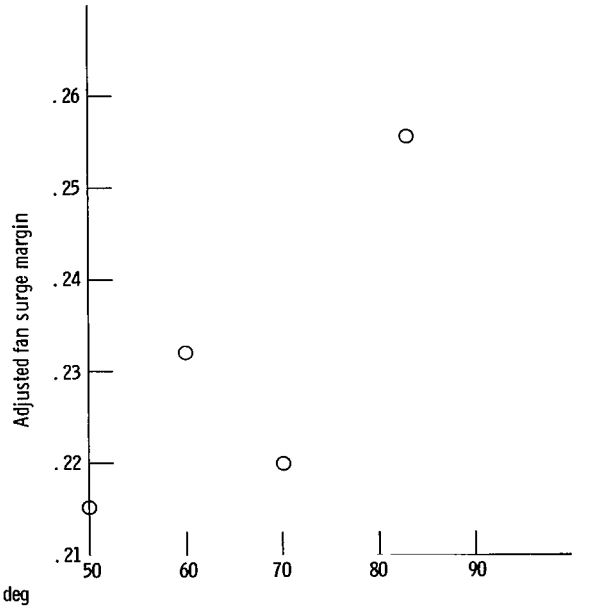

(h) Adjusted fan surge margin.

Figure 33. - Continued.

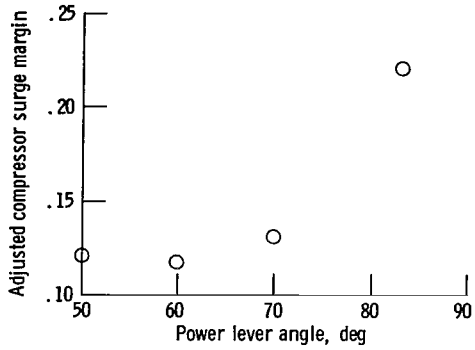

(i) Adjusted compressor surge margin.

Figure 33. - Concluded.

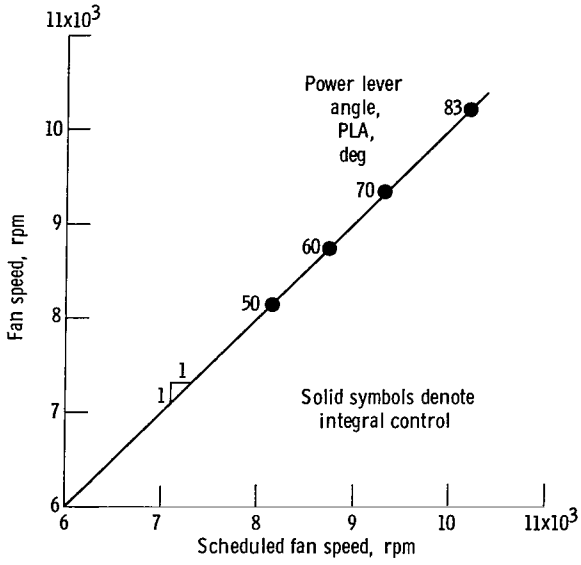

(a) Fan speed.

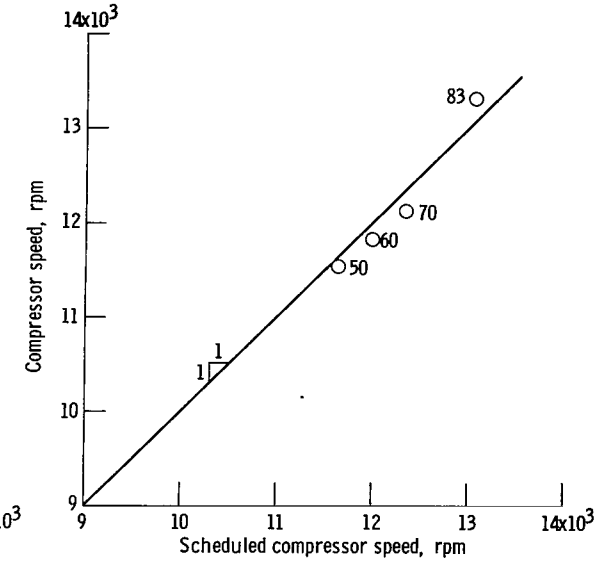

(b) Compressor speed.

Figure 34. - Steady-state, uninstalled performance of F100 real-time simulation with multivariable control. Altitude, 3.048 kilometers; Mach number, 1.2; standard-day conditions.

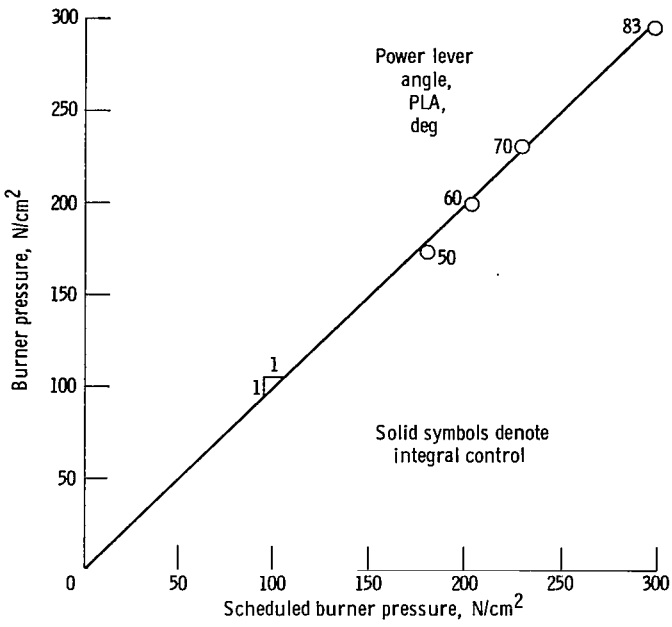

(c) Burner pressure.

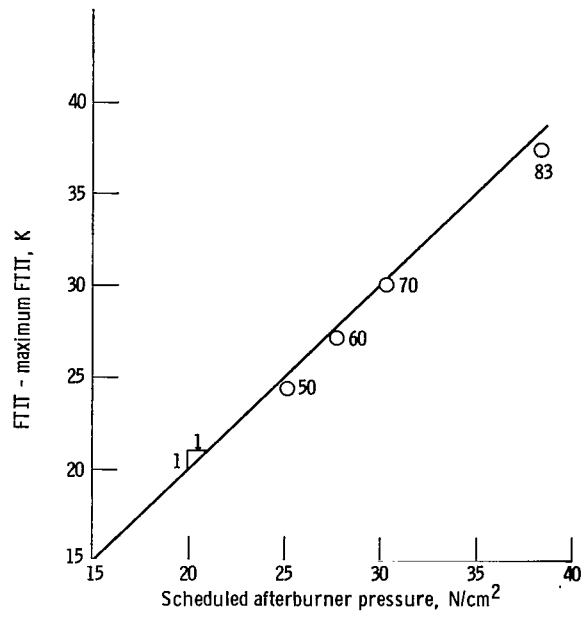

(d) Afterburner pressure.

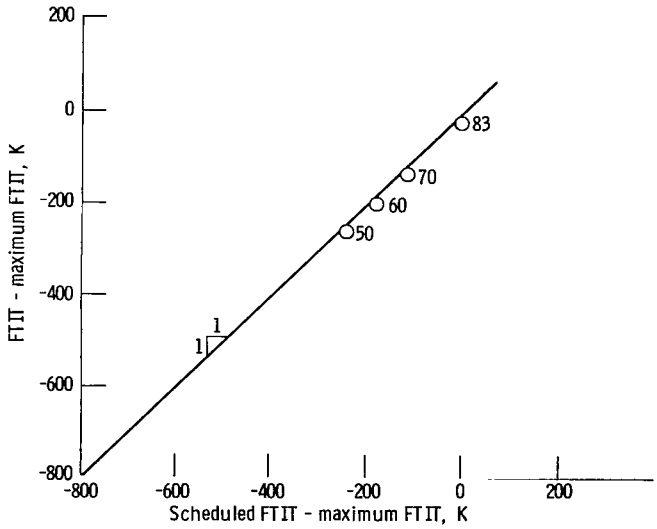

(e) Fan turbine inlet temperature.

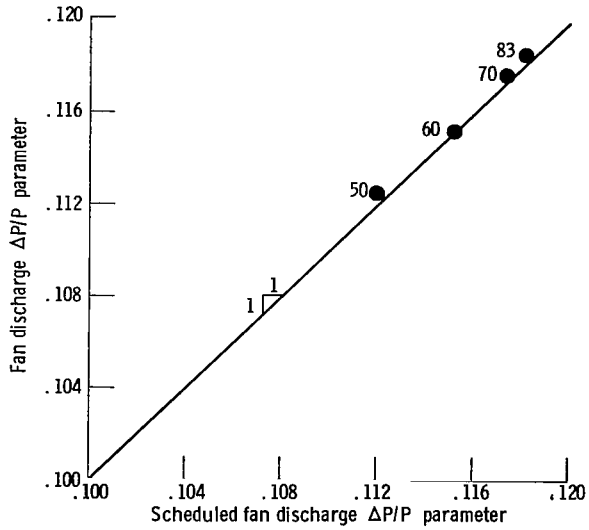

(f) Fan discharge ΔP/P parameter.

Figure 34. - Continued.

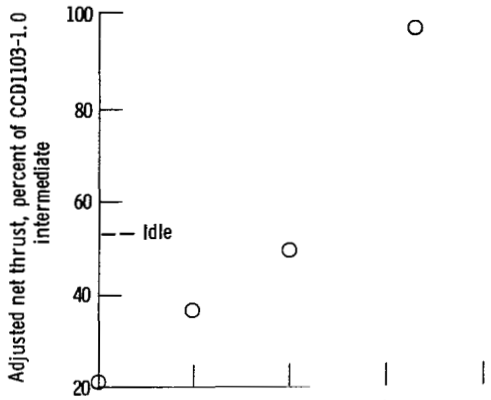

(g) Adjusted net thrust.

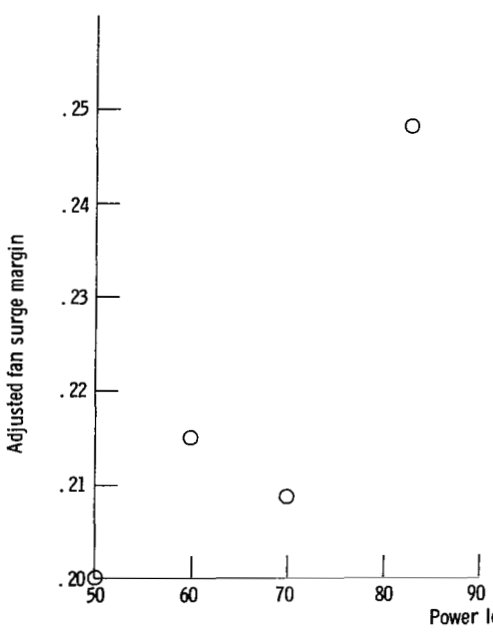

(h) Adjusted fan surge margin.

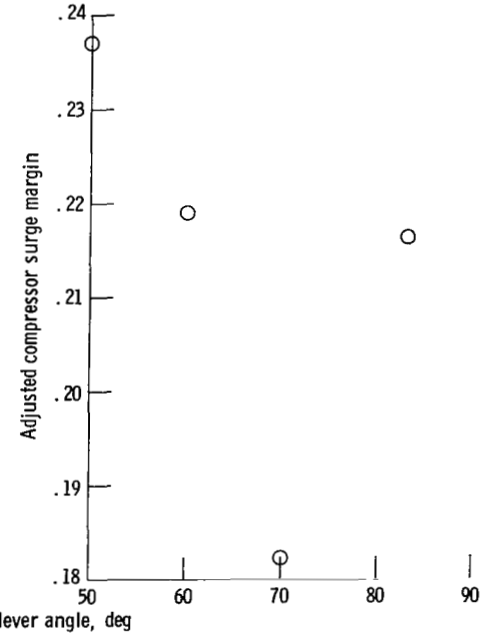

(i) Adjusted compressor surge margin.

Figure 34. - Concluded.

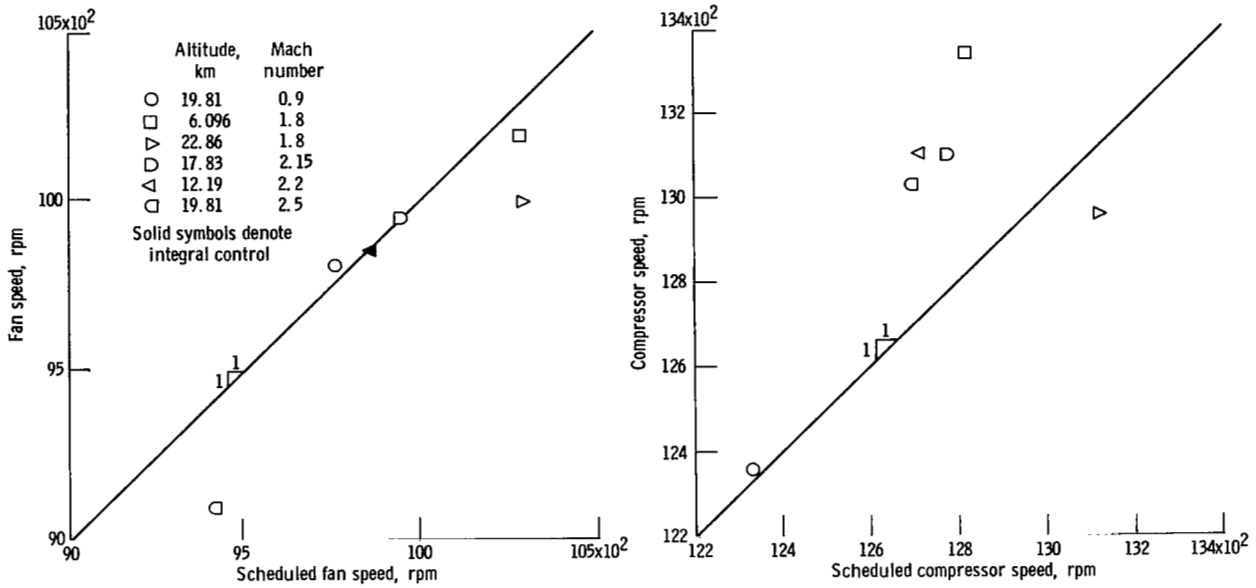

Figure 35. - Steady-state, uninstalled performance of F100 real-time simulation with multivariable control. Standard-day conditions; intermediate power.

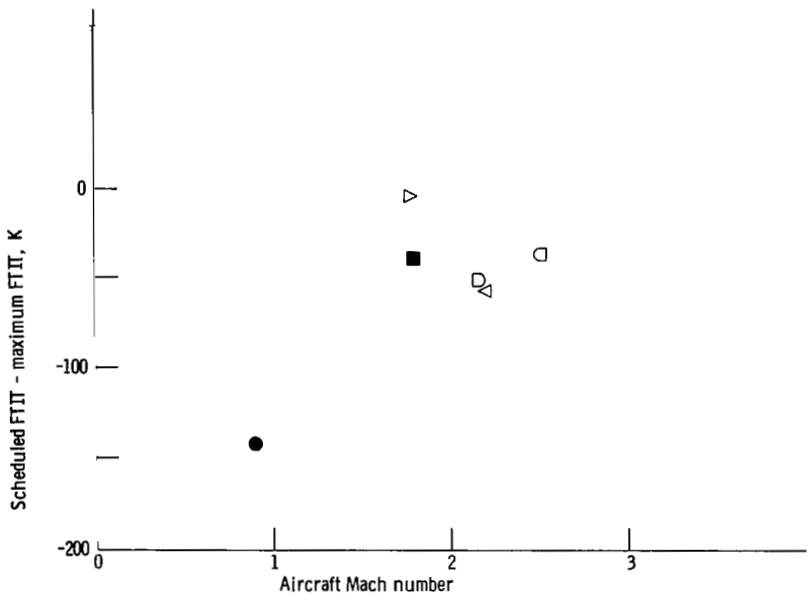

(e) Fan turbine inlet performance.

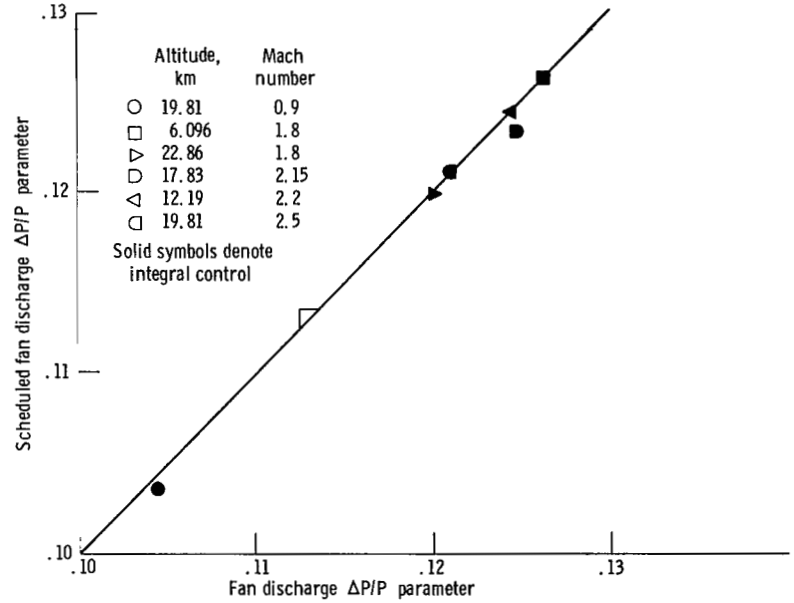

(f) Fan discharge ΔP/P parameter.

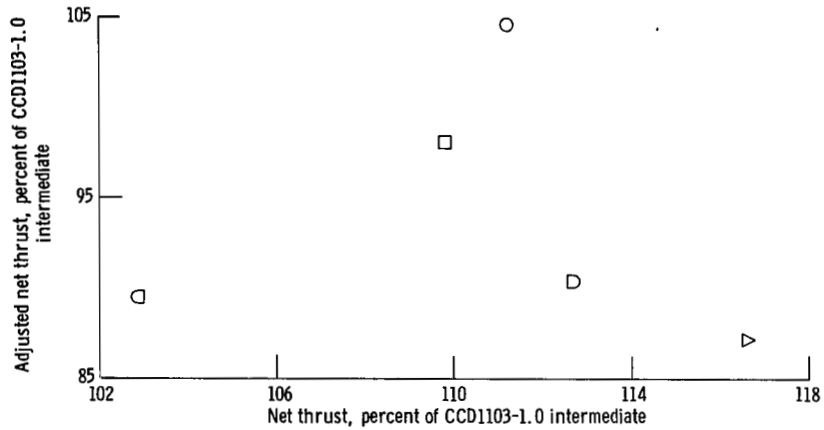

(g) Net thrust.

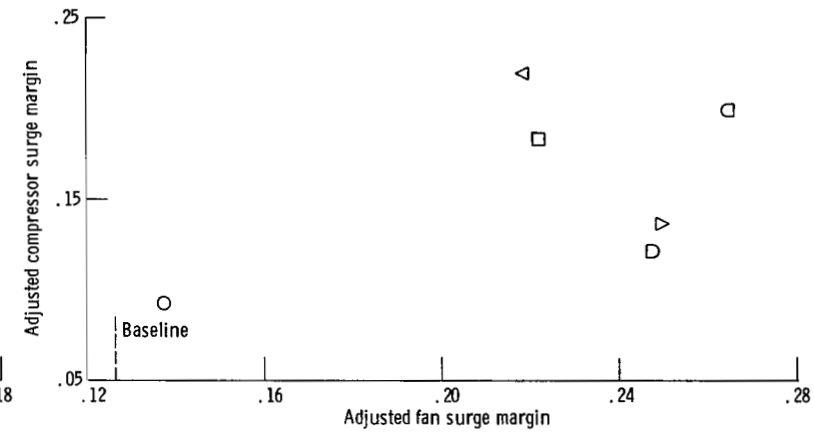

(h) Adjusted surge margins.

Figure 35. - Concluded.

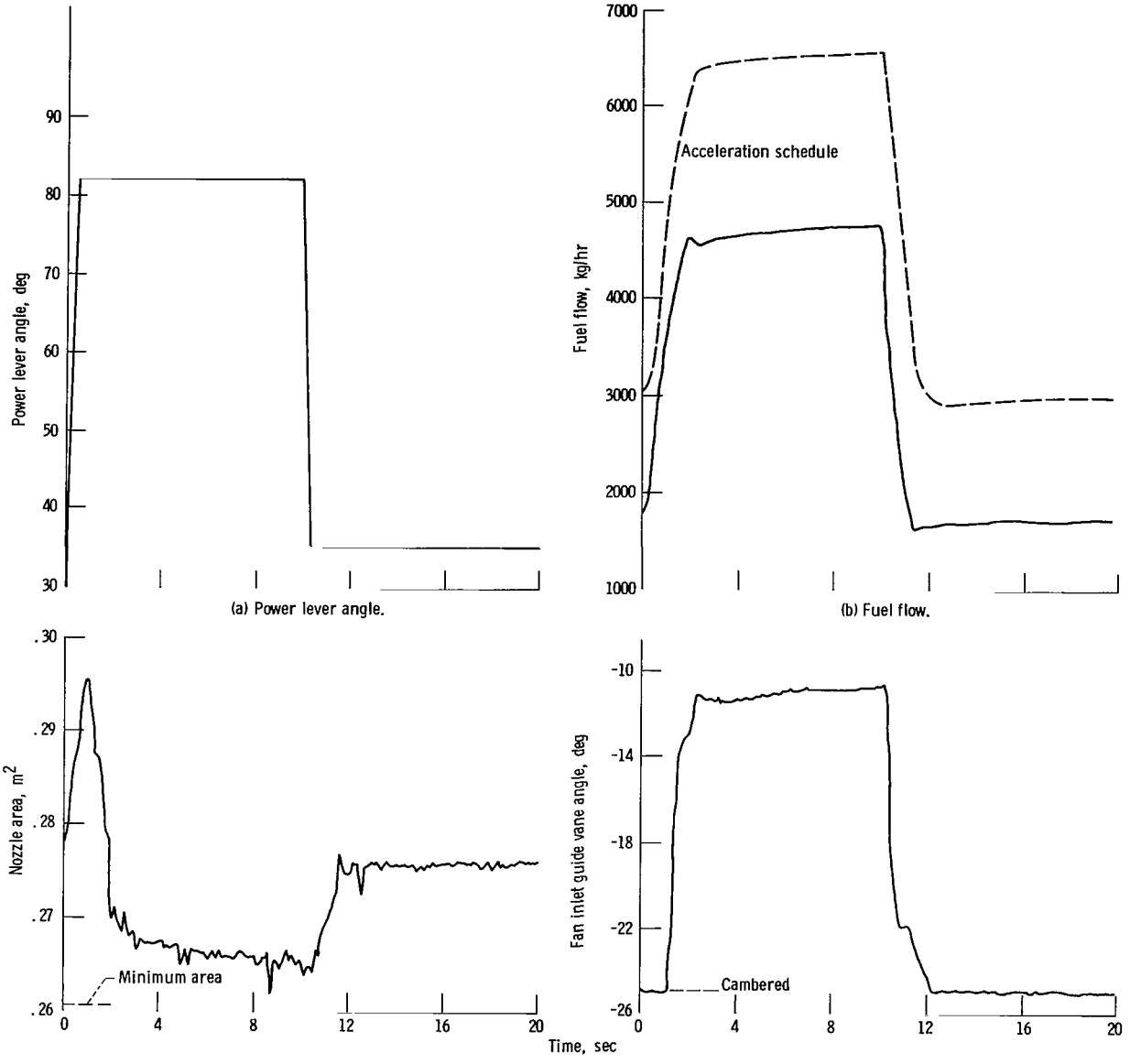

Figure 36. - Simulated F100 response to 35^0 to 83^0 power lever angle (PLA) snap at 3.048 kilometers and Mach 0.9. Multivariable control; PLA = 35^0 provides 30-percent thrust.

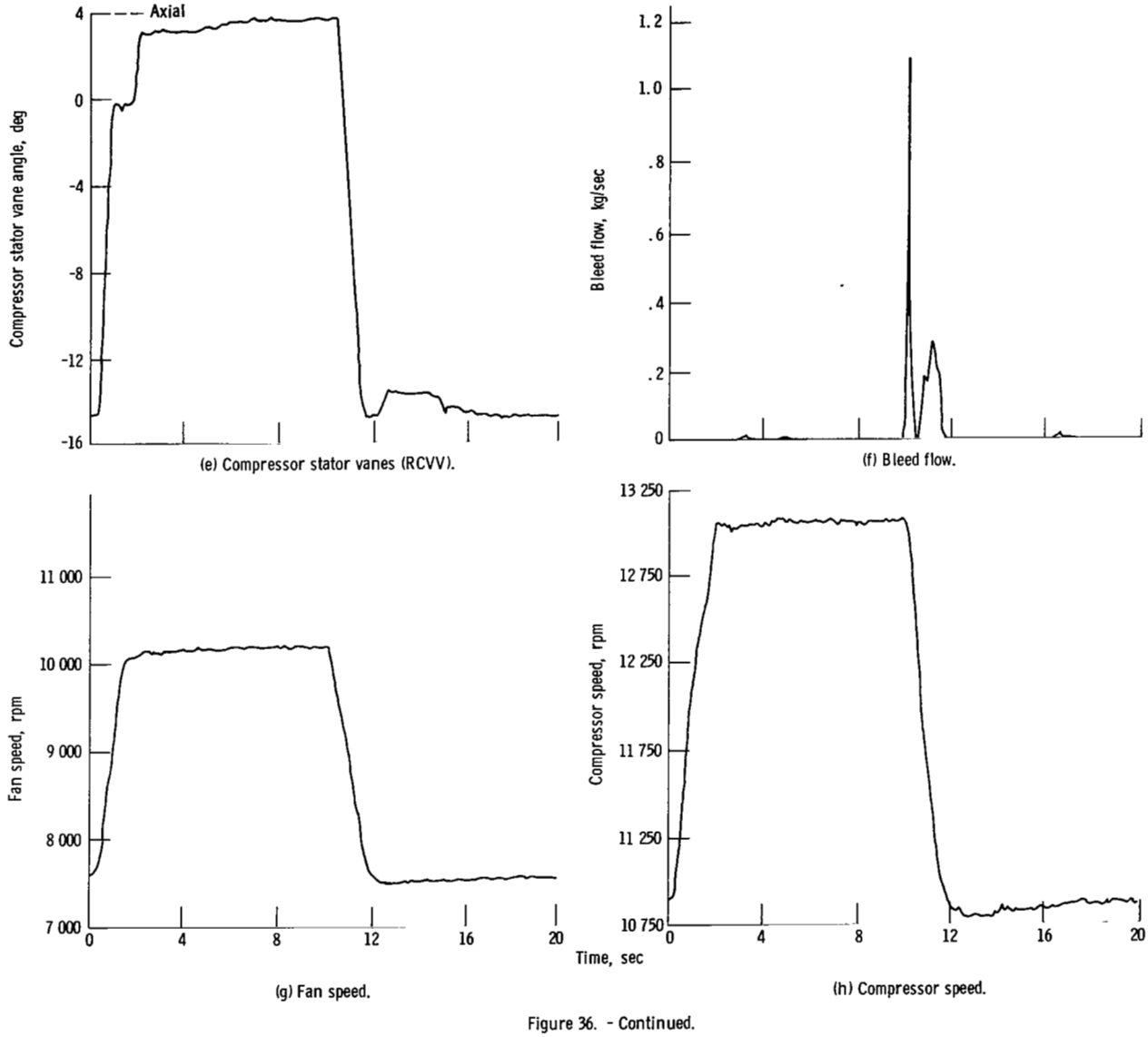

(e) Compressor stator vanes (RCVV).

(f) Bleed flow.

(g) Fan speed.

(h) Compressor speed.

Figure 36. - Continued.

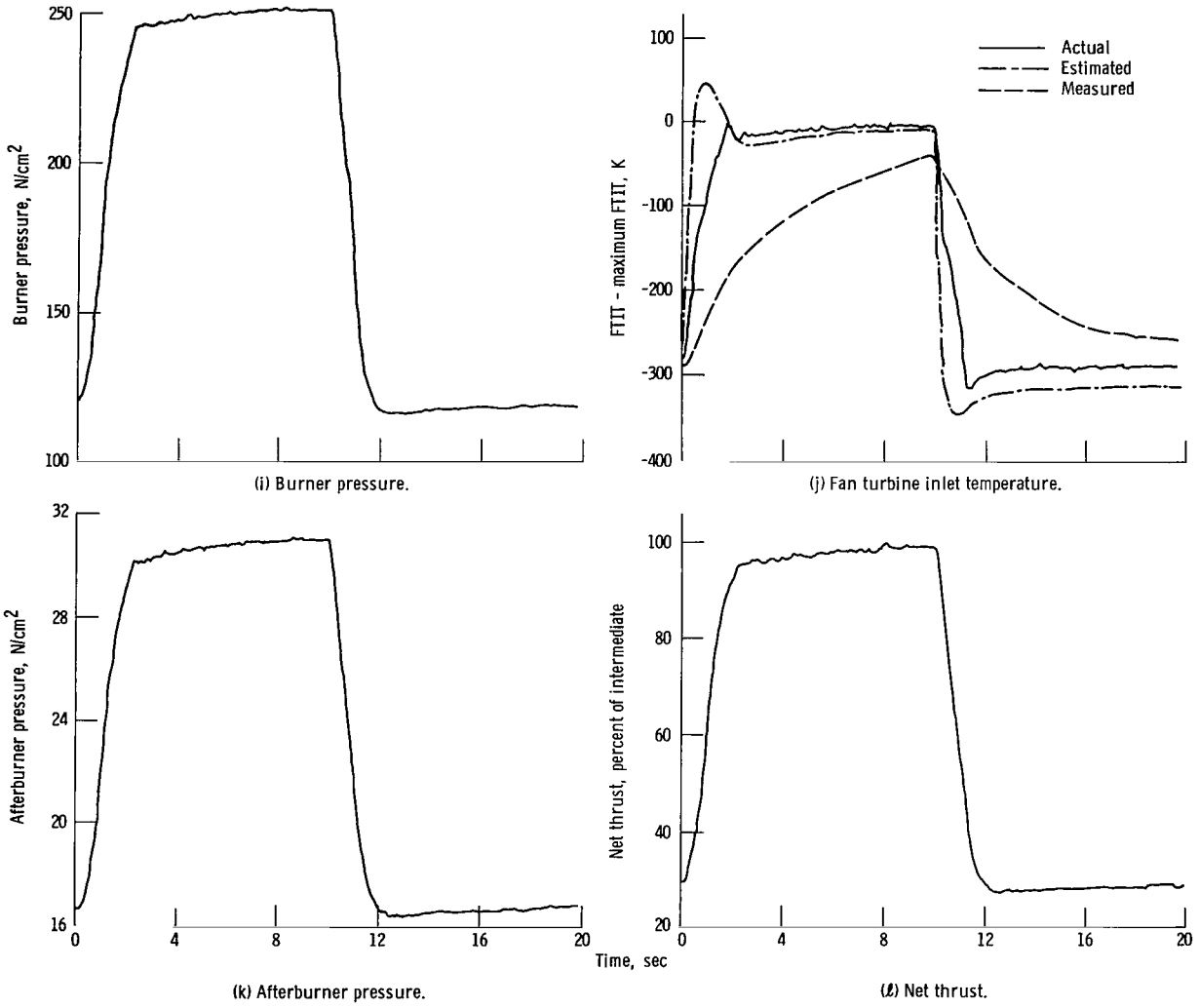

(i) Burner pressure.

(j) Fan turbine inlet temperature.

(k) Afterburner pressure.

(l) Net thrust.

Figure 36. - Continued.

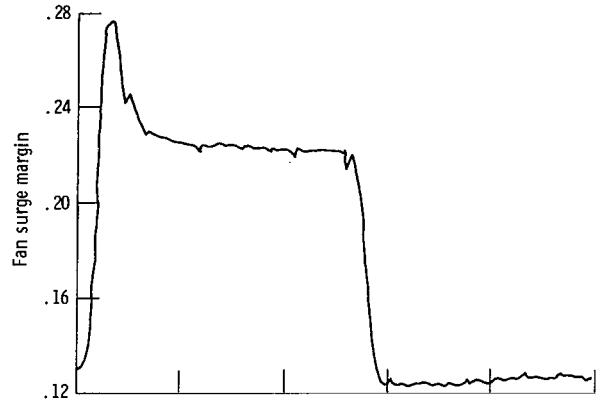

(m) Fan surge margin.

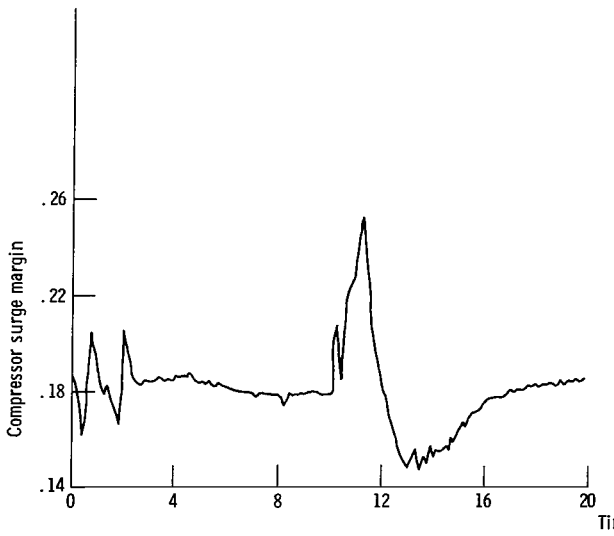

(n) Compressor surge margin.

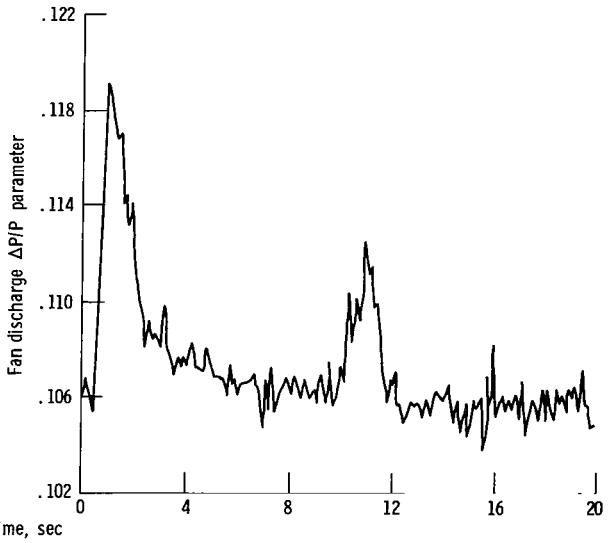

(o) Fan discharge ΔP/P parameter.

Figure 36. - Concluded.

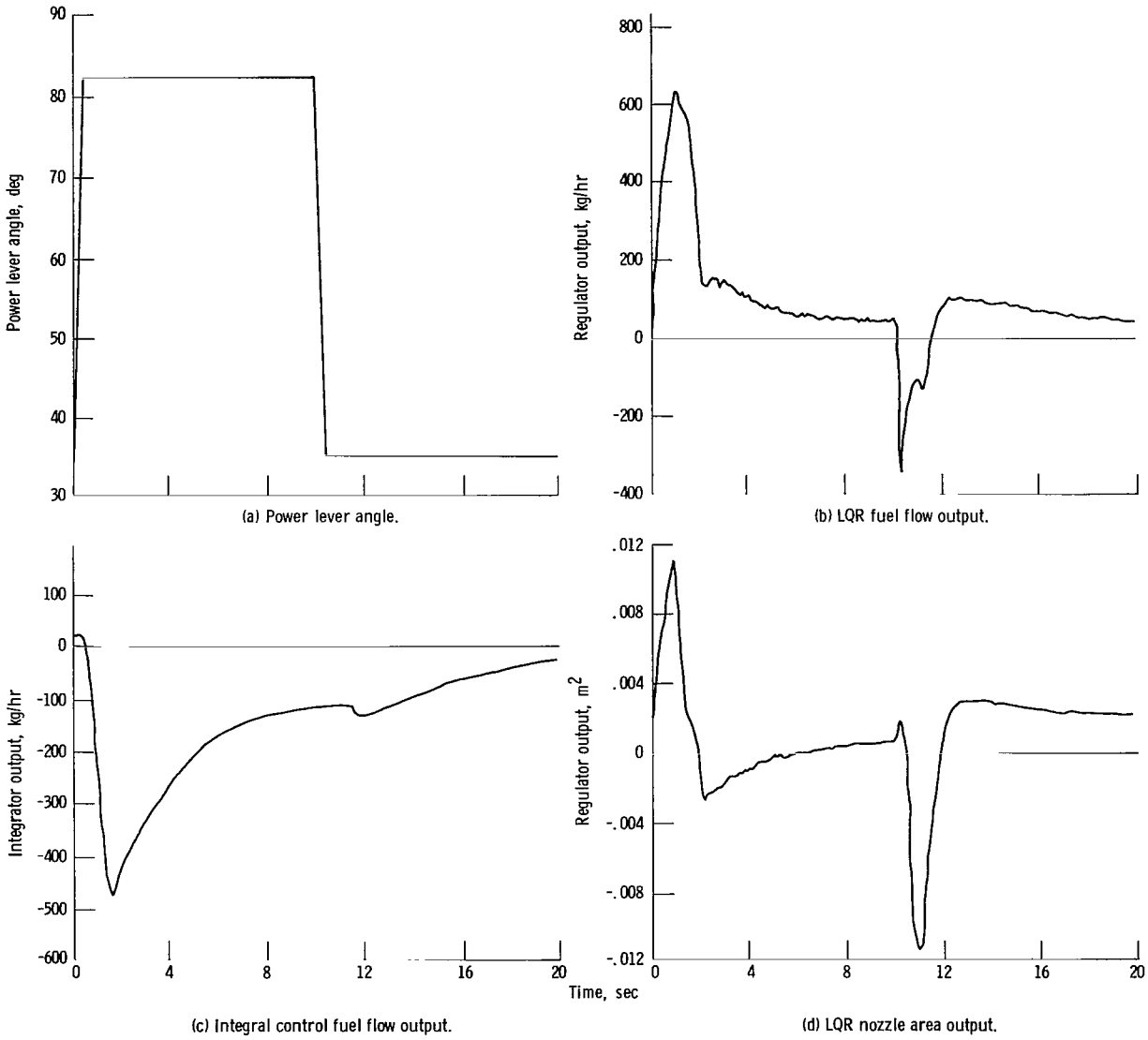

Figure 37. - Multivariable control performance for 35^0 to 83^0 power lever angle (PLA) snap at 3.048 kilometers and Mach 0.9. PLA = 35^0 provides 30-percent thrust.

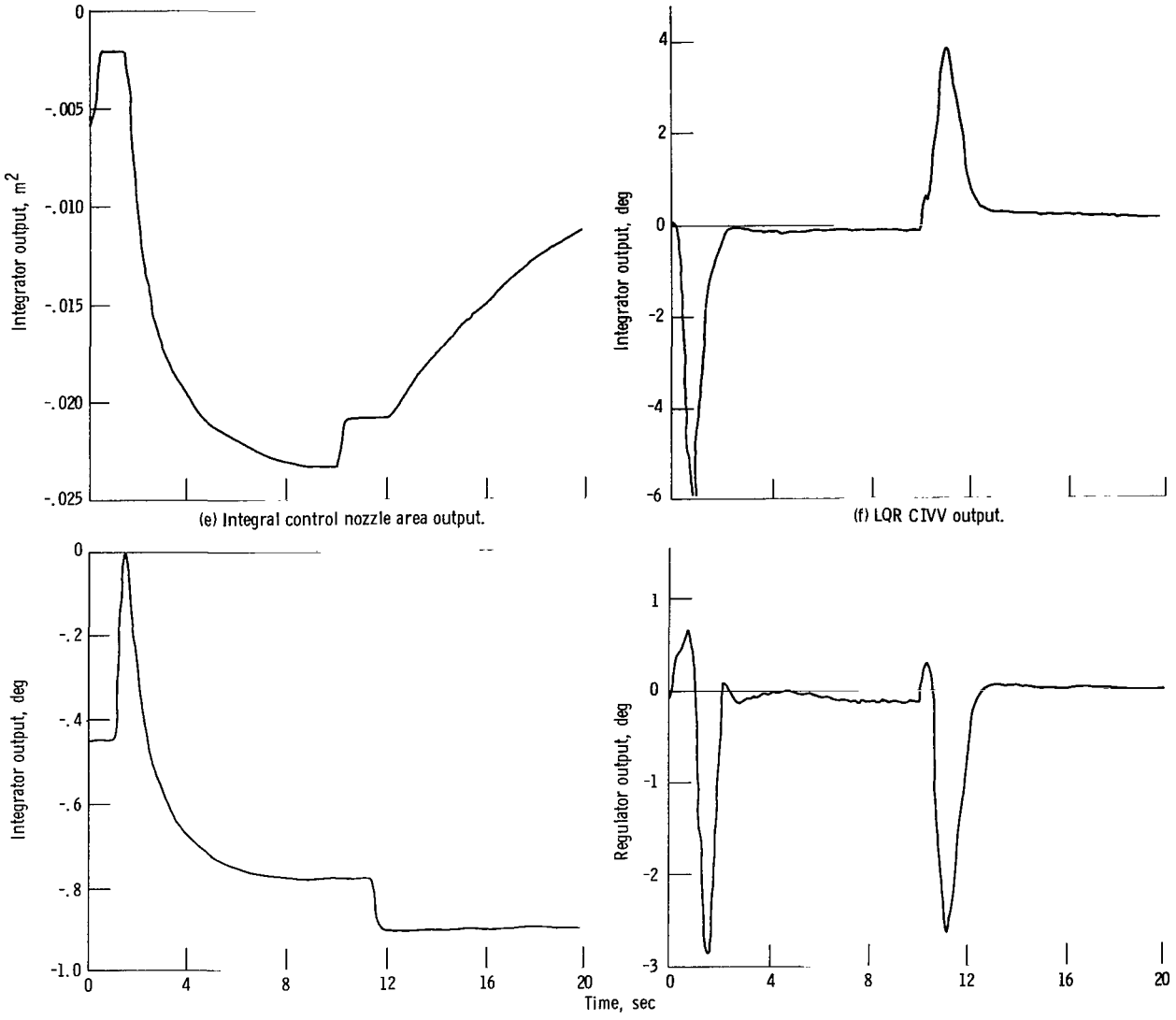

(e) Integral control nozzle area output.

(f) LQR CIVV output.

(g) Integral control CIVV output.

(h) LQR RCVV output.

Figure 37. - Continued.

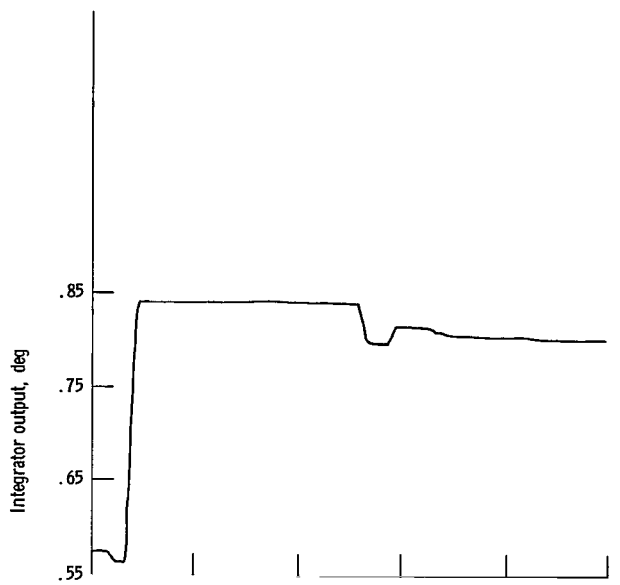

(i) Integral control RCVV output.

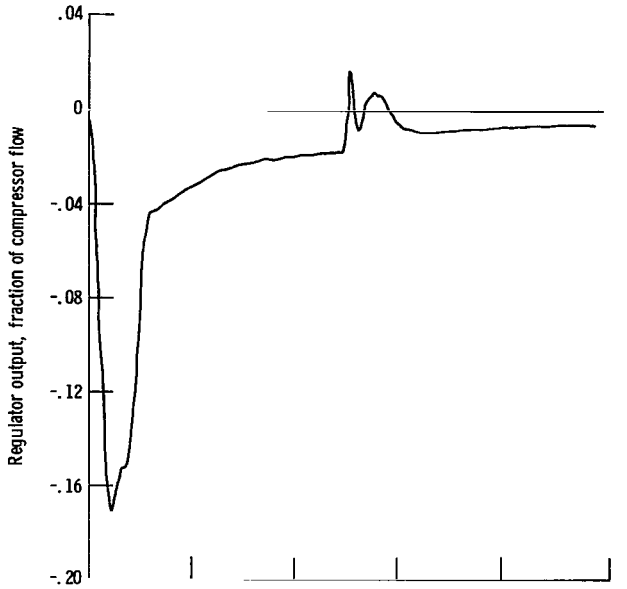

(j) LQR bleed flow output.

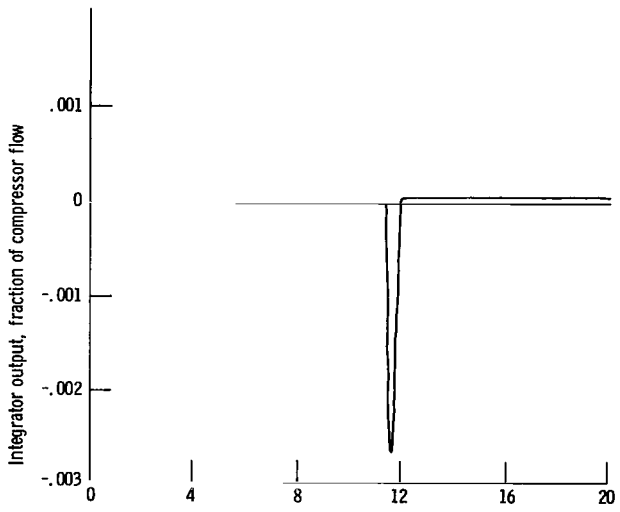

(k) Integral control bleed flow output.

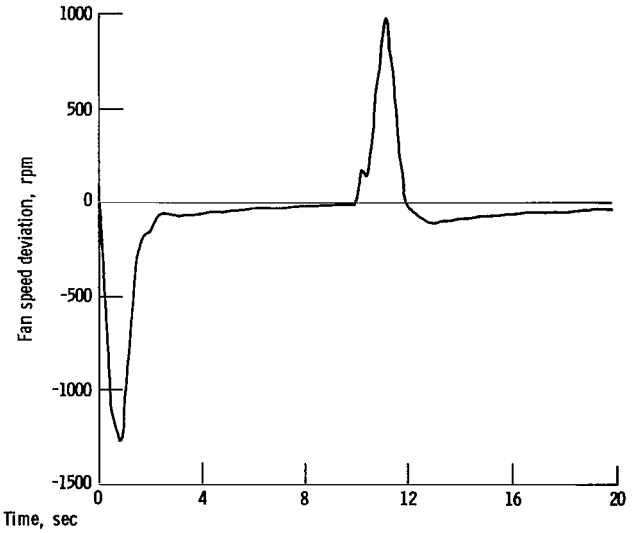

(ℓ) Fan speed deviation.

Figure 37. - Continued.

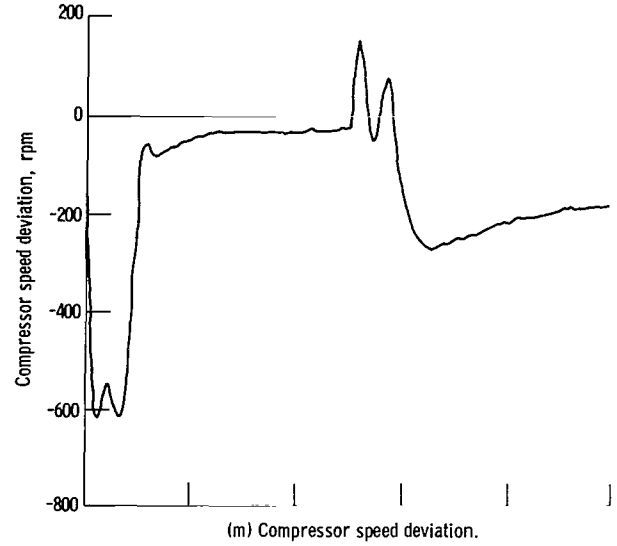

(m) Compressor speed deviation.

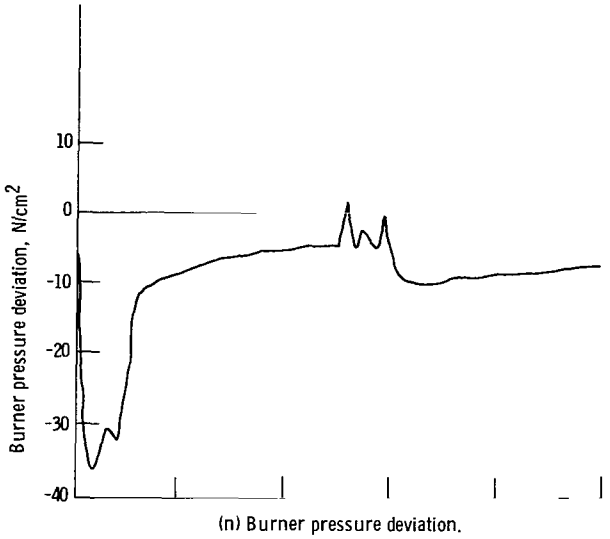

(n) Burner pressure deviation.

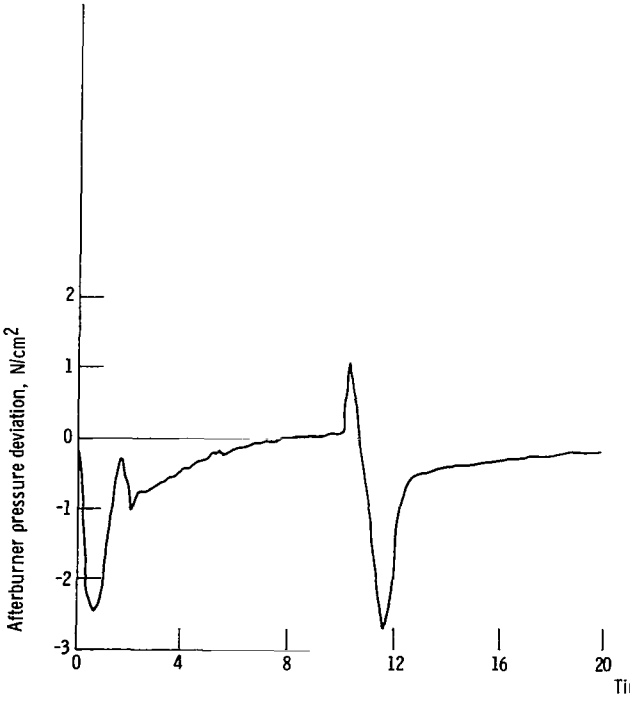

(o) Afterburner pressure deviation.

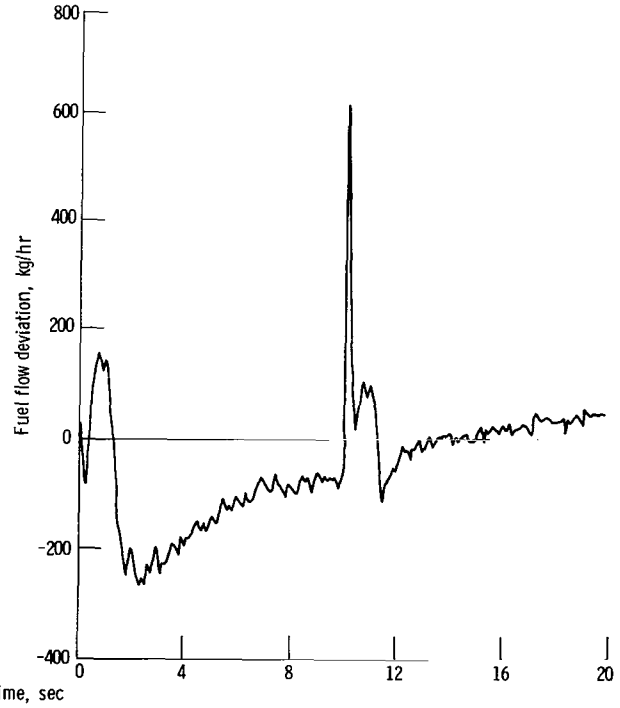

(p) Fuel flow deviation.

Figure 37. - Concluded.

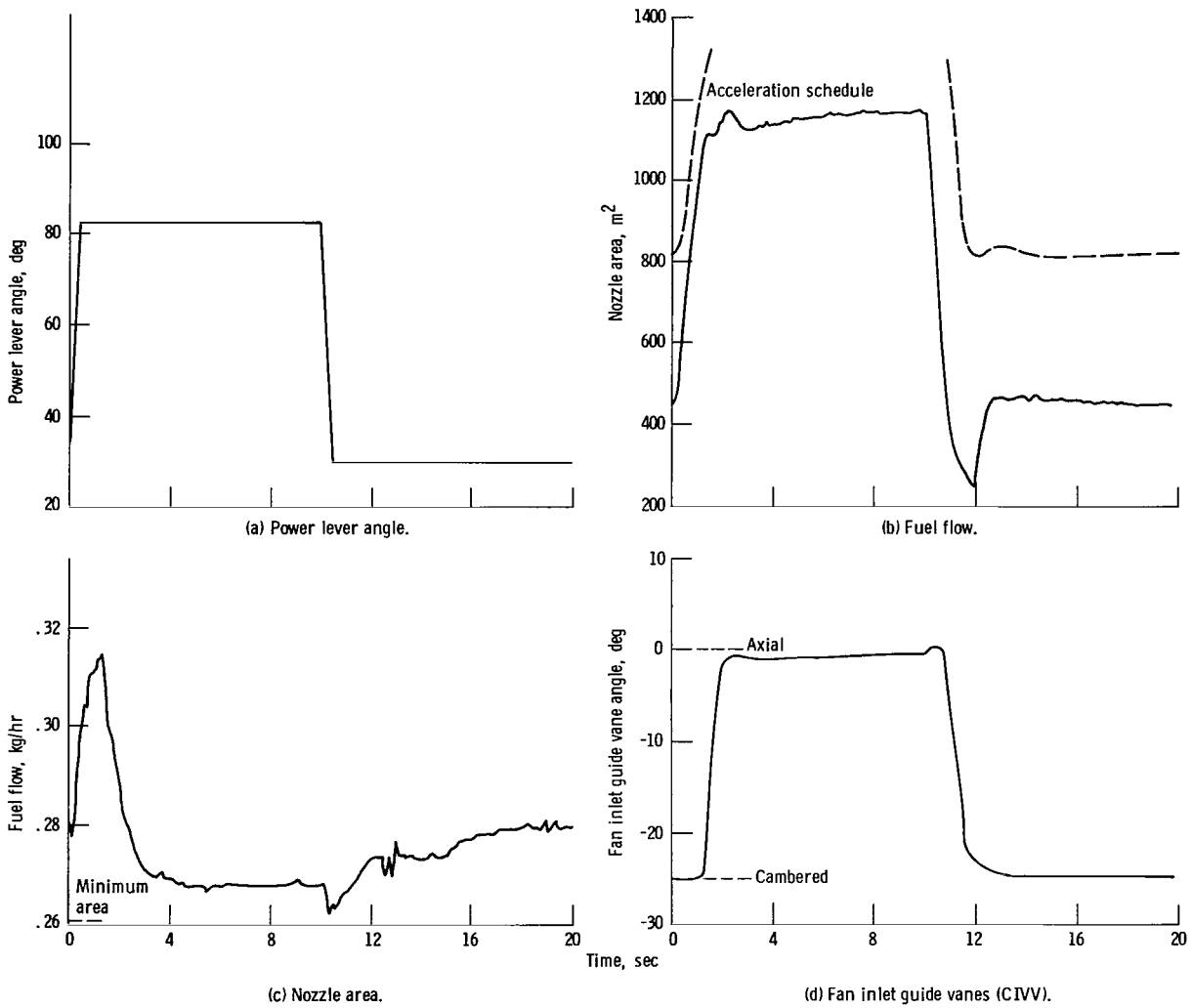

Figure 38. - Simulated F100 response to 30^0 to 83^0 power lever angle (PLA) snap at 13.72 kilometers and Mach 0.9. Multivariable control; PLA = 30^0 provides 40-percent thrust.

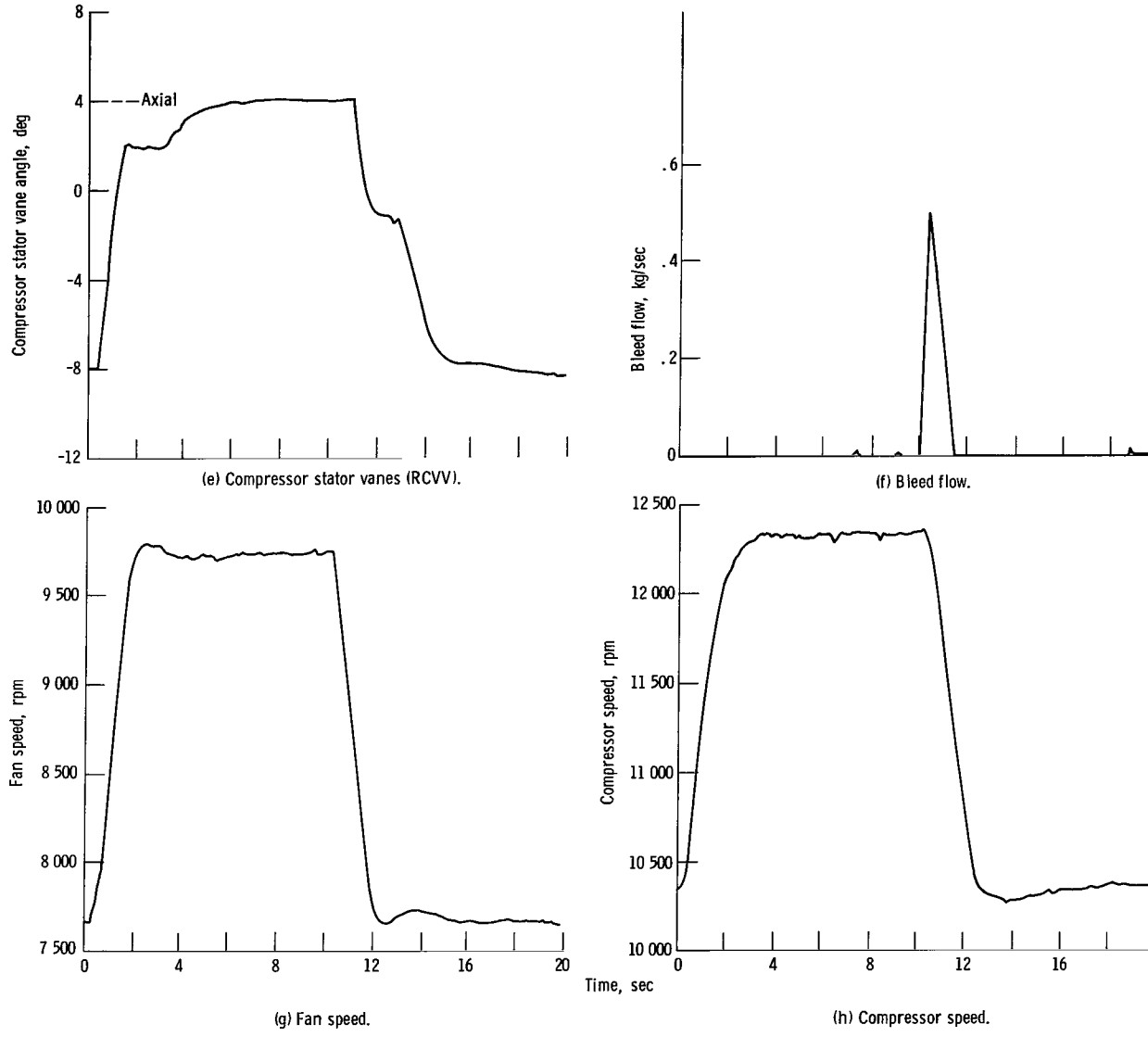

Figure 38. - Continued.

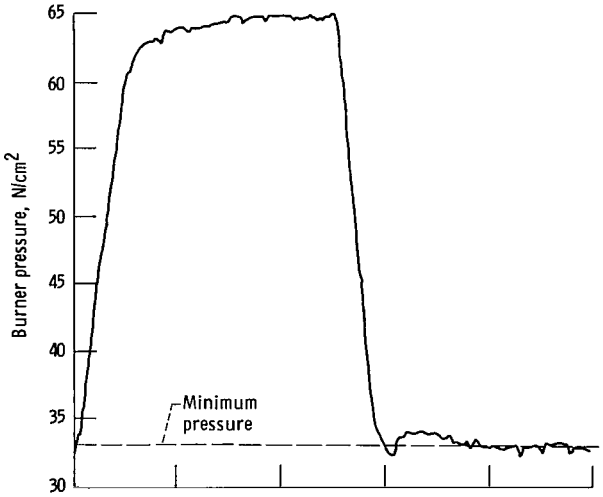

(i) Burner pressure.

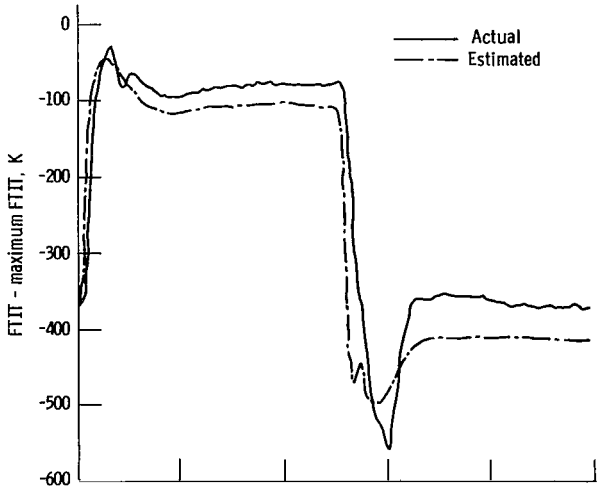

(j) Fan turbine inlet temperature.

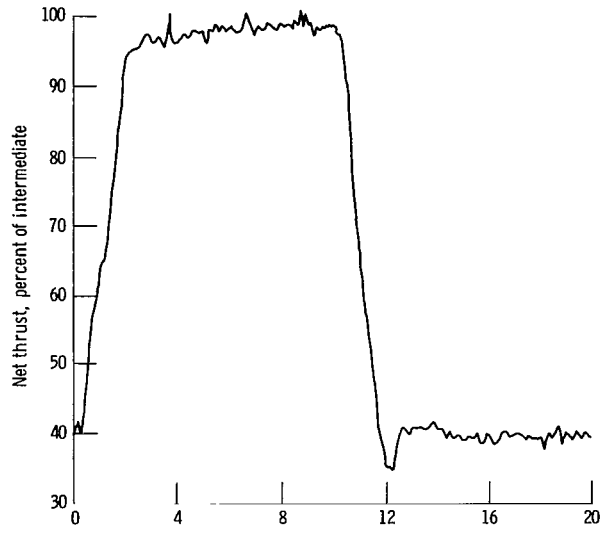

(k) Net thrust.

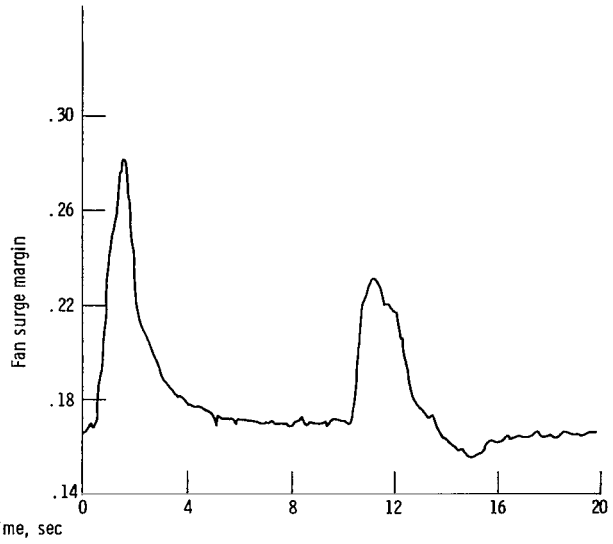

(ℓ) Fan surge margin.

Figure 38. - Continued.

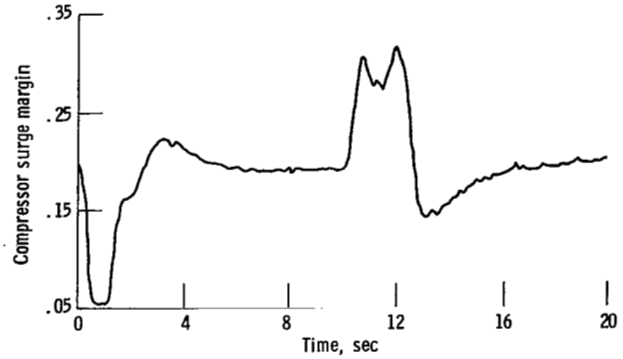

(m) Compressor surge margin.

Figure 38. - Concluded.

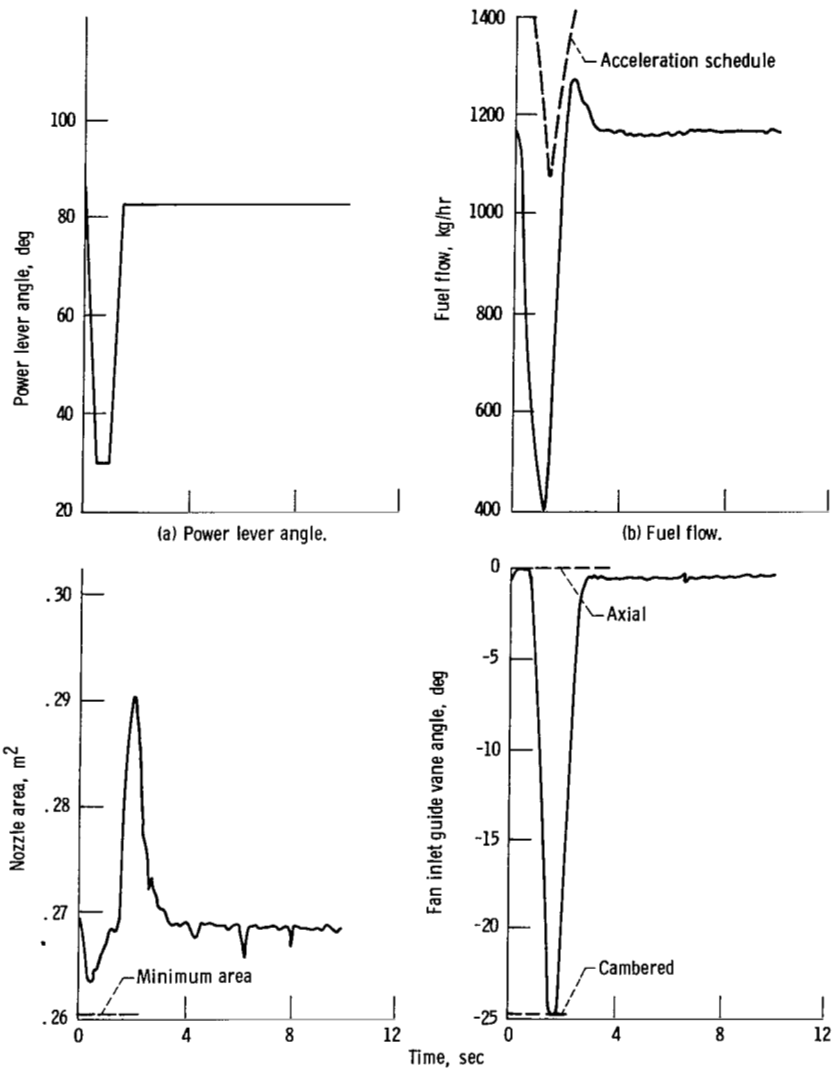

(a) Power lever angle.

(b) Fuel flow.

(c) Nozzle area.

(d) Fan inlet guide vanes (CIVV).

Figure 39. - Simulated F100 response to 83^0 to 30^0 to 83^0 power lever angle (PLA) bodie at 13.72 kilometers and Mach 0.9. Multivariable control.

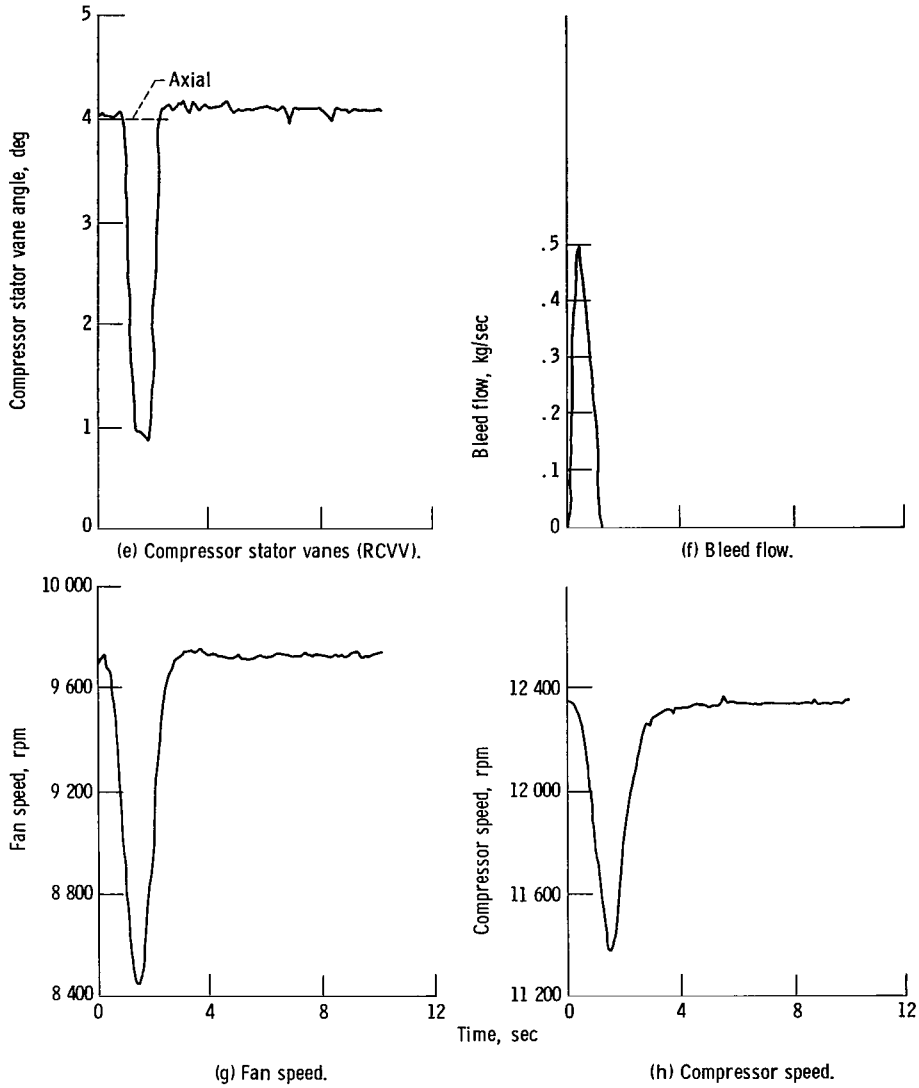

Figure 39. - Continued.

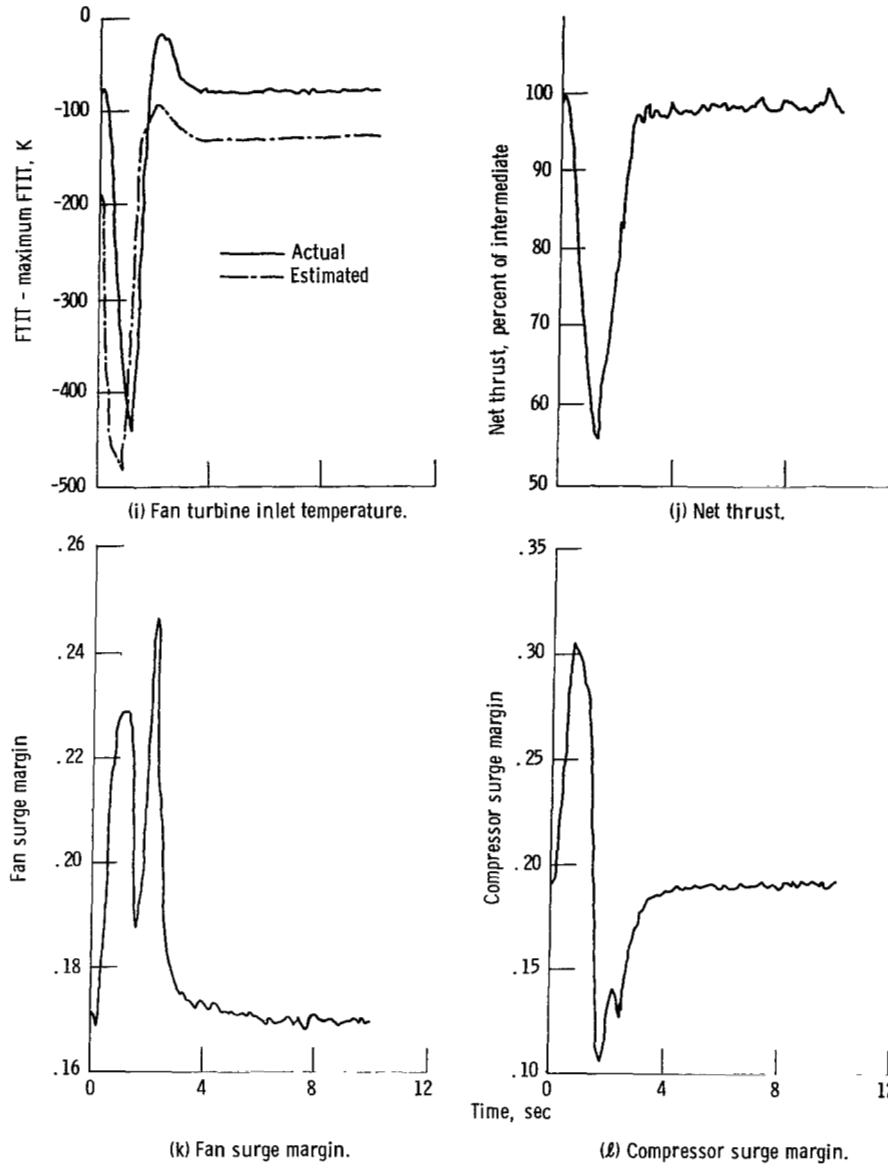

(i) Fan turbine inlet temperature.

(j) Net thrust.

(k) Fan surge margin.

(ℓ) Compressor surge margin.

Figure 39. - Concluded.

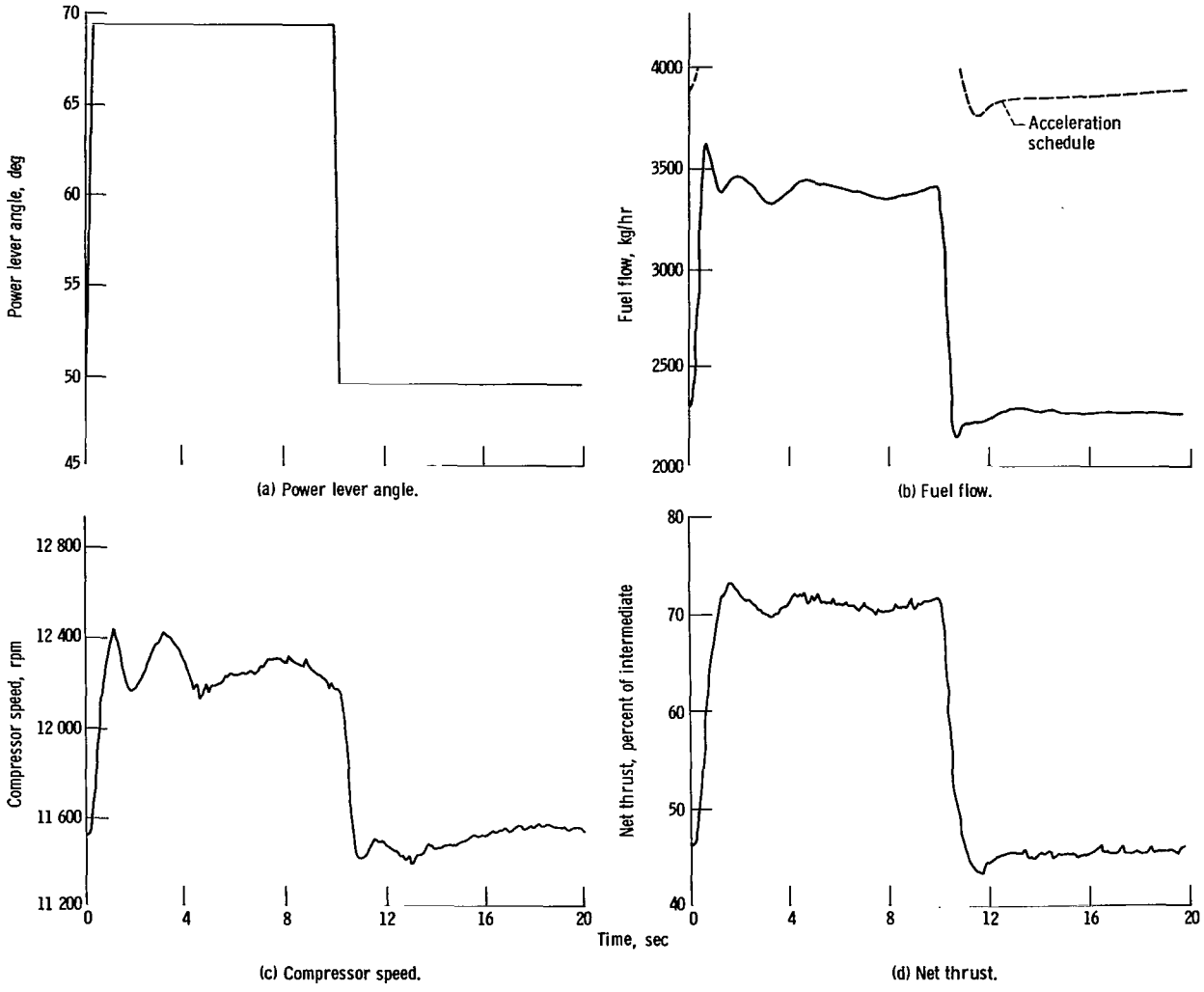

(a) Power lever angle.

(b) Fuel flow.

(c) Compressor speed.

(d) Net thrust.

Figure 40. - Simulated F100 response to 50^0 to 70^0 power lever angle (PLA) snap at 3.048 kilometers and Mach 0.9. Multivariable control.

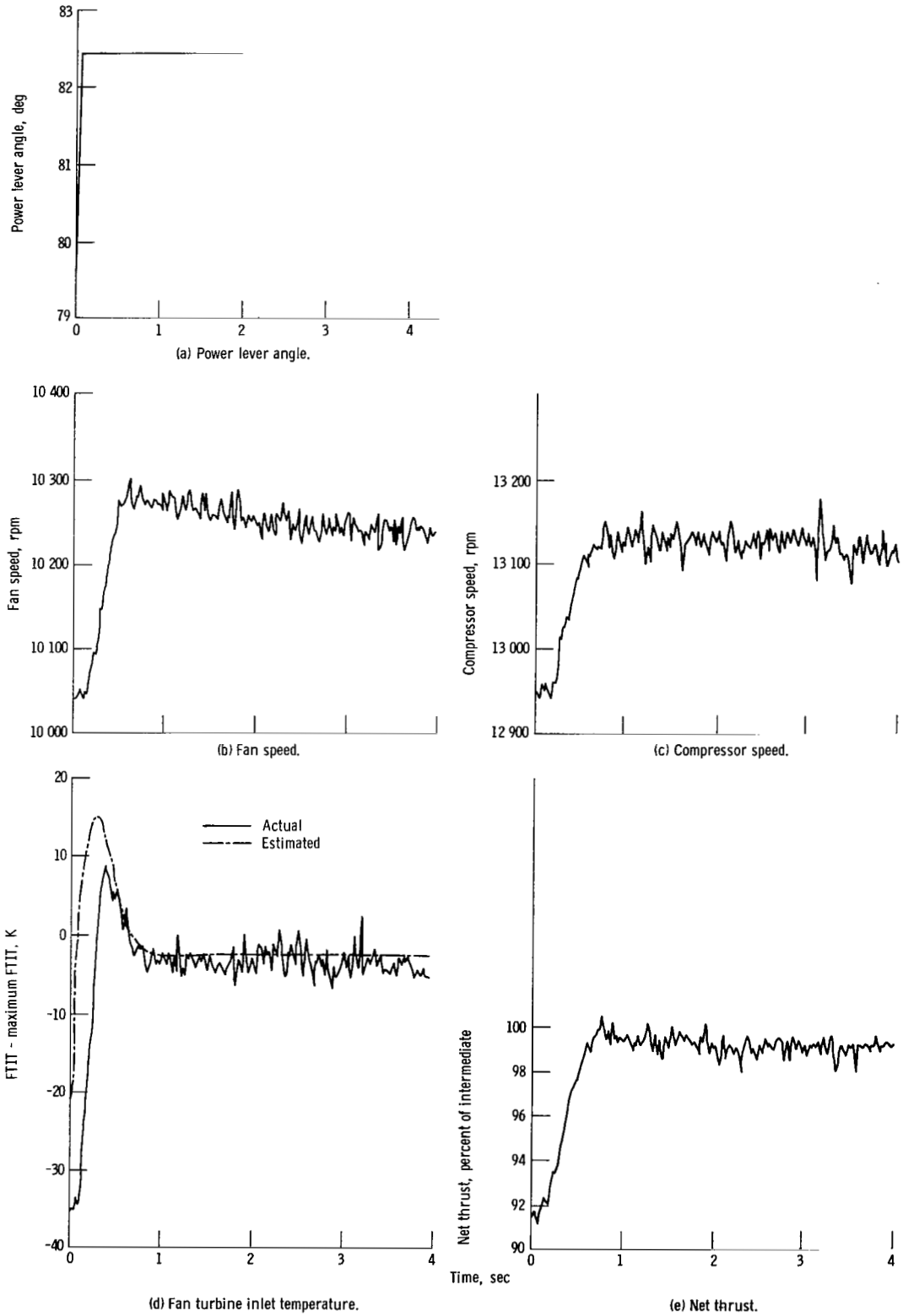

Figure 41. - Simulated F100 to 3^0 power lever angle (PLA) snap at 3.048 kilometers and Mach 0.9. Multivariable control; initial PLA = 79.4^0.

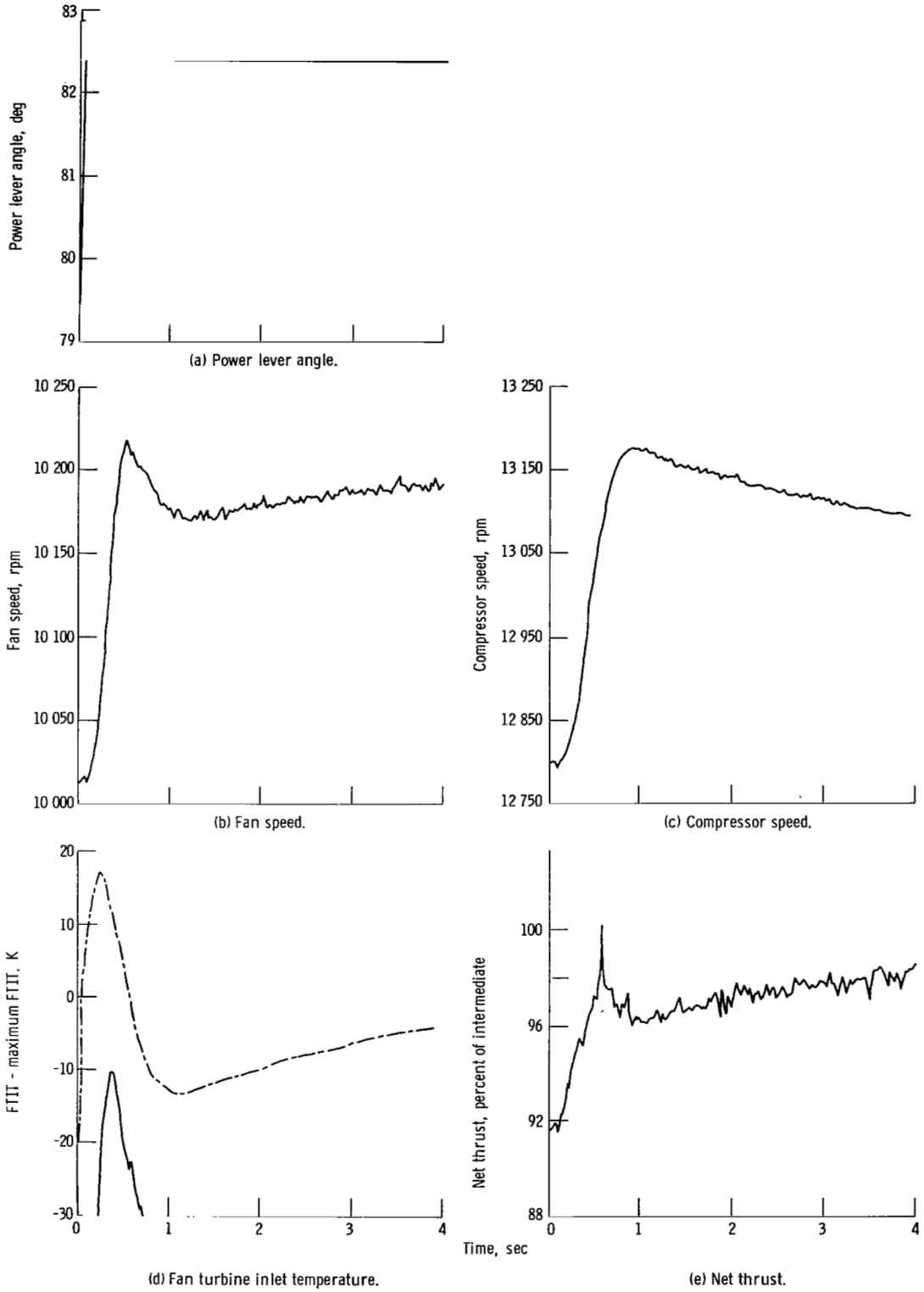

Figure 42. - Simulated F100 response to 3^0 power lever angle (PLA) snap at 3.048 kilometers and Mach 1.2. Multivariable control; initial PLA = 79.4^0.

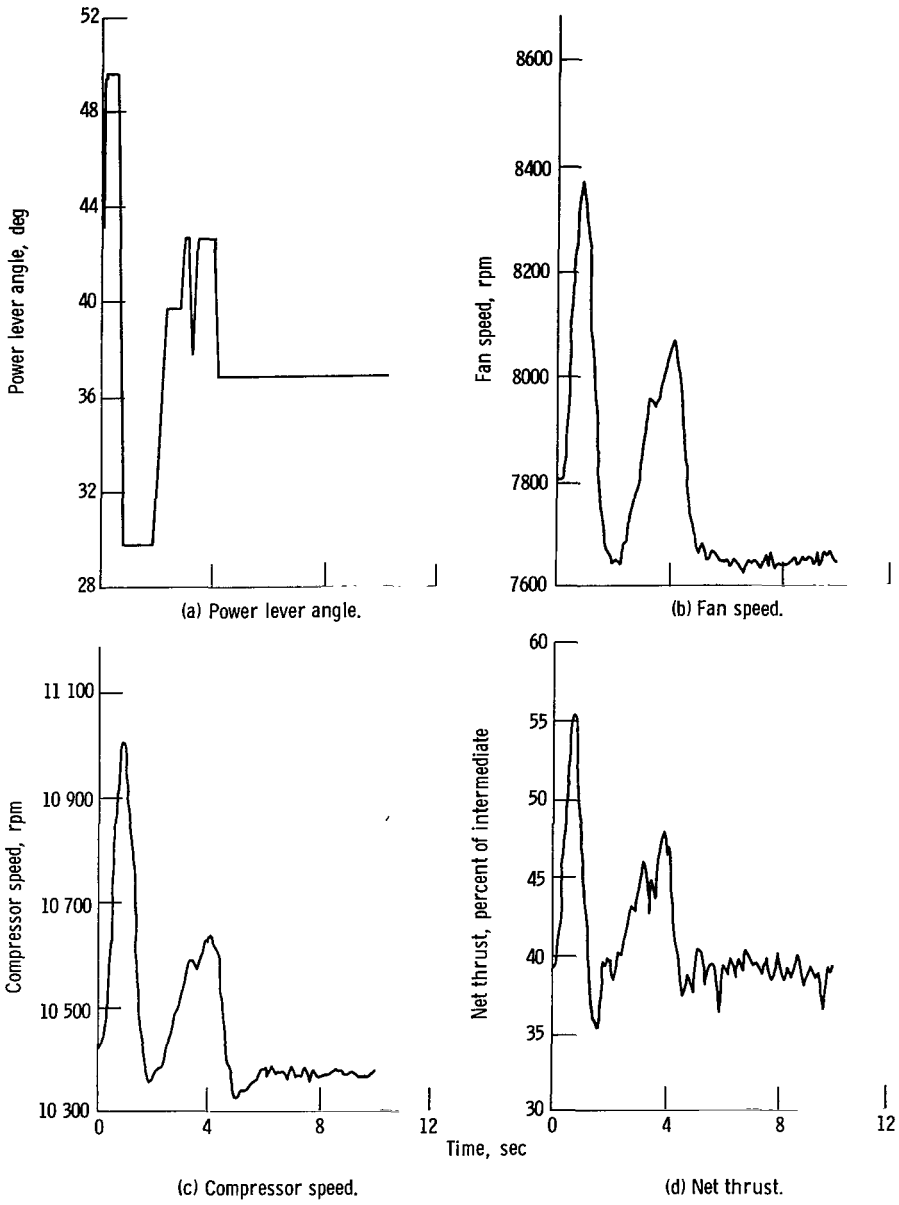

Figure 43. - Simulated F100 response to cyclic power lever angle (PLA) movement at 13.72 kilometers and Mach 0.9. Multivariable control; initial PLA = 40^0.

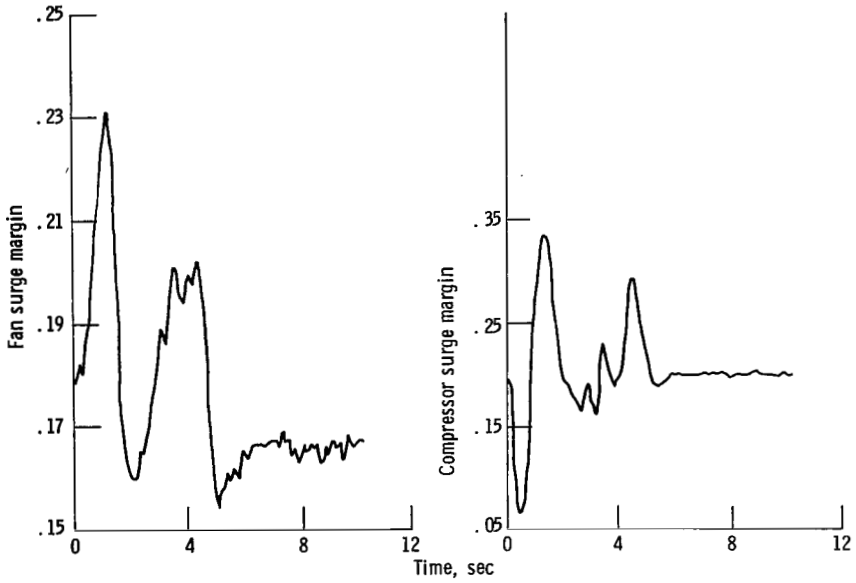

(e) Fan surge margin. (f) Compressor surge margin.

Figure 43. - Concluded.

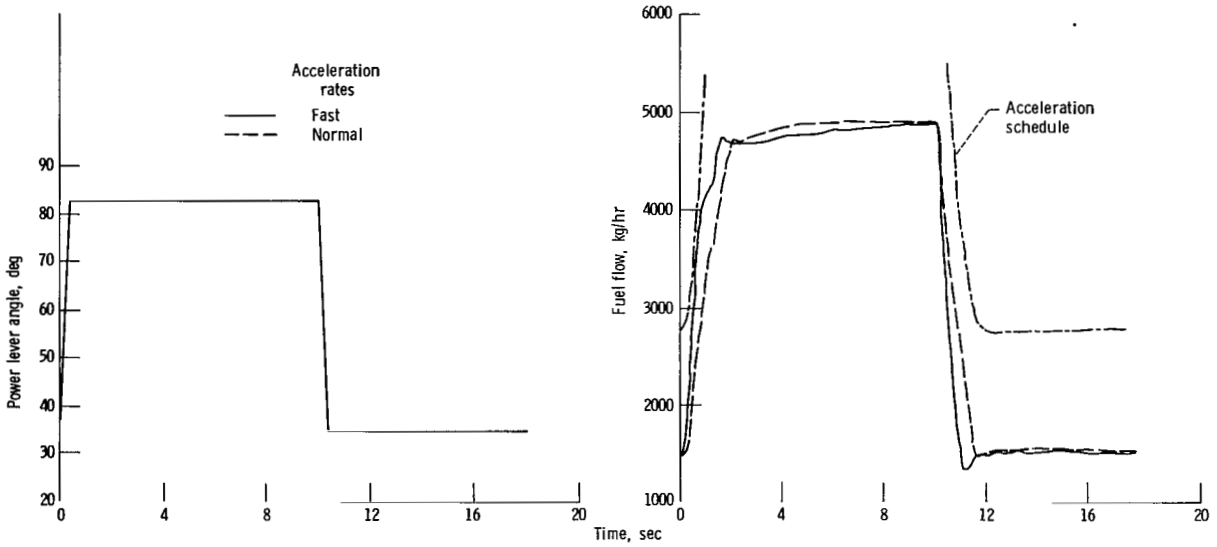

(a) Power lever angle. (b) Fuel flow.

Figure 44. - Comparison of normal and fast F100 simulation responses to 35^0 to 83^0 power lever angle (PLA) snap at sea-level, static conditions. Multivariable control.

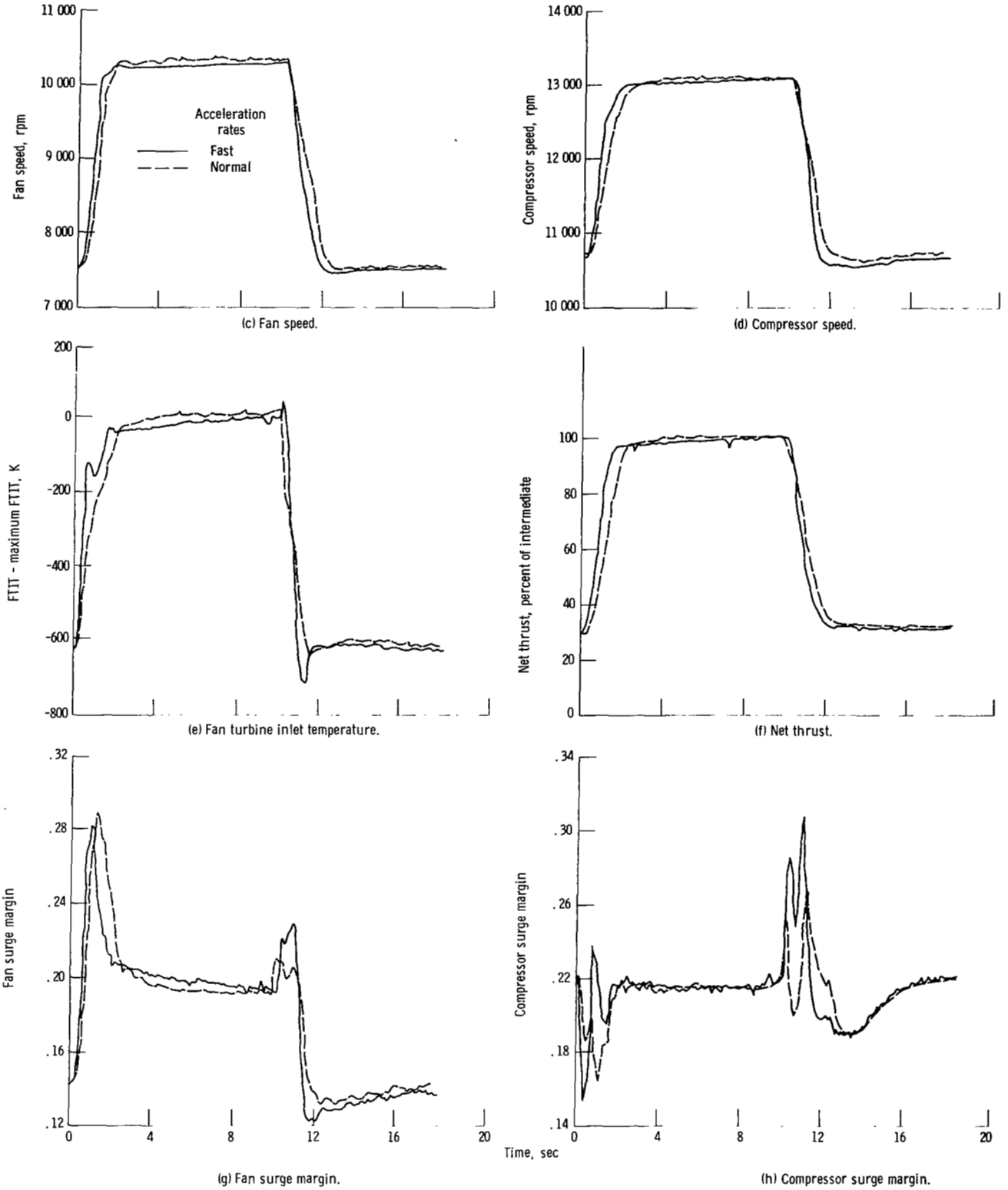

(c) Fan speed.

(d) Compressor speed.

(e) Fan turbine inlet temperature.

(f) Net thrust.

(g) Fan surge margin.

(h) Compressor surge margin.

Figure 44. - Concluded.

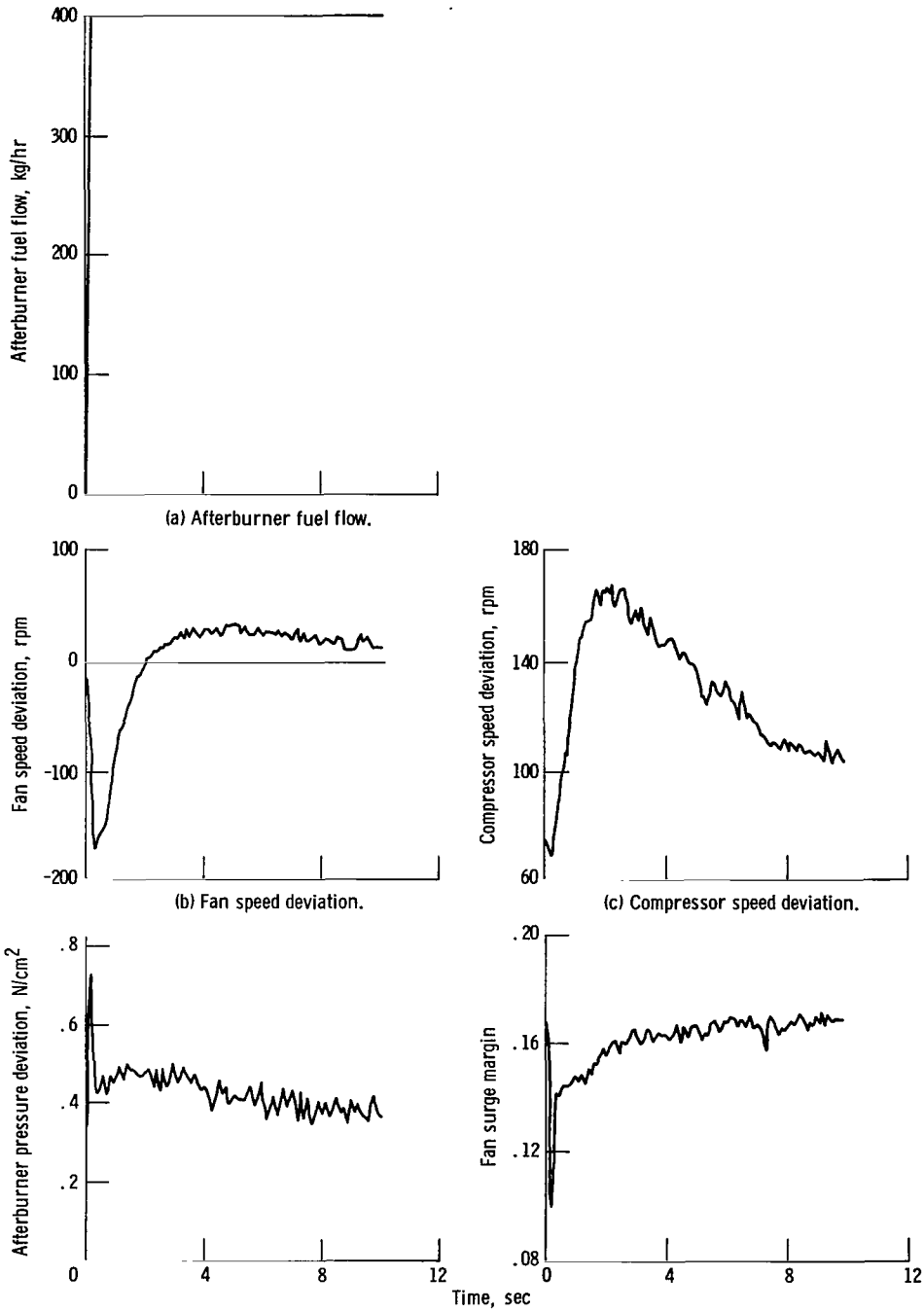

(a) Afterburner fuel flow.

(b) Fan speed deviation.

(c) Compressor speed deviation.

(d) Afterburner pressure deviation.

(e) Fan surge margin.

Figure 45. - Simulated F100 response to afterburner ignition at 13.72 kilometers and Mach 0.9. Multivariable control; PLA = 83^{0}.

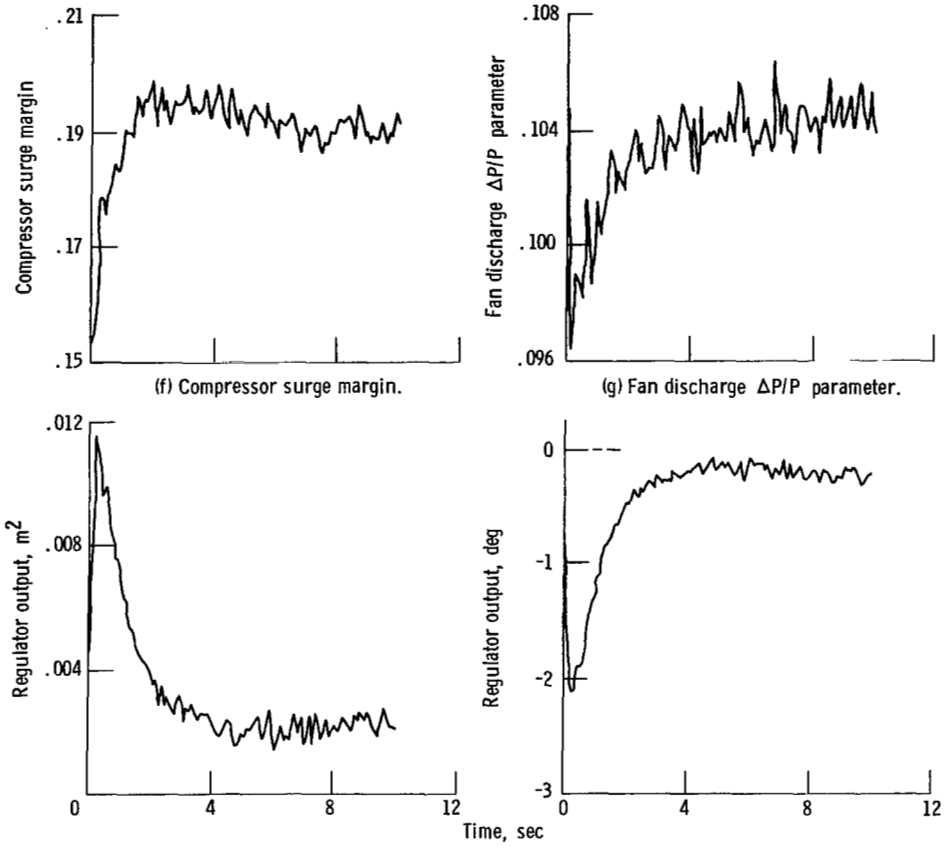

(f) Compressor surge margin.

(g) Fan discharge ΔP/P parameter.

(h) LQR nozzle area output.

(i) LQR CIVV output.

Figure 45. - Concluded.

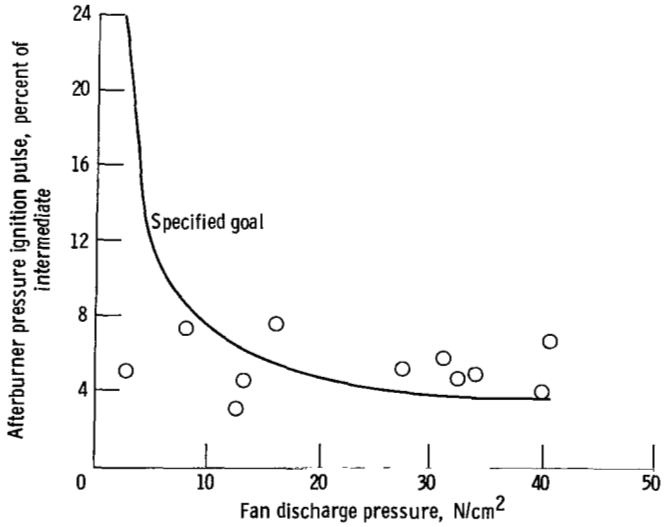

Figure 46. - Simulated F100 afterburner ignition pressure pulse amplitudes. Multivariable control; PLA = 83°; ignition, $\dot{w}_{F,7}/P_4$ = 5.92 kg-cm²/N-hr.

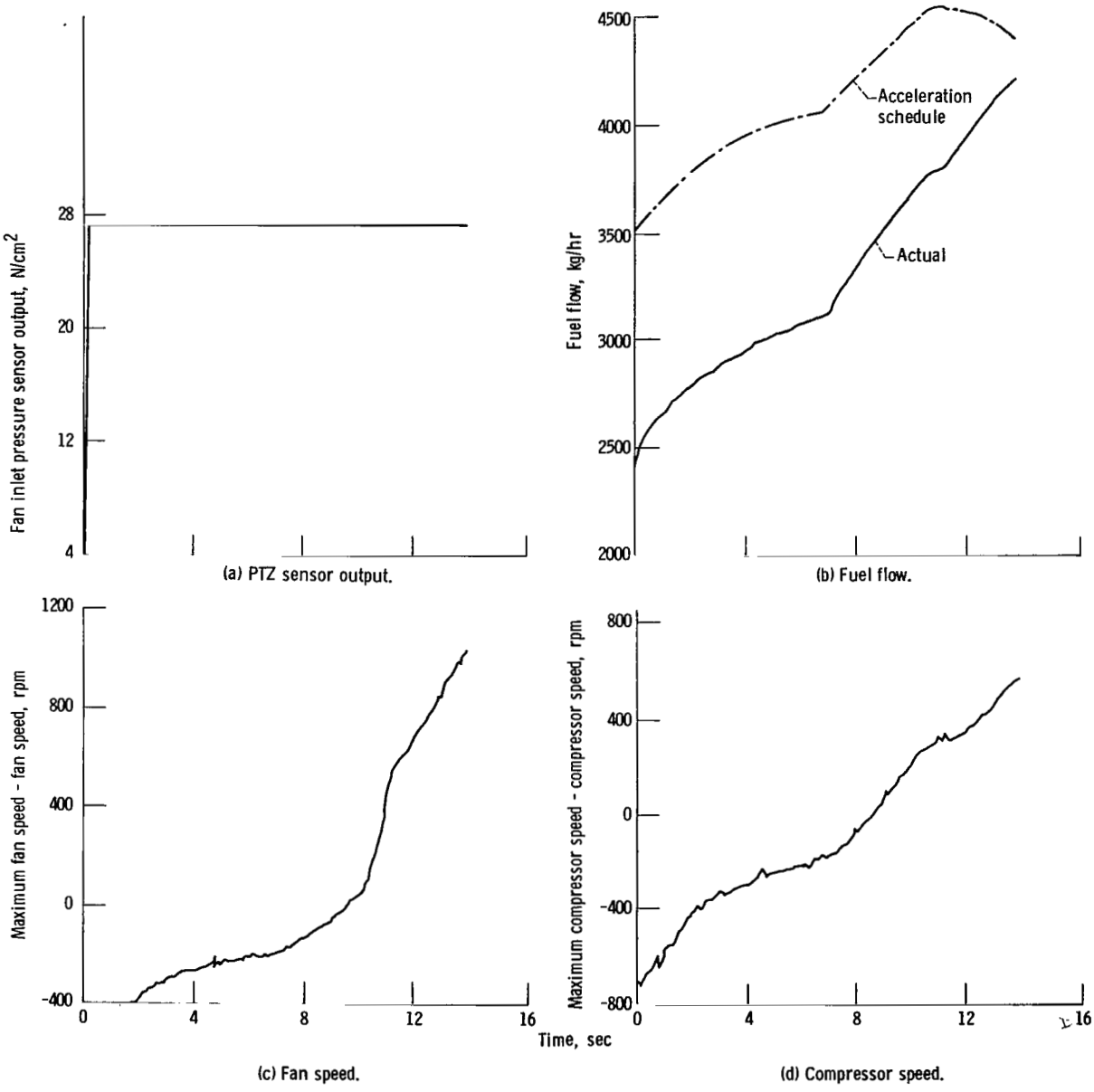

Figure 47. - Effect of fan inlet pressure sensor saturation on simulated F100 performance at 9.144 kilometers and Mach 0.9. Multivariable control; PLA = 83^0.

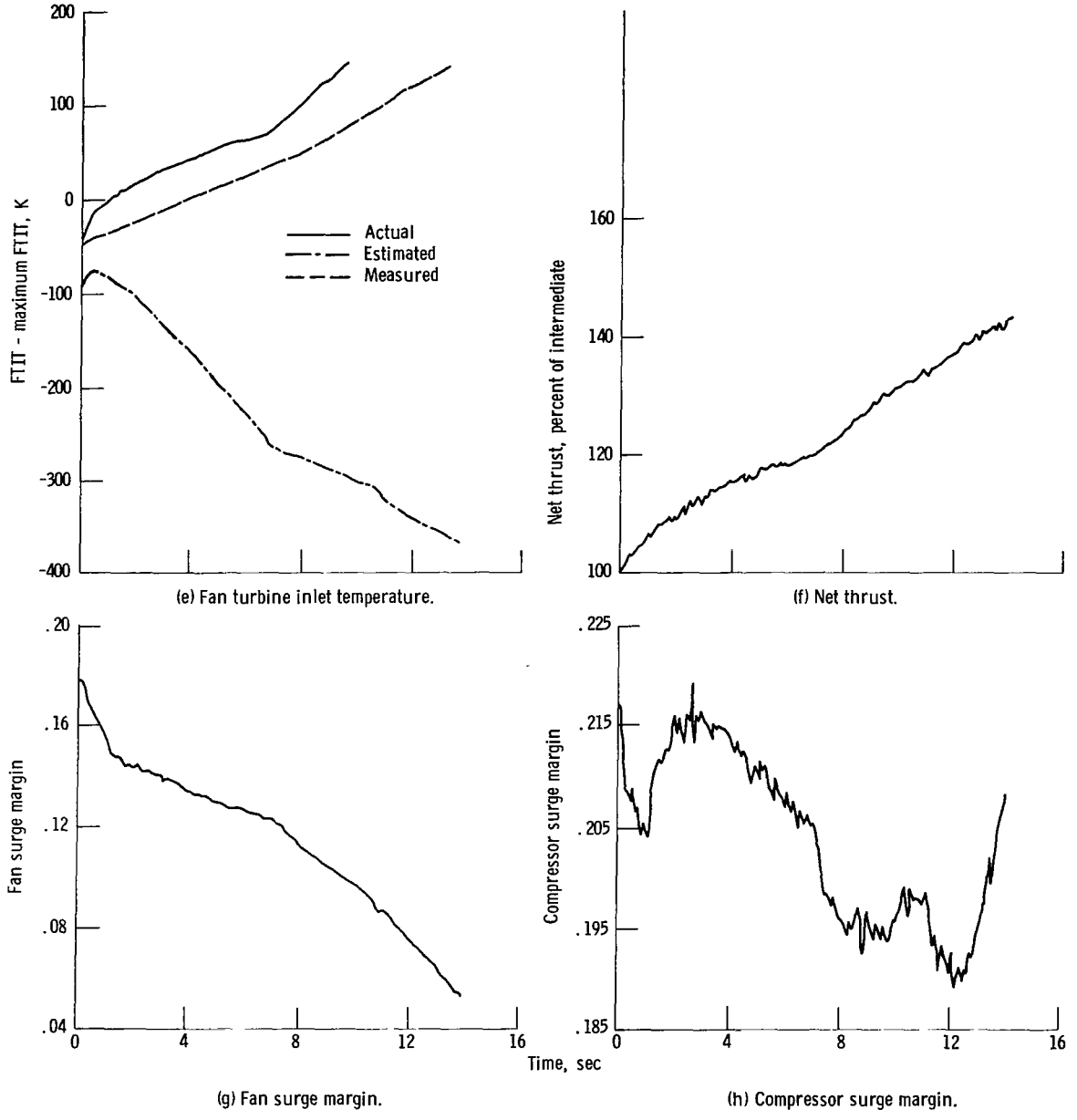

(e) Fan turbine inlet temperature.

(f) Net thrust.

(g) Fan surge margin.

(h) Compressor surge margin.

Figure 47. - Concluded.

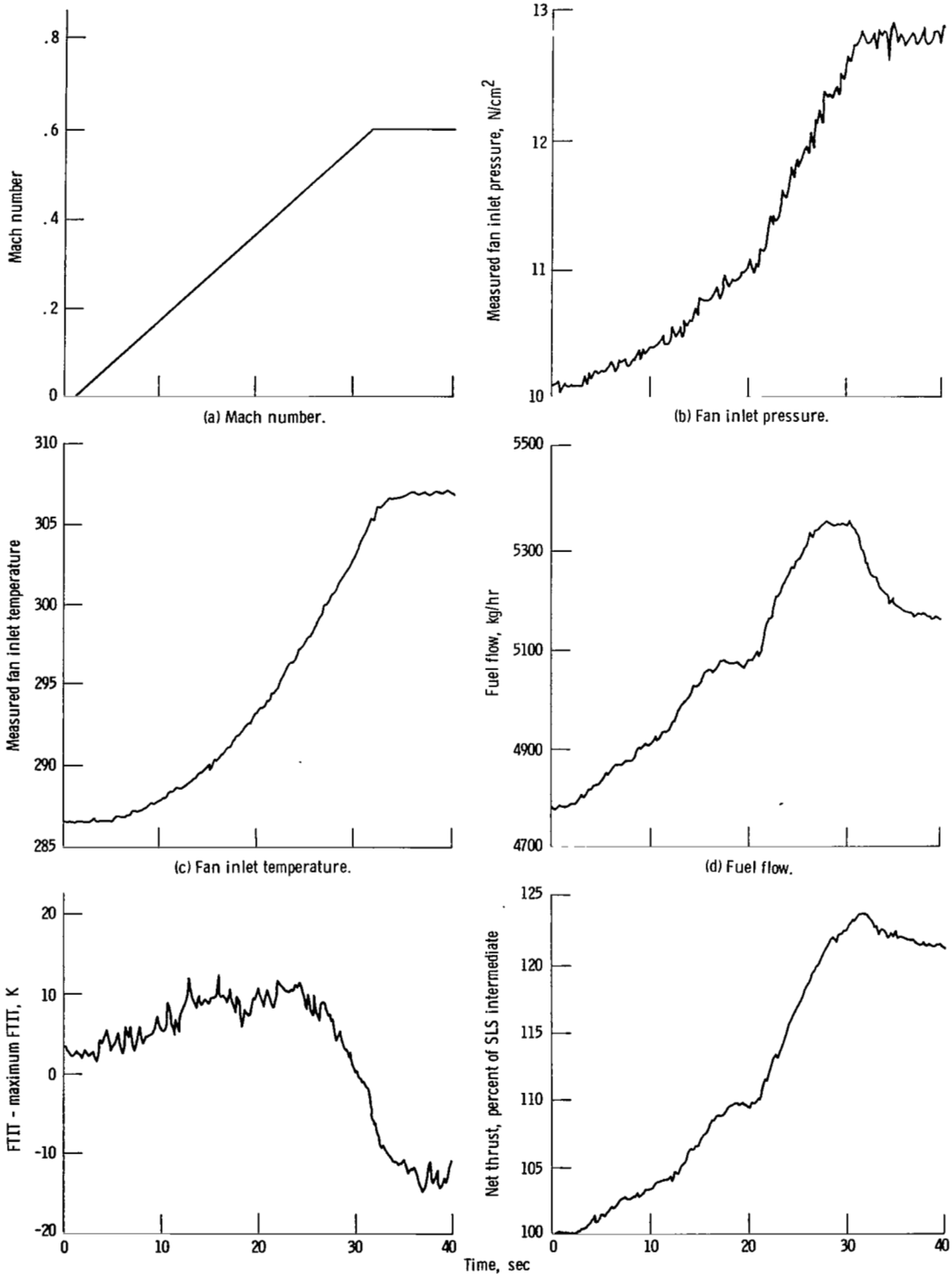

Figure 48. - Simulated F100 response to aircraft acceleration at sea level. Multivariable control; PLA = 83^0.

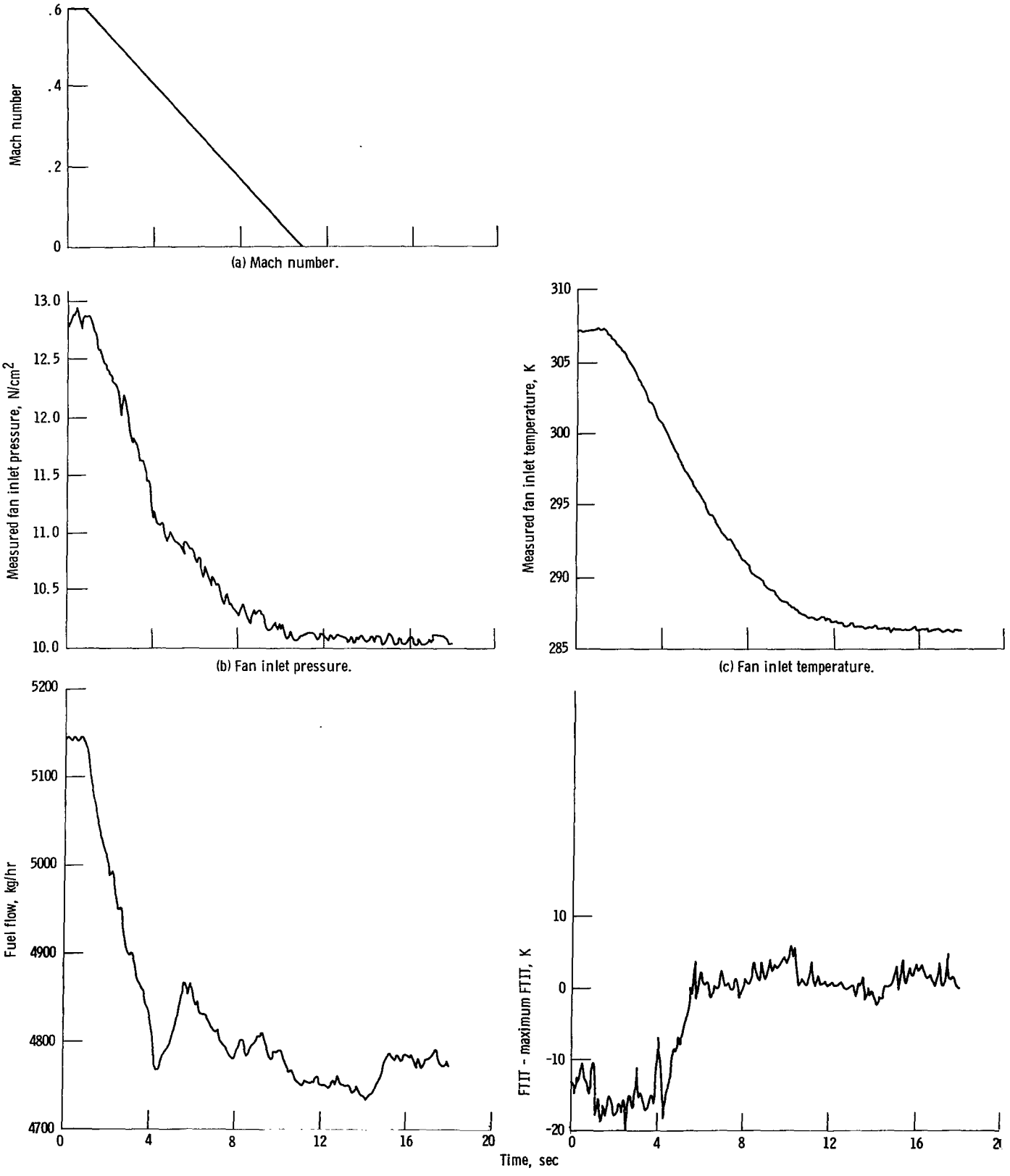

Figure 49. - Simulated F100 response to aircraft deceleration at sea level. Multivariable control; PLA = 83°.

1. Report No.	2. Government Accession No.	3. Recipient's Catalog No.
NASA TP-1056		

4. Title and Subtitle	5. Report Date
F100 MULTIVARIABLE CONTROL SYNTHESIS PROGRAM - EVALUATION OF A MULTIVARIABLE CONTROL USING A REAL-TIME ENGINE SIMULATION	October 1977
	6. Performing Organization Code
7. Author(s)	8. Performing Organization Report No.
John R. Szuch, James F. Soeder, Kurt Seldner, and David S. Cwynar	E-9170
	10. Work Unit No.
9. Performing Organization Name and Address	505-05
National Aeronautics and Space Administration Lewis Research Center Cleveland, Ohio 44135	11. Contract or Grant No.
	13. Type of Report and Period Covered
12. Sponsoring Agency Name and Address	Technical Paper
National Aeronautics and Space Administration Washington, D. C. 20546	14. Sponsoring Agency Code

15. Supplementary Notes

16. Abstract

The F100 Multivariable Control Synthesis program is a cooperative effort by the Air Force Aero-Propulsion Laboratory and the NASA Lewis Research Center aimed at accomplishing the design, evaluation, and testing of a practical, multivariable, linear quadratic regulator control for the F100 turbofan engine. This report covers the NASA evaluation of the multivariable control logic and implementation. The evaluation utilized a real-time, hybrid computer simulation of the engine. The results of the evaluation are presented, and recommendations concerning future engine testing of the control are made. The results indicated that the engine testing of the control should be conducted as planned.

17. Key Words (Suggested by Author(s))	18. Distribution Statement
Simulation; Hybrid computer; Real-time; Turbofan; Multivariable control	Unclassified - unlimited STAR Category 07

19. Security Classif. (of this report)	20. Security Classif. (of this page)	21. No. of Pages	22. Price*
Unclassified	Unclassified	103	A06

* For sale by the National Technical Information Service, Springfield, Virginia 22161

National Aeronautics and Space Administration

Washington, D.C.
20546

Official Business
Penalty for Private Use, $

THIRD-CLASS BULK RATE

Postage and Fees Paid
National Aeronautics and
Space Administration
NASA-451

U.S.MAIL

2 1 1U,A, 092377 S00903DS
DEPT OF THE AIR FORCE
AF WEAPONS LABORATORY
ATTN: TECHNICAL LIBRARY (SUL)
KIRTLAND AFB NM 87117

S

NASA

POSTMASTER: If Undeliverable (Section 158 Postal Manual) Do Not Return